REMOTE SENSING OF A DYNAMIC SUB-ARCTIC PEATLAND RESERVOIR USING OPTICAL AND SYNTHETIC APERTURE RADAR DATA

by

Jarod Lee Larter

A Thesis submitted to the Faculty of Graduate Studies of

The University of Manitoba

in partial fulfillment of the requirements of the degree of

MASTER OF SCIENCE

Department of Environment and Geography

University of Manitoba

Winnipeg, Manitoba, Canada

THE UNIVERSITY OF MANITOBA
FACULTY OF GRADUATE STUDIES
*****
COPYRIGHT PERMISSION

Remote Sensing of a Dynamic Sub-Arctic Peatland Reservoir Using Optical and
Synthetic Aperture Radar Data

A Thesis/Practicum submitted to the Faculty of Graduate Studies of The University of
Manitoba in partial fulfillment of the requirement of the degree
of

Master of Science

Jarod Lee Larter © 2010

ABSTRACT

Stephens Lake, Manitoba is an example of a peatland reservoir that has undergone physical changes related to mineral erosion and peatland disintegration processes since its initial impoundment. In this thesis I focused on the processes of peatland upheaval, transport, and disintegration as the primary drivers of dynamic change within the reservoir. The changes related to these processes are most frequent after initial reservoir impoundment and decline over time. They continue to occur over 35 years after initial flooding. I developed a remote sensing approach that employs both optical and microwave sensors for discriminating land (i.e. floating peatlands, forested land, and barren land) from open water within the reservoir. High spatial resolution visible and near-infrared (VNIR) optical data obtained from the QuickBird satellite, and synthetic aperture radar (SAR) microwave data obtained from the RADARSAT-1 satellite were implemented. The approach was facilitated with a Geographic Information System (GIS) based validation map for the extraction of optical and SAR pixel data. Each sensor's extracted data set was first analyzed separately using univariate and multivariate statistical methods to determine the discriminant ability of each sensor. The initial analyses were followed by an integrated sensor approach; the development of an image classification model; and a change detection analysis.

Results showed excellent (> 95%) classification accuracy using QuickBird satellite image data. Discrimination and classification of studied land cover classes using SAR image texture data resulted in lower overall classification accuracies (~ 60%). SAR data classification accuracy improved to > 90% when classifying only land and water, demonstrating SAR's utility as a land and water mapping tool. An integrated sensor data

approach showed no considerable improvement over the use of optical satellite image data alone. An image classification model was developed that could be used to map both detailed land cover classes and the land and water interface within the reservoir. Change detection analysis over a seven year period indicated that physical changes related to mineral erosion, peatland upheaval, transport, and disintegration, and operational water level variation continue to take place in the reservoir some 35 years after initial flooding.

This thesis demonstrates the ability of optical and SAR satellite image remote sensing data sets to be used in an operational context for the routine discrimination of the land and water boundaries within a dynamic peatland reservoir. Future monitoring programs would benefit most from a complementary image acquisition program in which SAR images, known for their acquisition reliability under cloud cover, are acquired along with optical images given their ability to discriminate land cover classes in greater detail.

ACKNOWLEDGEMENTS

DEDICATION

It has been a long haul for me and an even longer one for my wife. She has put up with books, papers, and my laptop on the dining room table and my constantly wandering mind for many a year now. Without her I could not have completed this project. She has helped me by helping our family through difficult times, and taking control of situations that I was unable or didn't know how to take control of. I am extremely grateful to have someone who can continue to motivate me and talk to me when I am feeling unfocused or down. She even took some time out of her schedule to give birth to our beautiful daughter. I love her for it and I dedicate this work to her.

TABLE OF CONTENTS

LIST OF TABLES

LIST OF FIGURES

LIST OF ABBREVIATONS AND SYMBOLS

ANOVA	analysis of variance
ASD	Analytical Spectral Devices
ASL	above sea level
CCRS	Canadian Centre for Remote Sensing
CDOM	coloured dissolved organic matter
DN	digital number
DOC	dissolved organic carbon
EMR	electromagnetic radiation
EMS	electromagnetic spectrum
GIS	geographic information systems
GPS	global positioning system
GS	generating station
KHLP	Keeyask Hydropower Limited Partnership
LDA	linear discriminant analysis

NDVI	normalized difference vegetation index
NIR	near-infrared
NWWG	National Wetlands Working Group
PCA	principal component analysis
VIS	visible
VNIR	visible/near-infrared
RAR	real aperture radar
SAR	synthetic aperture radar
$\sigma°$	radar backscatter coefficient

CHAPTER 1 : INTRODUCTION

1.1 RATIONALE

In this thesis I explore the potential of using optical and microwave satellite remote sensing technologies to effectively map the dynamic physical changes that can occur within northern peatland reservoirs, with an emphasis on sub-arctic/high-boreal hydroelectric peatland reservoirs. Specifically I introduce the use of high spatial resolution optical, visible and near-infrared (VNIR) data, and synthetic aperture radar (SAR) data to discriminate land primarily occupied by floating peatlands, forested land, and barren land from water as a means to map and monitor reservoir change.

Timely mapping of land and water has important implications for existing and proposed hydroelectric developments. The physical environment in which a reservoir lies has a direct effect on how it changes over time. Reservoirs found in the Canadian Shield such as those along the Winnipeg River have relatively stable bedrock and mineral shorelines. Stephens Lake, Manitoba along the Nelson River, by contrast is an example of a sub-arctic peatland reservoir that has undergone significant change in a relatively short period of time. Three main processes can be attributed to ongoing change in this reservoir: 1) water level management - Stephens Lake is cycled on a weekly basis according to hydroelectric demand; 2) mineral shoreline erosion – the glacio-lacustrine deposits in the shore zone can be easily eroded as a result of wave action and slope failure; 3) dynamic peatland processes (i.e. upheaval, transport, disintegration) – the process by which intact peripheral peatlands are continuously breaking down through lateral water movement within peatland soils. The third of these three processes is the

focus of this thesis. The rate and extent of shoreline erosion and breakdown in a reservoir is important in determining changes to both the terrestrial and aquatic environments. Peatland reservoirs are unique in that the erosion of an organic shoreline is different than the erosion of a mineral shoreline. Peatland reservoirs can expand laterally over time due to shore zone peatland disintegration processes. Initial inundation as a result of waterway impoundment causes some peatlands to detach from their parent material and float to the surface leaving other peatlands on the bottom of the reservoir. This process is known as *peatland upheaval*. This initial upheaval process, aided by the low bulk density of peat relative to water, has been shown to be rapid within the first few years, with limited occurrence after 10 years (Keeyask Hydropower Limited Partnership (KHLP) 2010). The resulting floating peatlands or peat islands can persist in a reservoir for many years by staying anchored to their parent material, or they can become completely detached and thus move throughout the reservoir via wind and water currents. Over time floating peat islands and peripheral shore zone peatlands go through a process of change which can involve various degrees of buoyancy, sometimes resulting in sinking of peat to the reservoir bottom, in addition to fragmentation or breakdown. This process has been described as *peatland disintegration* (KHLP 2010) and has seen limited study.

Peatland upheaval, transport, and disintegration has been linked with: 1) increases in carbon dioxide (CO_2) and methane (CH_4) greenhouse gases (Duchemin et al. 1995; Kelly et al. 1997); 2) increased concentrations of methylated mercury in the aquatic environment (St.Louis et al. 2004); 3) changes to aquatic habitat quality as a result of fluctuations in pH and oxygen demand (Rahel 1984); 4) physical hazards or barriers to navigation, and recreational use, and hydroelectric generating station operation, as a

result of peat debris lodged against turbine intakes (Balgurov 1967; Ronka and Uusinoka 1976); and 5) physical changes to the land and water boundary areas and composition of available aquatic and terrestrial habitats. The ability to quantify reservoir extent over time is not only required to understand the local terrestrial and aquatic habitats, but also potentially to meet the operational needs of a hydroelectric generating station.

Therefore there is a need to efficiently and accurately map and monitor the processes of peatland upheaval, transport, and ongoing disintegration, and mineral erosion both in the short term after reservoir initiation, when peatland upheaval and transport causes the most rapid change, and in the long term as shoreline evolution gradually continues with lateral expansion of the reservoir. Historically, the mapping and monitoring of peatland upheaval, transport, and disintegration, and mineral erosion processes in reservoirs relied upon the interpretation of multi-date aerial photography coupled with intensive field surveys (Ronka & Uusinoka 1976; Grondin and Ouzilleau 1980; Dryade 1984; Belanger et al. 1991; Robert 2000; Saint-Laurent et al. 2001; Manitoba Hydro and NCN 2003; Asada et al. 2005; KHLP 2010). These historical mapping and monitoring processes require extensive resources and time. In this thesis, I propose a spaceborne remote sensing approach that could potentially be incorporated into an operational framework for mapping and monitoring the dynamic land and water boundary changes of remote peatland reservoirs.

1.2 THESIS OBJECTIVES AND ORGANIZATION

The primary objective of this thesis is to develop an approach to discriminating land (floating peatlands, forested land, and barren land) from open water using optical and microwave remote sensing data in Stephens Lake, Manitoba. It is expected that this research may provide an operational monitoring context for routine discrimination of the land/water boundary in a dynamic peatland reservoir that is affected by water level management, mineral shoreline erosion, and peatland disintegration. This approach will also be robust enough to discriminate floating peatlands and peat islands from mineral shore zones and islands, which can lead to future inventories of floating peatland area and volume within the reservoir. This overarching thesis objective is achieved through four supporting thesis objectives, addressed in Chapters 3 - 6:

1. Determine the optical spectral reflectance and microwave backscattering signatures of the four dominant reservoir land cover classes that form the land/water reservoir boundary. The second part of this objective is to determine if optical visible and near-infrared (VNIR) and microwave synthetic aperture radar (SAR) data are able to successfully discriminate between the four broad land cover classes. This objective is addressed in Chapter 3 (optical) and Chapter 4 (SAR) respectively.

2. Determine whether optical, microwave, or a combination of these two remotely sensed data types is a better method of discrimination and classification of peatland reservoir classes. This objective is addressed in Chapter 5.

3. Develop a land cover image classification model to map floating peatlands, forested land, open water, and barren land cover classes, which comprise the reservoir's land/water boundary. This objective is addressed in Chapter 5.

4. Implement a change detection analysis using a land/water classification model and a historical land/water mask. This objective will demonstrate the changes that still occur in a relatively short time frame (7 years) in a dynamic sub-arctic peatland reservoir 35 years after initial impoundment. This objective is addressed in Chapter 6.

Chapter 2 provides a background and rationale for this thesis. I begin by introducing the thesis setting, I then review relevant literature pertaining to the overall thesis objectives including: wetland and peatland classification, development and ecology; peatland change related to hydroelectric development; optical and microwave remote sensing fundamentals; and the use of optical and microwave remote sensing technologies in wetland/peatland and reservoir applications. Chapter 2 is important as it provides the context for the content in research chapters 3-6.

Chapter 7 is a closing chapter summarizing each thesis chapter, their results, and the overall thesis conclusions as well as providing recommendations for future work utilizing optical and microwave remote sensing technologies to map and monitor peatland reservoir change.

CHAPTER 2 : THESIS SETTING, PEATLAND DYNAMICS, AND REMOTE SENSING

In this chapter I provide a thesis setting, explore the concepts of peatland ecosystems and the dynamic process of peatland upheaval, transport, and disintegration. I then discuss optical and microwave remote sensing principles and technologies and relate them to the mapping and monitoring of wetland and reservoir environments.

2.1 THESIS SETTING

The study area for this thesis is focused on Stephens Lake (56°23'N, 95°03'W), which is an approximately 280 km^2 hydroelectric reservoir along the lower Nelson River created by the impoundment of Kettle Generating Station (GS) forebay in 1970. The impoundment flooded 220.55 km^2 (Manitoba Hydro 1996a) of land resulting in the connection of the Nelson River with North and South Moose Lakes, now known as the north arm. Kettle GS is a peaking-type plant, with mean daily water levels in a one-week period fluctuating by as much as 1.9 m (Manitoba Hydro 1996a).

The Nelson River drainage area encompasses the prairie regions of Alberta, Saskatchewan, Manitoba, Montana, Minnesota and North Dakota as well as the boreal regions of Ontario, Manitoba and Saskatchewan (Figure 2.1). In total, the drainage area accounts for greater than 1 million km^2 (Rosenberg et al. 2005). The Nelson River extends from the northern outlet of Lake Winnipeg to Hudson Bay and transitions from the Canadian Shield to the Hudson Bay Lowlands and through the boreal and sub-arctic eco-zones as it exits northeastern Manitoba to Hudson Bay (Figure 2.1). This area of

Manitoba is known to have some of the highest concentrations of organic wetlands in Canada (Tarnocai et al. 2000). The extensive drainage area and relatively high slope is conducive to large scale hydroelectric development, with average slope from Split Lake to the estuary at 57 cm/km (Rosenberg et al. 2005). Beginning in 1961, Manitoba Hydro began harnessing the Nelson River's hydroelectric potential with the commissioning of Kelsey Generating Station, which is a run-of-river plant. In 1976 Manitoba Hydro completed the Churchill River Diversion (CRD) and Lake Winnipeg Regulation (LWR) projects. These two water management projects increased flows to the Nelson River system with CRD diverting a portion of the water flow from the Churchill River system to the Nelson River for hydroelectric power generation (Manitoba Hydro 1996b).
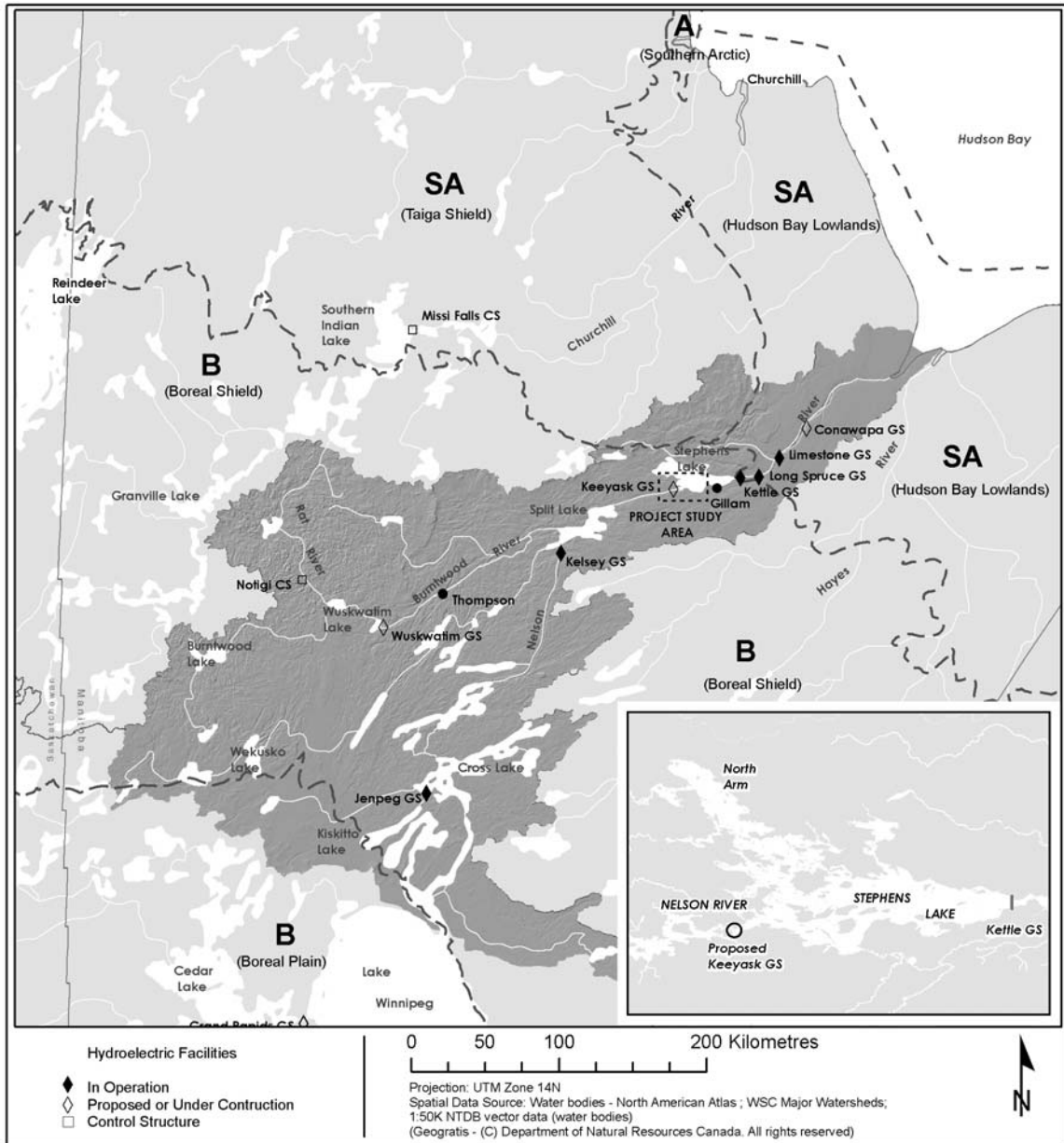
Figure 2.1. Location of Stephens Lake along the lower Nelson River in northeastern Manitoba.

2.1.1 Climate

The climate of the Stephens Lake area is a typical continental climate, with marine influences from Hudson Bay. The mean annual temperature for Gillam, Manitoba, which is situated along what is now the south shore of Stephens Lake, is -4.2°C. The

average January temperature is -25.8°C, while the average July temperature is 15.3°C. The climate is susceptible to extreme weather which has created extreme record lows of -46.1°C and record highs as much as 35.5°C. Average annual rainfall is 313.5 mm, while average annual snowfall is 228.6 mm (Canadian Climate Normals 1971 – 2000; Environment Canada 2007). As a result of these climatic conditions much of the area surrounding Stephens Lake is affected by discontinuous permafrost, which has played an important role in development of the adjacent peatlands.

2.1.2   Physiography

The Pleistocene glaciations assisted in the formation of the two major physiographic regions found in northern Manitoba, the Hudson Bay Lowlands, and the Precambrian shield (boreal shield), both of which are found in the area surrounding Stephens Lake. The surface mineral material in the area around Stephens Lake consists mainly of shallow to deep clay-textured lacustrine sediments underlain by loam to silt loam till. There are some areas which contain water-worked and eroded loam to silt-loam till and still fewer areas that contain discontinuous loam to coarse sand and gravelly glaciofluvial ridges (Mills et al. 1976). As a result the Nelson River system is known to be turbid (Rosenberg et al. 2005). Erosion of silt, sand, and clay glaciofluvial deposits within the watershed create an input of suspended and dissolved solids. This is more evident towards the Hudson Bay Lowlands where surface materials are more easily eroded (Rosenberg et al. 2005).

The terrain of the immediate area around Stephens Lake primarily owes its characteristics to an extensive, gently undulating to nearly level lacustrine plain,

elevations in the immediate area range between 120 and 180 m ASL. The surrounding

area is scattered with moderately rolling areas of drumlinized moraine, attributed to

glaciofluvial processes. In large low lying depressions peat landforms such as peat

plateaux, horizontal and patterned fen complexes dominate. On lower slopes gently

sloping thin (<1m) organic bog veneer covers the lacustrine sediments. The occasional

Precambrian rock outcrop also spots the area (Mills et al. 1976).

The Hudson Bay and James Bay Lowlands eco-climatic regions contain the

highest concentration of organic wetlands in Canada (Tarnocai et al. 2000). The

landscape around the southern periphery of Hudson Bay is dominated by over 75%

wetland. The region's high concentration of wetlands are attributed to the high positive

moisture indices, moderate evapotranspiration rates, low decomposition rates and non-

climatic factors such as low lying flat terrain and irregular drainage patterns.

The dominant soil orders in the area are Cryosolic and Organic. The Cryosolic

soils are organic, but affected by permafrost. The dominant organic soil types found in

the Stephens Lake area are Fibrisols and Mesisols (Scott 1996). Upland soils are

dominated by post-glacial and lacustrine deposits. These soils are predominantly

Luvisols. Where mineral soils are affected by saturated conditions Gleysols are also

found.

2.1.3 Vegetation

In the Low Subarctic and High Boreal transition zone near Gillam, Manitoba in

the vicinity of Stephens Lake, peat plateau bogs, polygonal peat plateau bogs, and palsa

bogs are common (Scott 1995). Vegetation of these peat landforms is dominated by an

open tree cover of *Picea mariana* (black spruce) mixed with the low shrub *Ledum groenlandicum* (Labrador Tea) and light-coloured lichens (*Cladonia* spp.). *Sphagnum* spp. and nutrient deficient soils create an inhospitable environment for higher order species (Scott 1995). In addition the landscape is also spotted with collapse scar fen peatland, which support graminoid species such *as Carex* spp (sedge) along with larger shrubs such as *Salix* spp. (willow) and *Myrica gale* (sweet gale) and where conditions permit *Larex lacerina* (tamarack).

The areas surrounding Stephens Lake are characterized by open lichen woodland, dominant tree species black spruce and tamarack in moist peatland areas and *Pinus banksiana* (jack pine) spotted in dry mineral upland areas. A number of deciduous trees thrive in the area including trembling aspen, birch, and willow. Smaller vegetation is dominated by bog and fen associated species, shrubs such as sweet gale, and willow, emergent aquatic species such as *Typha* spp. (cattail), graminoids such as grasses and sedges, some herbaceous species and assorted bryophytes dominated by *Sphagnum* spp..

2.2 PEATLANDS AND PEATLAND DYNAMICS IN RESERVOIRS

2.2.1 An Introduction to Wetlands, Peatlands and Floating Peatlands

The terms *wetland*, *peatland*, and *floating peatland* are used frequently throughout this thesis. They can be thought of as belonging to a hierarchical relationship (Figure 2.2) in which wetlands occupy the broad scale transition zone between open water and upland environments; peatlands, namely bog and fen, are wetland classes; and floating peatlands, a sub-class of peatlands, which form through either natural pathways or anthropogenic management of aquatic systems.
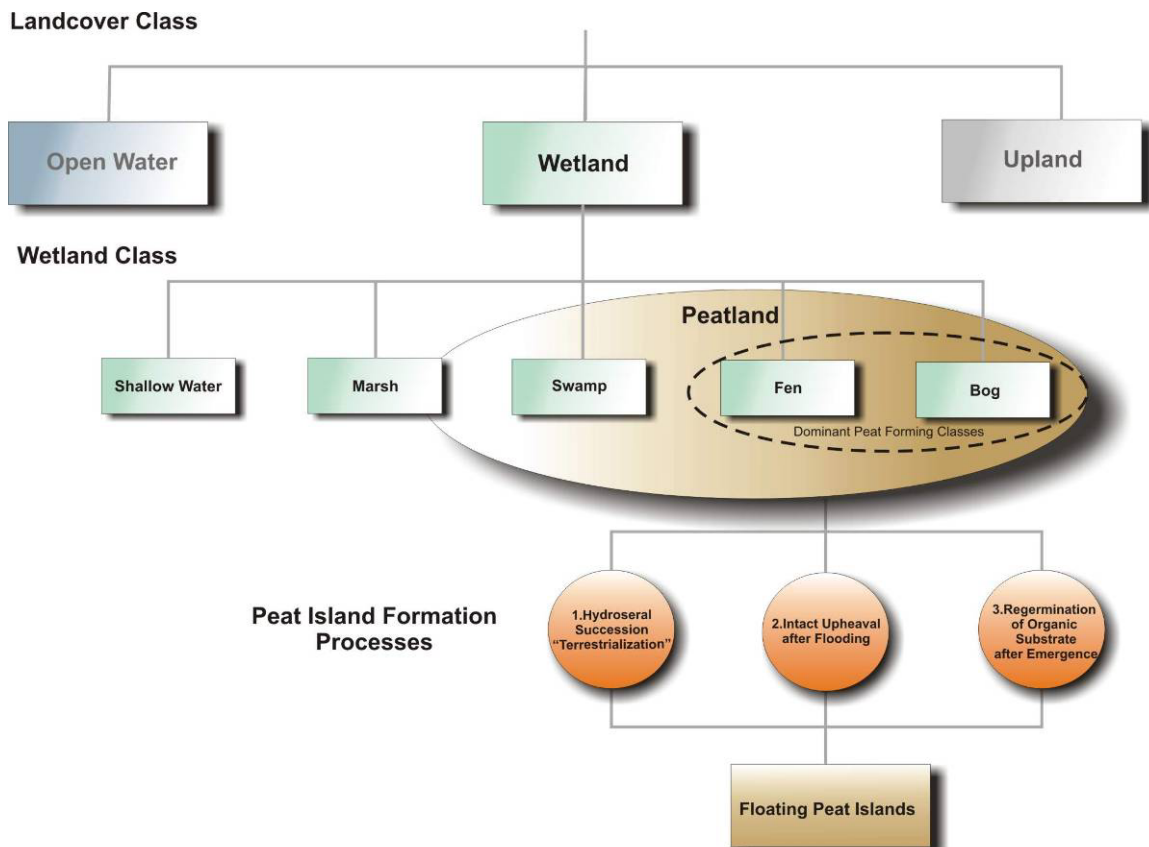
Figure 2.2. Hierarchical diagram of wetland land cover classes, primary peatland classes and pathways to peat island formation.

At first glance, the term *wetland* appears to be self-explanatory; however wetlands are complex, extensive, ecologically important, and globally distributed landforms. Terms such as *moor, schwingmoor, toubieres, muskeg*, *mire*, and *peatland* are synonymous with wetlands, and used around the world to describe some form of them. Because of their great significance, organizations such as the Canadian National Wetlands Working Group (NWWG) have spent many years defining and identifying land which should be classified as wetland. The NWWG provides a definition of wetlands which incorporates its related environment, defining a wetland as land that is saturated with water long enough to promote wetland or aquatic processes as indicated by poorly drained soils, hydrophytic vegetation and various kinds of biological activity which are adapted to a wet environment (National Wetlands Working Group 1997). The NWWG's Canadian Wetland Classification System defines five classes of wetland which include: shallow water, marsh, swamp, bog and fen, which exist along broad minerogenous to ombrogenous environmental gradients.

Peatlands are organic wetlands that contain 40 or more cm of peat, or partially decomposed organic matter, accumulation on which organic soils develop (NWWG 1997). Because of their ability to retain, purify and deliver fresh water, store large amounts of carbon, absorb environmental pollutants and support large numbers of floral and faunal species, of which many are endangered, peatlands have a great global environmental importance (Tarnocai et al. 2000). The geomorphological term peatland is derived from 'peat landform' and refers to biotic landforms that are composed of peat (Charman 2002). Peat is the building block of peat landforms or peatlands. Peat can be broadly classified on a first-order scale as being primarily moss, herbaceous, woody, or

detrital (Charman 2002). Peat is found where the partially decomposed remains of plants and animals or organic debris accumulate, or anywhere net primary production exceeds decomposition (Wieder et al 2006). A water-saturated anoxic environment can promote slow decomposition and accumulation of plant materials including woody parts, leaves, rhizomes, roots, and peat mosses (Rydin and Jeglum 2006). Peatlands are distributed throughout the globe, from warm tropical and sub tropical climates to the cooler boreal, sub-arctic and arctic climatic regions of the world. This research focuses on peatlands of the boreal and subarctic eco-climatic regions of Canada.

A floating peatland is a peatland or portion of a peat landform that remains buoyant in a water body due to its inherent low bulk-density relative to water, and increased gas release associated with increased microbial activity. Peat islands, either floating or anchored, are peatland ecosystems surrounded by open water that have either formed naturally through succession processes or as a result of changes to the environment through natural or anthropogenic flooding. The terms floating peatland and peat island are used interchangeably through out this thesis. Because of their buoyant nature, floating peat islands are in a constant state of change. Peat islands can move through an aquatic system via wind, wave, ice and water currents. Peat islands can fluctuate vertically in the water column as a direct result of natural or managed water level fluctuation or as a result of increased or decreased buoyancy resulting from microbiological productivity and subsequent gas liberation throughout the open water season (Ronka and Uusinoka 1976). The phenomena of floating peatlands or peat islands found in lakes or reservoirs has been documented in the past (Balagurov 1967; Ronka and Uusinoka 1976; Asada et al. 2005).

2.2.2 The Peatland Ecosystem

Peatlands ecosystems are dynamic. Peatland development is dictated by hydrology, climate, nutrient availability, landform, and biology (NWWG 1997; Charman 2002; Vitt 2006). The development and type of peatland can determine its susceptibility to upheaval after flooding. It is therefore important to understand the mechanisms that lead to peatland formation and evolution. This begins with understanding of peatland classification.

2.2.2.1 Peatland Classification

The Canadian Wetland Classification System (NWWG 1997) defines 7 wetland regions according to their similar topography, hydrography, and nutrient regime they include: arctic, subarctic, boreal, prairie, mountain, temperate, and oceanic. Manitoba has subarctic, boreal and prairie wetland regions. In Manitoba, peatlands are generally restricted to the boreal and subarctic wetland regions. Peat accumulation can occur in four out of five of the wetland classes defined by the Canadian Wetland Classification System (NWWG 1997).

Although fen and bog are the primary peat forming classes, it is possible for peat accumulation to occur in marsh and swamp classes (NWWG 1997). Succession between wetland classes is common. For example, a swamp may begin to accumulate peat and quickly transition to a fen environment.

The Canadian Wetland Classification System (NWWG 1997) contains three hierarchical levels, the first being class (open water, marsh, swamp, fen, and bog), followed by form and type. Form is determined according to surface morphology, surface

pattern, water type and morphology of underlying mineral soil. The type level relies on vegetation physiognomy to differentiate between wetland types.

Bogs are peatlands that are raised above the surrounding topography and are virtually unaffected by runoff or groundwater from surrounding mineral soils, thereby creating a nutrient deficient acidic ombrogenous environment. Fens are minerotrophic peatlands, which unlike bogs, have fluctuating water tables and are therefore rich in dissolved minerals. The Canadian Wetland Classification System lists 15 forms and an additional 4 subforms of bog peatland class, are 12 forms and an additional 7 subforms of fen class. Bog classes include: basin bog (situated in basins with no feeder streams), domed bog, palsa bog, and peat plateau bog. The fen classes include: collapse scar fen (formed by collapse due to melted permafrost), feather fen, horizontal fen and riparian fen. Both peatland classes have floating subforms. Floating peat bogs are sufficiently elevated from contact with mineral-rich waters of the water table, pond, lake, stream or river within which they are situated. Floating fens, unlike floating bogs, have a peat surface that is close to the surface of the water body upon which they are floating.

Table 2.1. Summary of primary differences between bog and fen peatland classes as defined by the Canadian Wetland Classification System (National Wetlands Working Group 1997).

Bog	Fen
1) all bogs have an accumulation of peat (at least 40cm)	1) all fens have an accumulation of peat (at least 40 cm);
2) the bog surface is raised or level with the surrounding terrain	2) the surface is level with the water table, and water flow occurs on the surface and through the subsurface
3) the water table is at or slightly below the surface and raised above the surrounding terrain	3) water table fluctuates and may be at or just below the surface
4) ombrogenous (water source is solely from precipitation)	4) minerogenous (water moving through the peatland is rich in nutrients, usually from surrounding mineral soils);
5) contains moderately decomposed *Sphagnum* peat with woody remains of shrubs	5) comprised mainly of decomposed sedge or brown moss peat
6) vegetation is dominated by *Sphagnum* mosses with tree, shrub (ericaceous) or treeless vegetation cover.	6) graminoids (sedges, grasses, reeds) and shrubs characterize the vegetation cover

Swamps, according to the Canadian Wetland Classification (NWWG 1997) can be classed as peatlands, however they are different than bogs and fens in that their vegetation is dominated by trees, shrubs and forbs. The only peatland form of swamp is the raised peatland swamp, which occur as raised plateaus similar to the domed bog form with the exception that they are influenced by mineral groundwater. Other forms of swamp occur in association with peatlands but would not be classes as such. Marshes are even less likely to contain peat accumulations greater than 40 cm. Organic soils may develop in permanently saturated lakeshore or delta marshes and under these conditions floating mats of vegetation form from sedge and aquatic mosses, which is a characteristic of a marsh transitioning to a rich fen. (NWWG 1997).

2.2.2.2 Peatland Structure and Soils

Bog and fen peatland classes have a common profile structure. This includes a living plant layer situated on top of an oxygen deprived slowly decomposing lower layer. Bogs are dominated by a Sphagnum decomposing layer; fen a sedge or graminoid layer; swamp a woody or tree peat layer; and marsh a sedge and aquatic moss layer, prior to transitioning to rich fen. From a hydrological perspective, peatlands are composed of two functional layers (Figure 2.3). The acrotelm (Charman 2002) is the portion of a peatland that remains above the water table; this layer consists of living plant material, such as mosses, graminoids, herbs, shrubs and trees and is generally rich in oxygen. Its thickness usually varies between 30 and 50cm (Quinty and Rochefort 2003). The catotelm is the portion of the peatland that remains permanently below the lowest position of the water table. It is an anaerobic environment where slow decomposition processes take place, it contains the decomposing peat (Charman 2002; Rydin and Jeglum 2006). In a floating peat island the acrotelm and catotelm fluctuate as the depth to the water table fluctuates according to the buoyancy of the floating peat island (Fechner-Levy and Hemond 1996).The internal hydrology of a peatland has a direct link with the slow decomposition rates and therefore soil development within the soil profile. The unique characteristics of peatland soil types are discussed below.
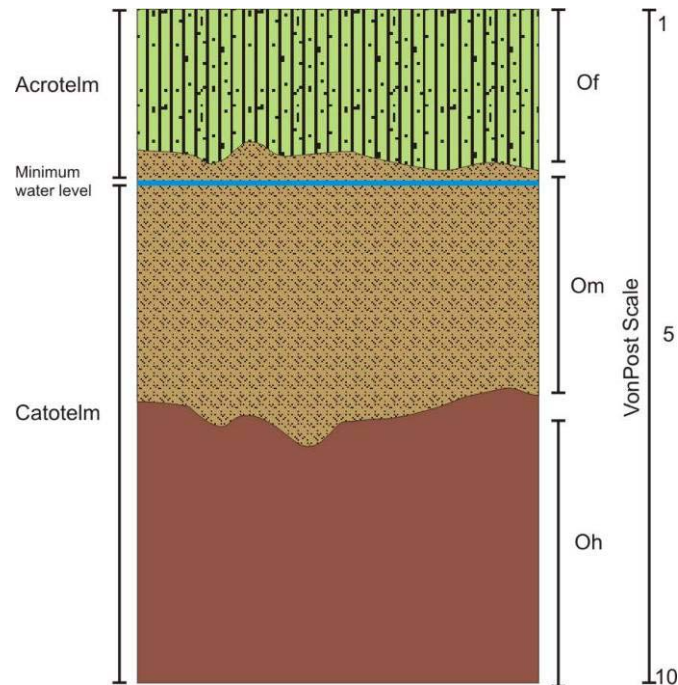
Figure 2.3. Typical peatland soil profile, showing the acrotelm and catotelm in relation to the water table, and the von Post scale in relation to the fibrisol (Of), mesisol (Om), and humisol (Oh) soil layers.

The Canadian System of Soil Classification (Agriculture and Agri-Food Canada 1998) identifies three soil orders that are associated with wetlands in Canada. These three soil orders include Organics, Cryosols and Gleysols. The Organic order contains Fibrisol, Meisisol, Humisol and Folisol great groups. According to the Canadian System of Soil Classification (Agriculture and Agri-Food Canada 1998), a soil is considered to be of the Organic order if it has greater than 30 % organic matter, although typically peatlands with large peat accumulations have between 80 and 90 % organic matter (Rydin and Jeglum 2006).

The first three organic soil great groups are associated with peatland development and are classed according to their level of decomposition, the forth organic great group (Folisol) is typically found in the under storey upland forest. Fibrisols (Of) are relatively non-decomposed soils, Mesisols (Om) are moderately decomposed soils and Humisols

(Oh) are heavily decomposed organic soils (Agriculture and Agri-Food Canada 1998). Organic soil order can be determined in the field by using the von Post scale (Von Post 1924). Well humified organic soils would be ranked closer to 10, with 10 being completely decomposed, unrecognizable material that escapes through the fingers when squished in the hand, indicative of a Humisol (Oh) (von Post 7-10). A von Post class of 1 indicates a relatively non-decomposed organic soil with intact plant material, the sample excretes a clear water with a yellow-brown tinge, indicative of a Fibrisol (Of) (vonPost 1-5) Mesisols (Om) are usually classified as being 5 or 6 on the von Post scale of decomposition. The degree of humification within a peat or organic soil profile is important in determining whether or not a peatland will become detached from its parent material when inundated by water, resulting in a floating peat island. The type of peat material or organic soil within the profile is dictated directly from the type of vegetation that is growing above it, a bog will likely be dominated by peat moss soils, while a rich fen would likely be primarily composed of peat sedge and roots, with only small amounts of peat moss.

Cryosolic soils are soils that are affected by permafrost. Cryosols can be either mineral or organic in nature. Organic cryosols dominate low lying areas of the subarctic and extend into high boreal regions. The process of cryoturbation, soil movement due to frost action, helps shape the peatland landscape and can result in hummocks, palsas, collapse scars, non-sorted nets, circles and polygons (Agriculture and Agri-Food Canada 1998).

The third soil order that is sometimes associated with peatland development are Gleysols, which occupy the transition between poorly drained organic soils and more

well drained upland mineral soil orders. The organic layer associated with a Peaty-phase Gleysol profile can accumulate to 40-60 cm before it needs to be reclassified as an organic or peatland soil (Scott 1995).

2.2.2.3 Peatland Flora

The vegetative composition of peatlands is dictated by a number of environmental gradients that include: water availability, water chemistry, nutrient availability and acidity. Plant species have developed to be competitive in the fen and bog environments. Nutrient rich fens tend to have the highest plant diversity, while nutrient poor fens tend to lack greater plant diversity, and bogs contain the lowest plant diversity (Rydin and Jeglum 2006).

Peatlands are composed of bryophytes, graminoids, herbs, aquatic vascular plants, shrubs and trees (Rydin and Jeglum 2006). Bryophytes include peat mosses (*Sphagnum*), brown mosses, liverworts, and feathermosses. The most common bryophyte species in peatland environments is *Sphagnum* spp., which is dominant in ombrotrophic bogs and often plays a secondary role in minerotrophic fens. Graminoid species in peatlands may include grasses, sedges, and rushes. Graminoid species such as *Carex* spp. often dominate rich fen peatlands, but are less diverse in *Sphagnum* dominated peatlands. The microtopography and position of the water table of a peatland also influences the vegetation that will grow. Hummocks will support shrub growth, and be dominated by *Sphagnum* species such as *Sphagnum fuscum* and *Sphagnum rubellum* while hollows and lawns will be dominated by hydrophytic species such as graminoids and have some loose colonies of *Sphagnum fallax* and *Sphagnum angustifolium* (Quinty and Rochefort 2003).

21

Various species of herbs can be found in rich fen communities but are more likely to be less abundant in bogs. Aquatic vascular plants including emergents such as *Typha* spp. (cattail) can be found along the edges of floating peat mats. Shrubs such as *Myrica gale* (sweet gale)*, Andromeda polifolia* (dwarf bog rosemary)*, Vaccinium oxycoccus* (small bog cranberry)*,* and *Salix spp.* (willow) are common among bogs in North America. Trees associated with peatlands in northern Manitoba are restricted to just a couple of species including: *Picea mariana* (black spruce), *Larix laricina* (tamarack), and to a lesser extent *Picea glauca* (white spruce) closer to upland areas. Table 2.2 lists a number of common peatland and peat island species that were encountered during surveys for this project.

Table 2.2. Species of vegetation commonly associated with peatlands and peat islands in the Stephens Lake study area.

Type	Family	Species	Common Name
Trees			
	Pinaceae	*Picea mariana*	Black Spruce
Shrubs			
	Salicaceae	*Salix spp.*	Willow
	Myricaceae	*Myrica gale*	Sweet gale
	Ericaceae	*Andromeda polifolia*	Dwarf bog rosemary
	Ericaceae	*Ledum groenlandicum*	Labrador tea
	Ericaceae	*Vaccinium oxycoccus*	Small bog cranberry
Graminoids			
	Cyperaceae	*Carex aquatilis*	Water sedge
	Cyperaceae	*Carex magellanica*	Few-flowered sedge
	Poaceae	*Calamagrostis canadensis*	Blue-joint grass
Aquatic Plants			
	Typhaceae	*Typha latifolia*	Common cattail
Herbs			
	Droseraceae	*Drosera rotundifolia*	Round-leaved sundew
	Rosaceae	*Potentilla palustris*	Marsh Cinquefoil (Five-finger)
Mosses			
	Sphagnaceae	*Sphagnum wulfianum*	Wulf's peat moss
	Sphagnaceae	*Sphagnum fuscum*	Common brown peat moss
	Sphagnaceae	*Sphagnum angustifolium*	Poor -fen peat moss
	Bracytheciaceae	*Tomenthypnum nitens*	Golden fuzzy fen moss
Lichens			
	Cladoniaceae	*Cladina rangiferina*	Reindeer lichen

In the Low Subarctic and High Boreal transition zone near Gillam, Manitoba in the vicinity of Stephens Lake, peat plateau bogs, polygonal peat plateau bogs, and palsa bogs are common (Scott 1995). Vegetation in these peat landforms is dominated by an open tree cover of *Picea mariana* (black spruce) mixed with the low shrub *Ledum groenlandicum* and light-coloured lichens. *Sphagnum* and nutrient deficient soils create an inhospitable environment for higher species (Scott 1995). The landscape is also

spotted with collapse scar fen peatland, which support graminoid species such as *Carex spp.* along with larger shrubs such as *Salix spp.* and *Myrica gale* and where conditions permit *Larex lacerina* (tamarack).

Of all the plant species in a peatland community the *Sphagnum* mosses are the most significant. Rydin and Jeglum (2006) identify the key features of *Sphagnum* spp. that make it important in the development of peatlands. Firstly, *Sphagnum* creates an environment that is acidic, nutrient poor, wet, and anoxic. Secondly it tolerates and requires low concentrations of nutrients and minerals. Third, it is naturally resistant to decay. And lastly, there are a number of species that specialize in different parts of the peatland gradient. Different groups of *Sphagnum* species are adapted to varying hydrological conditions. Quinty and Rochefort (2003) describe *Sphagnum* species of the *Acutifolia* group as being adapted to drier conditions and can be found on hummocks and peat plateaus, these include *Sphagnum fuscum* and *Sphagnum rubellum*. Species belonging to the *Cuspidata* group are not well adapted to retain water and can therefore be found growing in loose colonies in the lawns and hollows of a peatland, and include *Sphagnum fallax* and *Sphagnum angustifolium*.

2.2.2.4 Peatland Fauna

Boreal and subarctic peatlands are home to a wide variety of organisms. Beginning with methanogenic bacteria, and up to large foraging mammals such as moose, peatlands provide a healthy and diverse habitat. As with floral species, there are certain limiting factors that control species richness and abundance for a number of taxanomic groups. The amount of open space, density of forest cover, nutrient availability and

acidity (bog or fen), presence of pools and soil drainage are all factors that effect

populations of amphibians, reptiles, birds and arthropods (Desrochers and van Duinen

2006). Some organisms have a direct role in the formation, growth and alteration of the

peatland while others use it as a home and feeding ground. Table 2.3 summarizes some of

the organisms commonly found in northern peatlands.

Table 2.3. Species of bacteria and animals commonly associated with peatlands.

Organism Group	Taxonomy	Common Name	Organism Group	Taxonomy	Common Name
Bacteria[1]	Achromobacter	-	Amphibians[2]	*Bufo americanus*	American toad
	Actinomyces	-		*Hyla versicolor*	eastern gray tree frog
	Bacillus	-		*Plethodon cinereus*	red-backed salamander
	Chromobacerium	-		*Pseudacris crucifer*	northern spring peeper
	Clostridium	-		*Pseudacris triseriata*	western chorus frog
	Cytophaga	-		*Rana clamitans*	green frog
	Micrococcus	-		*Rana pipiens*	leopard frog
	Micromonospora	-		*Rana septrentrionalis*	mink frog
	Mycobacterium	-		*Rana sylvatica*	wood frog
	Nocardia	-			
	Pseudomonas	-	Birds[2]	*Geothlypis trichas*	common yellowthroat
	Streptomyces	-		*Melospiza lincolnii*	Lincoln's sparrow
				Passerculus sandwichensis	savannah sparrow
Invertebrates[2]	Coleoptera	beetles		Zonotrichia albicollis	white-throated sparrow
	Ciliates	-			
	Cladocerans	water fleas	Mammals[2]	*Alces alces*	moose
	Diptera	flies		*Castor canadensis*	beaver
	Hymenoptera	wasps, bees, etc.		*Clethrionomys* sp.	voles
	Lepidoptera	moths, butterflies		*Lynx* sp.	lynx
	Rhizopods	-		*Odocoileus virginianus*	deer
	Rhyncota	-		*Ondatra* sp.	muskrat
	Rotifers	-		*Sorex* sp.	shrews
				Synaptomys sp.	lemmings
Reptiles[2]	*Opheodrys* sp.	green snakes		*Ursus americanus*	black bear
	Thamnophis sp.	garter snakes			

1. From Rydin and Jeglum (2006).
2. From Desrochers and van Duinen (2006)

Bacteria are perhaps one of the most important peatland organisms. Because

bacteria populations are generally small in peatland environments relative to other

environments, decomposition rates are slow allowing the characteristic peat layers to

accumulate. Certain forms of bacteria (Table 2.3) present in a peatland will feed off of

organic material, breaking down the organic carbon of plant material to dissolved organic

carbon (DOC), methane (CH_4) in anaerobic environments, and carbon dioxide (CO_2) in

aerobic environments (Moore and Basiliko 2006).

Invertebrate communities are specious in boreal and subarctic peatlands. Peatland pools, despite their low pH, tend to have a rich invertebrate diversity; as such most invertebrate studies have focused on the open pools within the peatland (Rosenberg et al. 1987). High proportions of peatland invertebrate species are adapted to the unique peatland environment, and are considered to be specialists (Table 2.3). Other species are more generalist and can be found in other habitats in addition to peatland environments. (Desrochers and van Duinen 2006).

Amphibians, due of the osmotic exchanges that occur through their skin, are highly vulnerable to the biogeochemistry of their environment (Desrochers and van Duinen 2006). The low pH acidic environment of a raised bog would therefore not normally be conducive to productive amphibian habitat. There are, however, a number of species that are commonly found in boreal bog and peatland pool environments, due mainly to the presence of the rich invertebrate populations acting as an important food source. Lizard species are not commonly found in northern peatlands. Surveys of Canadian peatlands have revealed small populations of garter snakes and green snakes in the southeastern boreal regions, however very little quantitative data exists for lizard species (Desrochers and van Duinen 2006).

Birds are very abundant in peatlands. Although some birds may specifically choose nesting areas in a peatland, their occurrence in peatlands usually arises out of secondary dependence on invertebrate food sources or some other habitat requirement (Charman 2002). There are no known bird species that are found exclusively in peatlands (Desrochers and van Duinen 2006). Table 2.3 lists a few species that frequent boreal and subarctic peatlands.

Peatland mammals range from small voles and mice up to large species such as moose and black bear (Table 2.3). Beavers (*Castor canadensis*) have the ability to alter the peat landscape via the construction of dams and subsequent flooding (Mitchell & Niering 1993). When bog environments are flooded, the hydrology (water table), nutrient availability, and pH are altered in effect changing the vegetation communities that are able to live in the new conditions. These sorts of changes are discussed in greater detail in the section dealing with the formation of floating peat islands. Floating peat islands are known to be important primary habitat for muskrats (*Ondatra zibethicus*). Muskrat peat island usage was found to increase in low water years when mainland shore zones are exposed, while the floating peat island moves vertically with water level fluctuation (Manitoba Hydro and NCN 2003).

2.2.2.5 Peatland Formation and Distribution in Manitoba

Peatlands are unique environments that form over thousands of years. The vast expanses of boreal and subarctic peatlands that currently occupy the North American and Eurasian landmasses developed almost exclusively since the last glacial maximum (Kuhry and Turunen 2006). The current peat landscape in northeastern Manitoba is directly linked to the Wisconsinan Glaciation of the Pleistocene epoch (75000 – 8000 years B.P.) (Corkery 1996). In northern Manitoba's high boreal and low subarctic post-glacial landscape factors such as cool temperatures, low to moderate evapotranspiration rates, anoxic conditions, functionally limited decomposer communities, and litter and organic matter substrates that are naturally slow to decompose create an environment that is conducive to the development of peat (Moore and Basiliko 2006). Given these

prevailing physical and environmental conditions there are three main pathways to peatland formation commonly discussed in the literature. These pathways include primary peat formation, paludification, and terrestrialization, otherwise known as infilling or hydroseral succession (Rydin and Jeglum 2006; Vitt 2006).

Primary peat formation occurs directly on recently exposed wet mineral soil that has not experienced a drier period (Rydin and Jeglum 2006; Vitt 2006). This is the case for areas that have recently been exposed due to glacial retreat and subsequent 'isostatic rebound'. A glacier up to 3 km thick over Hudson Bay, caused a depression of the earth's crust by as much as 1000 m (Corkery 1996). As the glacier receded Hudson Bay and northeastern Manitoba began to rise and still rises today at a rate of 70 cm/century (Corkery 1996).

Further to the glacial recession and subsequent isostatic rebound, Manitoba's landscape was influenced by erosion of the Precambrian shield and limestone of the Hudson Bay Lowlands, deposition of glaciofluvial and glaciolacustrine till and sediments across the flat landscape, and large glacial lakes which deposited rich mineral sediments, which also resulted in an irregular drainage system of swamps, lakes and streams (Corkery 1996). The Hudson Bay Lowlands are dominated by fen peatland as a result of the combined influence of the carbonate-rich glacial deposits on groundwater and the lack of time since isostatic emergence from Hudson Bay, some low-lying fen areas close to the shores of the bay have only initiated in the last 1000 years (Scott 1995). The development of the subarctic peatlands of the Hudson Bay Lowlands would have been most rapid during the Holocene climatic optimum (~ 9000 – 5000 years BP) when climatic conditions would have been more like present day boreal conditions (Kuhry &

Turunen 2006). Peatland formation in the subarctic has since slowed due to cooler prevailing climatic conditions following the warm period. Primary peat formation can also occur on: fresh deposits such as dune sacks, alluvial plains, deltas, and volcanic deposits; open pit mines, gravel pits and quarries, mine spoils, and human created mineral surfaces (Rydin and Jeglum 2006).

Paludification, the most common of the three processes, is similar to primary peat formation except that in this process peat initiation occurs on top of previously drier, vegetated habitats over inorganic soils in the absence of a body of water (Vitt 2006). During this process there is an upward accretion of peat caused by a water table which rises sufficiently to be above the immediate influence of surrounding base-rich groundwater, and an outward accretion of peat over fen or previously dry land (Scott 1995). Therefore this can also be considered a succession process whereby land once occupied by fen peatland is transformed to a proto-bog and then eventually an ombrotrophic bog environment. This is evident further inland from Hudson Bay where exogenous paludification has allowed upward and outward accretion of bog over top of older mesotrophic fen, replacing ericaceous shrubs, mesotrophic sedges and mosses, and scattered white spruce with oligotrophic species such as peat moss, Labrador tea, tamarck, and black spruce (Scott 1995). Counter to paludification is the process of depaludification, whereby the peatland self-regulates and undergoes senescence, growth balances out and sometimes results in negative production , in the form of reversion back to a forest phase (Scott 1995).

The third peat formation pathway can be described as infilling, terrestrialization, or hydroseral succession. This process occurs in shallow bodies of water, which may

gradually be filled in by surrounding riparian vegetation, thereby terrestrializing the former aquatic habitat (Vitt 2006). In the Canadian Wetland Classification (NWWG 1997) this formation pathway is associated with the floating subforms of riparian bog (floating bog) and fen (floating fen). These peat mats may be floating or grounded to the base of the shallow water body.

As a result of these unique landscape, hydrologic and climatic conditions, Manitoba contains the highest percentage of wetland (41%) and peatland (38%) cover by total area compared to the rest of the Canadian provinces (Figure 2.4). The highest densities of peatlands in Canada are found adjacent to the Hudson Bay in the Hudson Bay and James Bay Lowlands. In these areas peatland land cover is greater than 50 % and in some areas above 75 %. Canada's land cover is comprised of 12% peatland, and is considered to be the largest area of peatlands in the world, comprising almost one quarter of the world's total (Tarnocai et al. 2000; Scott 1995). Boreal and subarctic peatlands make up to 97 % of the total peatland area in Canada (Tarnocai 2006).

Canadian Peatland Distribution

% of Land Cover
- 0 - 1
- >1 - 25
- >25 - 50
- >50 - 75
- >75 - 100

0 250 500 1,000 1,500 2,000 2,500 Kilometres

Province or territory	Wetland Area		Peatland Area	
	ha x 10^3	% of land area	ha x 10^3	% of land area
Alberta	13704	21	12673	20
British Columbia	3120	3	1289	1
Manitoba	22470	41	20664	38
New Brunswick	544	8	120	2
Newfoundland-Labrador	6792	18	6429	17
Northwest Territory	27794	9	25111	8
Nova Scotia	177	3	158	3
Ontario	29241	33	22555	25
Prince Edward Island	9	1	8	1
Quebec	12151	9	11713	9
Saskatchewan	9687	17	9309	16
Yukon Territory	1510	3	1298	3
Canada	127199	14	111327	12

Figure 2.4. Peatland concentration and distribution map (top) and provincial wetland and peatland area summary (Scott 1995) (bottom). (Spatial data source: Tarnocai, C. et al. 2002, Peatlands of Canada Database).

2.2.3 Peatland Change and Hydroelectric Development

Peatlands have a dynamic nature, they are constantly undergoing internal changes. They can respond rapidly or over long periods to changes in climate, changes in hydrology, forest fires, and animal and human activity. In the literature these changes are referred to autogenic and allogenic changes (Scott 1995; Charman 2002; Kuhry and Turunen 2006).

Autogenic change refers to internal changes that occur to a peatland as a result of natural ecosystem processes, whereas allogenic change occurs as a result of external factors (Charman 2002). These two processes interact with each other, in that allogenic influences may bring about autogenic changes. This thesis focuses on the external factors that bring about change. More specifically changes brought about by flooding of peatlands and subsequent changes due to the construction and operation of hydroelectric generating facilities.

A change in the hydrology of a peatland as a result of flooding leads to changes in nutrient status and pH and a change in vegetation cover, which is an example of allogenic anthropogenic change resulting in autogenic changes within the peatland. Flooding of peatlands due to hydroelectric dam construction and subsequent flooding is known to result in peatland upheaval, transport, and disintegration over time (Ronka and Uusinoka 1976; Dryade 1984; Belanger et al. 1991; Robert 2000; Manitoba Hydro and NCN 2003; KHLP 2010).

In the past few decades hydroelectric development in Canada has moved from the populated south to the unpopulated north (Rosenberg et al. 1997). Take for example the case of Manitoba where early hydroelectric development occurred exclusively on the

Winnipeg River relatively close to the capital region and now current and future

development is now concentrated on the remote lower Nelson River, which flows

through the boreal and subarctic peatlands of northeastern Manitoba.

Hydroelectric developments that use storage reservoirs (peaking type plant),

rather than run of the river designs, tend to have greater effects on the surrounding

aquatic and terrestrial environment due to increased flooding of the surrounding

landscape. In the formation of a peatland reservoir water first inundates the landscape. If

certain factors are present, the upper layer of a peatland can detach from the lower

organic soil layers and float to the surface of the newly formed reservoir, creating

floating peatlands in which buoyancy is aided by methanogenic bacterial gas liberation

and the low bulk density of the peat.

2.2.4 Floating Peatlands

Floating peatlands have been documented for some time, Lewis and Dowding

(1926) described the vegetative composition of surviving muskeg islands, after

inundation in a calcareous central Alberta lake occupying a basin of primarily

decomposed peat. Riparian forms of floating bog and fen peatland may form naturally

along lake, reservoir and river shorelines, as an initial stage in the process of

terrestrialization are described by the Canadian Wetland Classification (NWWG 1997). A

number of studies describe peat island formation after beaver dam construction in

peatland environments (;Mitchell & Niering 1993; Weyhenmeyer 1999).

Much of the earlier peer reviewed literature describing peatland upheaval and

floating peat islands in reservoirs comes out of Finland, Sweden and Russia from various

studies conducted in the late 1960s and 1970s (Balagurov 1967; Ivanov 1971; Ronka and Uusinoka 1976). In Canada, a number of consultant report studies commissioned by Hydro Quebec detail peatland disintegration, upheaval and floating peat islands in the hydroelectric reservoirs of Eastmain 1, La Grande 1, and Cabonga (Grondin and Ouzilleau 1980; Le Groupe Dryade 1984; Belanger et al. 1991; Robert 2000). Peatland and shoreline erosion and flooding associated with the Churchill River Diversion (CRD) and subsequent flooding of Southern Indian Lake and the Rat/Burntwood River System have been described (Beke 1975; MB Hydro and NCN 2003). Currently, Manitoba Hydro is conducting environmental studies that predict the effects of peatland disintegration related to hydroelectric development over time (KHLP 2010).

2.2.4.1 Pathways to Floating Peatland Formation

There are three common 'process pathways' to floating peatland formation. The first pathway, terrestrialization, also referred to as hydroseral succession (NWWG 1997; Somodi and Botta-Dukat 2004), is a process whereby riparian fen and bog peat grows laterally to form floating peat peninsulas. These peatlands form next to ponds or lakes extending outwards from the shore. In a reservoir, these floating peat mats may become detached from the shore as a result of wind, wave or current action, allowing them to migrate and move throughout the reservoir. The surfaces of peat mats, which often extend 0.5 m above the surface of the lake, are comprised of the roots of intertwined graminoids, (grasses, sedges and rushes) and other vegetation. The floating fens' buoyancy can be assisted by trapped methane in the submerged portion of the lake (NWWG 1997).

In the second peat island formation pathway, non-vegetated organic substrates become delaminated from deeper mineral sediments and float to the surface as a result of seasonal water fluctuations. These dead organic substrates may contain viable rhizomes, which may germinate shortly thereafter. (Clark and Reddy 1998; Somodi and Botta-Dukat 2004). The floating organic substrate eventually becomes vegetated and forms a floating peat mat.

The third pathway to peatland formation is the upheaval of intact peat mats shortly after artificial or natural flooding of a peatland. The inundation of peatlands due to increase in lake or river water levels can often result in detachment or rupture and upheaval of the upper fibric layer of the inundated peatland. These floating peatlands may persist relatively untouched, rapidly degrade, have seasonal vertical fluctuations, or migrate throughout the reservoir. There are number of studies that discuss the factors that lead to the formation of floating peatlands via this pathway (Ronka and Uusinoka 1976; Ouzilleau 1977; Le Groupe Dryade 1984; Hogg & Wein 1988; Belanger et al. 1991; Fechner-Levy & Hemond 1996; Robert 2000; St.Louis et al. 2004; KHLP 2010)

2.2.4.2 Peatland Upheaval

The flooding of peatlands can result in peat upheaval and the creation of floating peat islands (Figure 2.5), their subsequent translocation and eventual disintegration due to reservoir forces. A number of factors determine whether or not a flooded peatland will become a floating peat island. Other determining factors will determine how long a floating peat island will remain intact and in place. A number of studies have been conducted that document the upheaval of peatlands after the creation of hydroelectric

reservoirs (Ronka & Uusinoka 1976; Hogg & Wein 1988; Fechner-Levy & Hemond 1996); Ouzilleau 1977; Le Groupe Dryade 1984; Belanger et al. 1991;Robert 2000;St.Louis et al. 2004; KHLP 2010). These studies identify the various processes and factors that determine peatland upheaval and peat island evolution after flooding.

Figure 2.5. Photograph of a peat island formation in O'Neil Bay at Stephens Lake, Manitoba (photo credit: P.Cooley 2006)

The process of peatland upheaval is summarized in four general processes or requirements (Figure 2.6). These include:

1) Shallow flooding of a peatland (< 6 m). If flooding is greater than 6 metres, the low density of the fibric portion of the peatland and microbiological gas build up may not be able to overcome the resulting hydrostatic pressure of the flood waters;

2) The thickness of the upper fibric (Of) horizon, it's bulk density relative to the flood waters, the amount of *Sphagnum* present, and the degree of decomposition

in the profile are all considered important factors in peat uplift. During initial

flooding, some peatlands will rupture and detach immediately from their meisic to

humic organic soil parent material and float to the surface;

 3) Increased gas build up. A result of increased microbial activity after

inundation, an increase in methane (CH_4) aids in peat uplift and buoyancy;

 4) Rupture or detachment from parent material. If the low bulk density of the

fibric (Of) peat horizon and increased gas ebullition is enough to overcome the

hydrostatic pressure of the flood water the fibric peat layer will rupture and detach

from the underlying meisic (Om) and humic (Oh) peat horizons and float to the

surface.
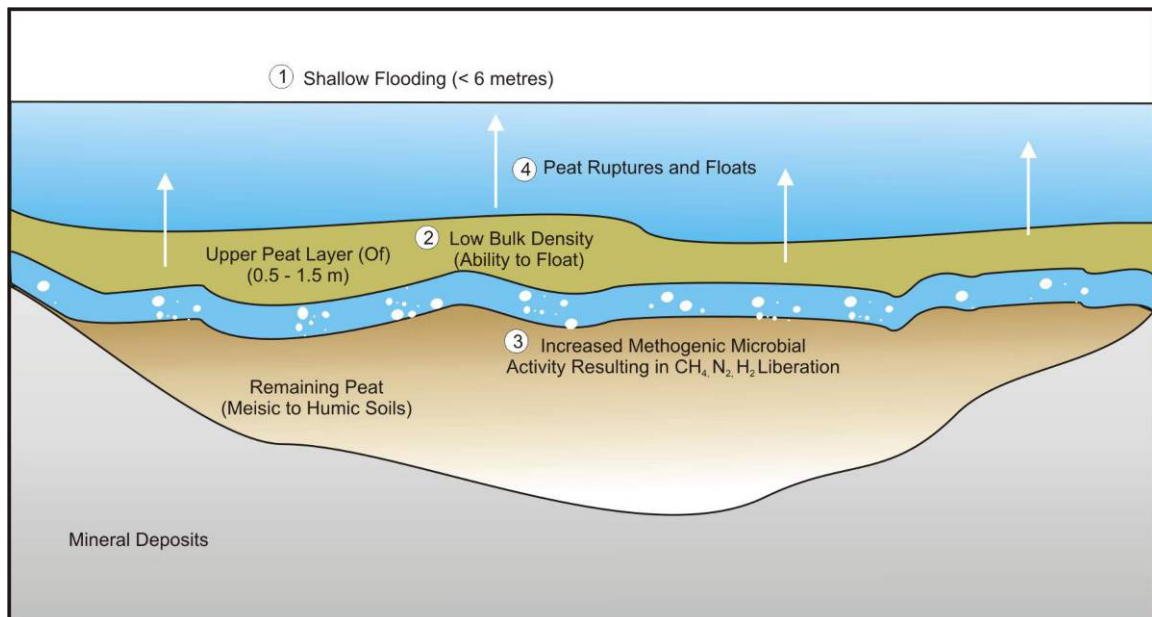
Figure 2.6. The generalized process of peat upheaval after flooding of a peatland.

As stated above, the depth to which a peatland is flooded is an important

determining factor in peat upheaval. Studies have shown (Robert 2000; KHLP 2010) that

when a peatland is flooded at a depth greater than 6 m, the low density of the peatland

and the build up of microbiological gas is unable to overcome the force of hydrostatic and atmospheric pressure. This would also be dependent on the rate at which the reservoir was filled. Most peatlands experience upheaval as the reservoir is initially flooded (Ronka & Uusinoka 1976; Ouzilleau 1977; Le Groupe Dryade 1984; Belanger et al. 1991; Robert 2000; KHLP 2010). Therefore, peatlands that do not surface immediately after flooding are unlikely to float to the surface when the water column over top of them is greater than 6 m, implying that most secondary upheaval occurs in the shallow areas of the newly formed reservoir. One study has predicted 80 % of upheaval to occur in shallow water that is less than 2 m in depth (KHLP 2010).

The physical characteristics of the fibric (Of) peat horizon are an important consideration in peat uplift dynamics. The thickness of the Of horizon, the degree of decomposition within the peat profile, the bulk density of the Of horizon, and the presence of *Sphagnum* species all play an important role in peat uplift.

According to a study of a Quebec hydroelectric reservoir the thickness of the fibric soil layer of the peatland is considered to be the most important factor in upheaval potential of peatlands, as a thick cohesive Of horizon will limit the roots getting caught on denser lower peat horizons (Belanger et al. 1991). In a study at Stephens Lake it was found that approximately 94% of floating peatlands were comprised of fibric peat (KHLP 2010). The thickness of floating peat islands is variable. Robert (2000) stated that studies have shown floating peat islands to have an average thickness of 1 m and can range in thickness from 0.7m to 1.6 m. Median floating peat thickness in Kettle Reservoir was found to be 90 cm (KHLP 2010).

The degree of decomposition within the peat profile is considered to be the second most important characteristic of a peatland that determines probability of upheaval (Belanger et al. 1991; Robert 2000). When the degree of decomposition of the peatland is greater than 3 on the von Post scale, it will not float (Belanger et al. 1991). The degree of decomposition in lower peat layers therefore determines where the fibric upper layer of the peatland will incur a horizontal rupture and float to the reservoir surface (Ronka & Uusinoka 1976).

Density is considered to be the third most important peatland characteristic leading to potential upheaval (Belanger et al. 1991; Robert 2000). The bulk density of the upper fibric layers of a peatland is typically lower than that of water, thereby allowing peat to float. Hogg and Wein (1988) identify density as being one of two major mechanisms responsible for the floatation of peat mats.

The presence of *Sphagnum spp.* increases the buoyancy of the island, and promotes detachment of the fibric peat profile from lower layers due to weak cohesion of the Sphagnum stems and leaves (Belanger et al. 1991). However, it is possible for peat composed of other vegetation types to float.

Increased gas release resulting from increased microbiological activity after initial inundation of a peatland is important to the peatland upheaval process, and peat buoyancy. The 'marsh gas' produced during anaerobic decomposition aids in initial rupture and upheaval of the floating peat island from its parent peatland. The primary gases that constitute 'marsh gas' are methane (CH_4) , nitrogen (N_2), and hydrogen (H_2), at a proportion of 70%, 20%, 10%, respectively (Ronka & Uusinoka 1976). Hogg and Wein (1988) consider the production of bubbles from a CH_4 nucleus by anaerobic

decomposition and bubble entrapment within the mat one of two major mechanisms

causing the floatation of peat mats after wetland inundation. Fechner-Levy and Hemond

(1996) reported that this bubbling of methane, or ebullition, is the primary mode of CH_4

transport in many anaerobic environments created after flooding. Methanogenic bacteria

present in peatlands favor the anoxic environment created after flooding, which removes

the zone of oxidation usually present in an undisturbed wetland and creates an

environment that has a warmer temperature, resulting in increased microbial activity and

subsequent increases in levels of relatively insoluble CH_4 eventually causing sections of

the peatland to float to the surface as it bubbles (St.Louis et al. 2003).

Most peatland upheaval occurs within the first year or so after flooding (Robert

2000; KHLP 2010). Peat that does not float during initial flooding will typically surface

within the first year if its bulk density is low enough, a sufficient volume of gas builds

up, and flooding is not greater than 6 m. Upheaval can still occur years after initial

flooding, but these islands will not have a living vegetation cover (Robert 2000; Asada et

al. 2005). One study predicts that after 10 years of hydroelectric operation after initial

filling of a peatland reservoir, peat resurfacing will essentially cease (KHLP 2010).

2.2.4.3 Peat Transport, Disintegration and Reservoir Expansion

Peat upheaval, transport, and disintegration in a hydroelectric reservoir is a

dynamic ongoing process. After a peatland has surfaced following inundation, certain

characteristics will dictate how long it will remain resistant to disintegration, and whether

or not it will migrate throughout the reservoir (Figure 2.7a). Not all uplifted peat can be

described as a free floating island. Some floating peatlands will remain attached to

shorezone peatlands, forming floating peat peninsulas. Some peat islands will be floating but remain attached to their underlying parent material because of roots, or permafrost (Figure 2.7b). Other peat islands will initially float but then sink due to a lack of buoyancy. And yet other floating peat islands will remain intact and move throughout the reservoir like rafts, pushed by wind, waves, and water currents. Adjacent shoreline peatlands that are not initially susceptible to floatation due to reservoir flooding may, over time, break down contributing to overall reservoir expansion (Figure 2.7c).
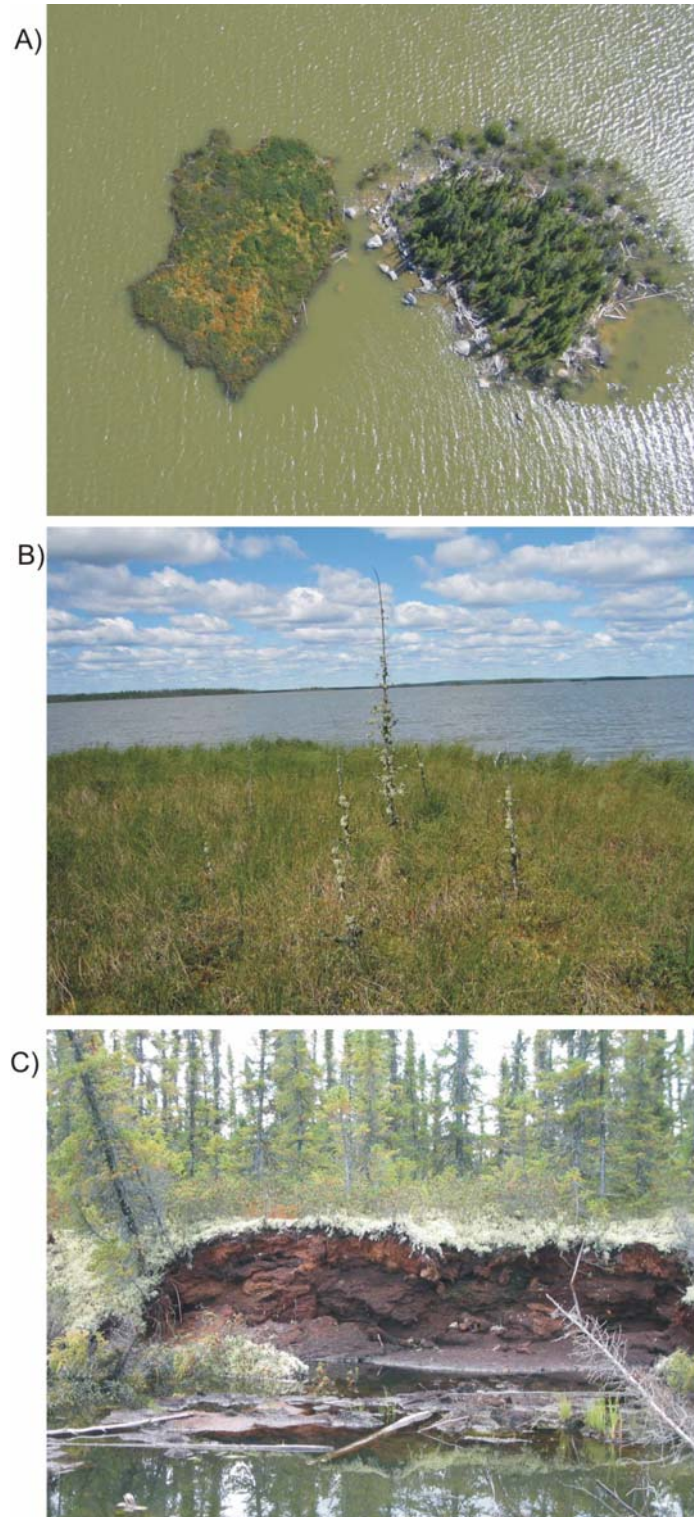
Figure 2.7. Examples of dynamic peatland processes showing A) A sweet gale dominated floating peat island lodged against a black spruce mineral island (transport); B) a sedge dominated peat island with black spruce remnants; and c) shoreline peatland disintegration underway.(Photo Credit: J.Larter 2006)

In general, studies have found that little time is required for peatland upheaval after initial flooding of the peatland, peat island structure and vegetation can change over time, certain islands appear to more resilient to degradation and retain their size and shape over time, and peat islands are capable of migration over long distances (Ouzilleau 1977; Grondin and Ouzilleau 1980; KHLP 2010). Floating peatland movement is affected by many factors such as location, wave energy, current as well as wind direction, frequency and strength field observations have shown they can move several km or more within a few days based on these criteria (KHLP 2010). The smaller the island is and the presence of water ponds seems to favor rapid disintegration, whereas larger islands tend to be impervious to changes in shape and size (Ouzilleau 1977). Islands that are treed and discontinuous in structure will tend to have a life span of less than 5 years before fragmentation and breakdown, where as islands without trees and uniform structure will remain intact for more than 5 years (Grondin and Ouzilleau 1980). Peat islands that remain intact over extended periods tend to be concentrated in back bays and between mineral islands where they are protected from erosive elements such as wind/wave action, water currents and ice flows (Ouzilleau 1977). In fact these floating peat mats found in sheltered locations may actually expand horizontally and/or vertically as new peat is formed by plants growing on the surface, therefore experience a net decrease or increase in volume, area and mass over a given period (KHLP 2010).

Peatland disintegration is directly linked with reservoir expansion over time. Intact peatlands along the initial reservoir shoreline break down, and when considered along with mineral shoreline erosion processes, contribute to an increase in reservoir size over time (KHLP 2010). Peat plateau banks have been shown to erode at a mean rate of 4

m/year during the first four years of flooding, declining afterwards, in the Kettle

Reservoir (KHLP 2010). This process can occur for many years after whereby shorezone

peatlands experience collapse due to permafrost melt, primarily in peat plateau bogs,

subsequent floating and detachment from the shorezone, followed by either breakdown or

transport throughout the reservoir.

2.2.4.4 Floating Peatland Vegetation

Vegetation change after peatland flooding is common (Mitchell and Niering 1993;

Asada et al. 2005). Floating peat islands, can quickly reestablish their pre-flood

vegetation community after resurfacing, however tree species (black spruce, jack pine,

and tamarack) often become chlorotic and die off by the end of the first season of

flooding (Asada et al. 2005). In most cases the skeletal-branch remains of dead trees will

remain vertical, amongst a living shrub, sedge, and moss community on a floating peat

island. Other peat islands may immediately float to the lake surface after flooding without

any apparent signs of vegetation die off.

Changes in peatland hydrology can lead to a succession of peatland vegetation

communities, whereby bog communities are replaced by fen and marsh communities.

The experimental flooding of a boreal peatland, saw a shift from a bog-dominated

ombrotrophic vegetation community to a fen and marsh minerotrophic community

(Asada et al. 2005). While species richness did not change greatly in the floating peatland

they found that species turnover was common. Bog indicator species such as *Picea*

mariana, *Pleurozium schreberi*, *Rhododendron groenlandicum*, and *Sphagnum fuscum*

disappeared or declined, while more minerogenous and/or hydric species such as *Typha*

latifolia, *Myrica gale*, *Carex rostrata*, *Scirpus cyperinus*, and *Eriophorum angustifolium* appeared or increased in abundance.

2.2.4.5 Floating Peatland Classification

Unlike the Canadian Wetland Classification (NWWG 1997) there is no widely accepted classification of floating peatlands. The documented studies that do exist have classified peat islands according to their vegetation composition (Ouzilleau 1977; Dryade 1984; Belanger et al. 1991; Robert 2000; Manitoba Hydro and NCN 2003). Classes of peat islands vary from study to study as they are based on local descriptions of peat island vegetation cover. In the Wuskwatim Environmental Impact Statement (EIS) (Manitoba Hydro and NCN 2003), floating peatlands, or aquatic peatlands were classed according to dominant vegetation cover, some classes included: Sedge, Ericaceous, Treed, Cattail, Bare, and Tall Shrub. Co-dominant species islands were referred to as mosaic classes of combinations of the above classes. In all, 13 classes were used to describe the Wuskwatim Lake area peat islands occurring either naturally or as a result of flooding caused by the Churchill River Diversion. Ouzilleau (1977) described four types of peat islands in the Cabonga reservoir in Quebec: Type I – shrub dominated with few trees; Type II – Shrub dominated peat islands with no trees; Type III – shrub and *Carex* dominated peat island; Type IV – shrub dominated peat islands with *Typha*. Another study out of Quebec (Dryade 1984) grouped floating peat islands in the Opinaca and La Grande 2 reservoirs by the percent composition of living and dead vegetation.

2.2.5 Environmental Impacts Associated with Peatland Flooding

Past research on the environmental effects of hydroelectric reservoirs has focused on local in-reservoir and down stream effects (Baxter 1977). More recent research has focused on cumulative large scale impacts (Rosenberg et al. 1997; Rosenberg et al. 2000). In these studies, effects such as reservoirs acting as greenhouse gas sources (CO_2, CH_4), mercury release into the aquatic ecosystem, sedimentation, and alteration of aquatic and terrestrial habitat, are awarded more attention.

A number of studies conducted at the Experimental Lakes Area (ELA) study site in northwestern Ontario have documented the effect of anthropogenic flooding on boreal wetlands (Scott et al. 1999; Saquet 2003; St.Louis et al. 2004; Asada et al. 2005). In 1991 the Experimental Lakes Area Reservoir Project (ELARP) was initiated as a long-term controlled field experiment designed to simulate the impacts of a large-scale shallow flooding by reservoirs on peatlands and shallow lakes (Asada et al. 2005). In 1993 ELA study-lake 979 was experimentally flooded in order to study the effects of flooding on a boreal peatland (Saquet 2003). The primary objective was to quantify net greenhouse gas (GHG) emissions from reservoirs (Kelly et al. 2007).

2.2.5.1 Greenhouse Gases

Peatlands act both as carbon sinks and carbon sources. Peat is composed primarily of partially decomposed plant material, a large source of organic carbon. Peatlands can be greater than 2 metres thick, and can therefore contain a massive volume of non-decomposed carbon based material. When a peatland is exposed to change through either flooding or increased temperature, bacterial activity within the peat mass is increased.

46

Methanogenic bacteria mineralize the peat and release methane (CH_4) and carbon dioxide (CO_2) gases. These two gases are said to be major gases that have a large influence on the global radiative balance contributing to the greenhouse effect (Saquet 2003). Studies at ELA in Ontario have measured increased CO_2 and CH_4 in flooded peatland reservoirs. Saquet (2003) found flooding initially caused CO_2 and CH_4 emission rates to increase and changed the ELA wetland from a small, natural carbon sink to a large source of carbon. Hydroelectric reservoirs have been found to be sources of greenhouse gases (GHGs) to the atmosphere as a result of organic carbon mineralization in flooded plants and soils to carbon dioxide (CO_2) and methane (CH_4) (St.Louis et al. 2003). Flux rates of important GHGs measured in artificial reservoirs have been found to be 5 to 10 times greater than the flux rates measured in equivalent natural wetlands (Duchemin et al. 1995; Kelly et al. 1997).

2.2.5.2 Mercury Methylation

Methylmercury (MeHg) is an organic form of mercury (Hg) produced during the microbial decomposition of organic materials. Mercury, from anthropogenic emissions in addition to natural emissions, can be transported long range through the atmosphere and deposited via precipitation and dry deposition in remote aquatic and wetland environments (Fitzgerald et al. 1998). Much of the mercury in boreal and subarctic peatlands is locked into the peat (bogs) due to lack of water flow. Flooding of peatlands promotes anoxic conditions, where methanogenic bacteria become active. Methylmercury is produced in conjunction with methane (CH_4) gas during the decomposition process. Once methyl mercury reaches the reservoir water supply it enters the food web and

47

bioaccumulates up the food chain. Methyl mercury accumulates in aquatic organisms to concentrations many orders of magnitude greater than found in either the water column or precipitation (Downs et al. 1997). Studies have quantified methylmercury in newly formed reservoirs. St. Louis et al. (2004) found a 40 fold increase in net MeHg production a year after experimental flooding of a boreal peatland reservoir. Methylmercury is a known neurotoxin and can be harmful to animals and humans (St.Louis et al. 2004).The human consumption of freshwater and marine fish contaminated with monomethylmercury is the primary public health concern related to Hg in the environment (Fitzgerald et al. 1998). Methylmercury contamination has been known to persist for 20-30 years after original reservoir impoundment (Bodaly et al. 1997; Rosenberg 1997).

2.2.5.3 Aquatic Habitat Alteration

Flooding and subsequent peatland disintegration alters the characteristics of aquatic habitat. Most notably there is an immediate loss of terrestrial habitat and increase and alteration to aquatic habitat resulting from flooded terrestrial habitat. Subsequent peatland disintegration and erosion of mineral shorelines, causes the reservoir to expand over time, in turn increasing the amount of available aquatic habitat.

Besides changes to the physical availability or quantity of aquatic habitat the quality of the newly created habitat is of concern. In addition to methylated mercury contamination, the increased decomposition of organic material, after flooding results in increased microbial production, thereby reducing available dissolved oxygen (DO) and creating an acidic and anoxic environment. Methanogenic bacteria present in peatlands

favor the anoxic environment created after flooding, which removes the zone of oxidation usually present in an undisturbed wetland and creates an environment that has a warmer temperature, resulting in increased microbial activity (St.Louis et al. 2003). Acidic and anoxic conditions are known to limit fish species richness (Rahel 1984). Temperature fluctuations can also limit use for a number of fish species, life stages, and activities (foraging or spawning).

2.2.5.4 Physical Impediments to Hydroelectric Operations, Navigation and Recreation

Environmental concerns associated with peatland ecosystem change are certainly more prevalent in the literature. However, floating peatlands as barriers to hydroelectric operation, boat navigation, and social recreation are also important considerations for the unique and dynamic process of peatland upheaval, transport, and disintegration.

Much of the earlier literature describes floating peat islands and other debris resulting from hydroelectric impoundments as impediments to the normal operation of turbines (Balagurov 1967; Ivanov et al. 1971; Vasilevskii et al. 1975). The problem of floating peat islands is described as an engineering issue, rather than an environmental issue. A number of mitigation options to minimize the impact of peatland uplift, transport and disintegration on hydroelectric operations after reservoir creation have been discussed. These options have included but area not limited to: land clearing prior to flooding, using dyking systems to limit the expansion of shorelines into peatlands over time, laying heavier substrates such as gravel over top of the peat landscape to limit the chances of peat upheaval and protecting water intakes with booms, or physically towing uplifted peat islands to dry land (Ivanov 1971; Ronka and Uusinoka 1976; KHLP 2010).

Ronka and Uusinoka (1976) outline some of the environmental and social problems associated with floating peat islands. They describe water pollution via the introduction of humic acids and certain elements such as nitrogen, sulfur, and iron, in addition to disintegration of peat and the presence of floating organic debris throughout the reservoir causing navigational hazards to recreational users, as primary concerns.

2.3 REMOTE SENSING IN PEATLAND ENVIRONMENTS

Mapping and monitoring of peatland change in reservoirs has been identified as being important to current and future hydroelectric developments and to the environmental assessments that support their licensing and operation (KHLP 2010). To date, peatland and peat island mapping and inventory studies have consisted almost entirely of low level aerial forestry surveys, aerial photography and ground based surveys (Ronka and Uusinoka 1976; Belanger et al. 1991; Grondin and Ouzilleau 1980; Le Groupe Dryade 1984; Robert 2000; Asada et al. 2005; KHLP 2010; Manitoba Hydro 2003). Monitoring peatland disintegration in a reservoir to date has required multi-date aerial photography over many years in order to track the progression of lateral reservoir expansion, peat upheaval, movement, and disintegration. A photo is required prior to flooding, shortly after flooding, and subsequent years after flooding, in order to accurately monitor peatland and reservoir change. In order to create land cover maps from aerial photography, it first needs to be successfully planned and flown and then needs to be processed. Processing steps may include: 1) digital scanning of negatives in the absence of digital camera; 2) correction for camera tilt, georeferencing or orthorectification of the imagery; 3) heads up or tablet based photo interpretation and digitizing of features. These steps are repeated for multiple dates of aerial photography. The process is effective but it can be time consuming, and relatively expensive. Current remote sensing technologies provide alternatives to this conventional approach.

An increased understanding of the importance of wetlands has led to an emphasis on wetland and peatland mapping and inventorying (Augusteijn and Warrender 1998). As a result satellite remote sensing has become a common tool for mapping environmental

changes in wetlands. Recent advances in the spatial and spectral resolution capabilities of commercial high-resolution optical satellites such as IKONOS, Orbview, and GEOEYE, QuickBird and WorldView, have provided enhanced detail from which environmental changes can be mapped. Microwave systems such as RADARSAT-1 and 2, operated by MDA Corporation; also provide a formidable alternative to traditional air photo based surveys. There are a number of advantages to using these sensors, which include: 1) optical satellite image resolution has approached that of aerial photography (40 – 50 cm); 2) archived image products can be accessed immediately; new acquisitions can be requested at any time and distributed via DVD media or internet download within days of successful acquisition; 3) satellite image products are a cost effective solution when compared to the amount of resources and processing time that factors into aerial photography production; 4) multispectral remote sensing has been proven to be successful in discriminating between land cover types. For these reasons, satellite remote sensing solutions should be considered for mapping and monitoring the dynamic processes related to peatland reservoirs.

2.3.1 An Introduction to Remote Sensing

Remote sensing is defined as the acquisition of information about an object without being in physical contact with it (Elachi and van Zyl 2006). The principles and fundamentals of remote sensing are well documented (Lillesand and Kieffer 2000; Mather 2004; Elachi and van Zyl 2006). A brief summary of the basic concepts of remote sensing is provided.

Remote sensing technologies measure the response of electromagnetic radiation (EMR) reflected from earth-based targets. The scale of large to small wavelengths of EMR make up the electromagnetic spectrum (EMS) and includes the sub-millimeter wavelength energies of gamma-rays, x-rays, ultraviolet, visible blue, green and red, near infrared, far infrared and the larger wavelengths such microwaves and radio waves (Figure 2.8). Remote sensing satellites, orbiting the earth, have sensors that operate in different portions of the EMS. Passive sensors record the energy reflected back from earth targets illuminated by the sun. These sensors commonly operate in the optical portion of the EMS, which includes the visible and infrared wavelengths (0.3 µm to 14 µm). Active sensors emit their own energy source and record the amount of energy reflected back from earth targets. These sensors commonly operate in the microwave (1 mm to 1 m) portion of the EMS. Remotes sensing systems are not exclusive to the orbit above earth, they can be ground-based (Doppler radar), water-based (sonar system), and air-based (aerial photography). They all record energy response from a remote location, to allow scientists to make quantitative and qualitative measurements over varying study area sizes and scales.

© CCRS

http://www.ccrs.nrcan.gc.ca/resource/tutor/fundam/images/waveleng.gif
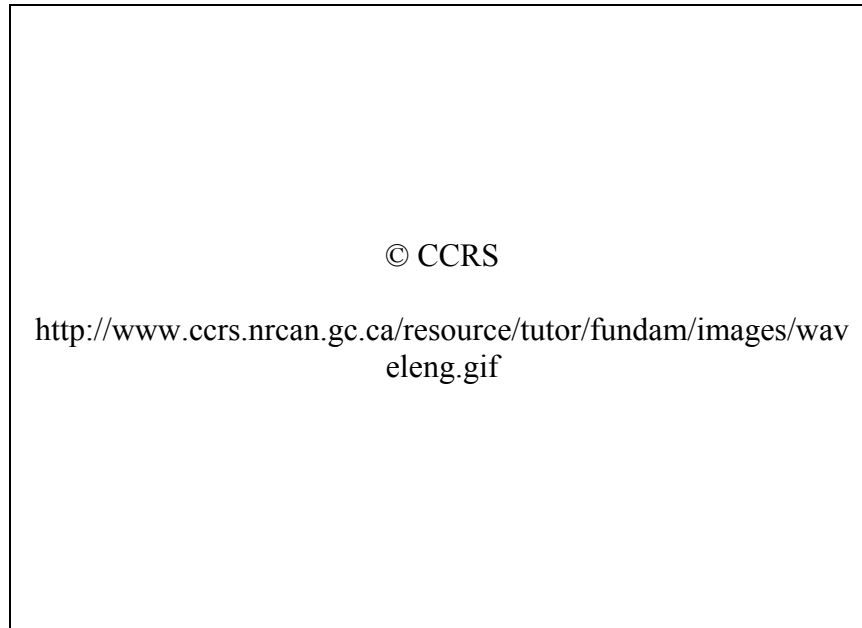
Figure 2.8. The electromagnetic spectrum (EMS) identifying the various portions, with examples of optical and microwave sensors. Copyright: Canadian Centre for Remote Sensing (CCRS), with permission for non-commercial reproduction).

Electromagnetic energy interaction with ground surface features can be described by the following energy balance equation (Lillesand and Kieffer 2000):

$$E_I(\lambda) = E_A(\lambda) + E_R(\lambda) + E_T(\lambda) \tag{2.1}$$

Where E_I (incident energy) is the sun's or active sensor's incident energy, E_A (absorbed energy) is energy absorbed by the target, E_R (reflected energy) is energy reflected off of the target, and E_T (transmitted energy) is energy transmitted through the target. The amount of reflected energy returning to a sensor can tell us a great deal about the ground target. The imagery produced during a satellite acquisition, once converted from analog to digital format, is in an array of digital numbers (DN) representing the returned or reflected energy from the ground target, across one or more spectral bands. This quantity of reflected energy can be expressed as a percentage, as a ratio of the amount of energy reflected from an object over the amount of energy that was originally incident upon it and is termed spectral reflectance. Factors such as energy transmission

through the atmosphere, angle of the sensor with respect to the target, position of the target on a sloped terrain, and the way in which energy interacts with ground targets, whether they act as net diffuse, lambertian, or specular reflectors, can greatly influence the amount of energy reflected to the sensor. Understanding how these variables alter reflection back to the sensor becomes more crucial when analyzing multi-date imagery, where environmental conditions and imaging parameters may be different. A comprehension of these basic underlying principles allows scientists to apply remote sensing to numerous earth resource applications, including wetland and hydrology applications.

Optical and microwave satellite remote sensing imaging technologies have been used in wetland and peatland applications(Augusteijn & Warrender 1998; Sawaya et al. 2003; Li and Chen 2005; Bartsch et al. 2008). There are benefits and drawbacks to using each of these technologies for earth remote sensing applications. The fundamentals of optical and microwave remote sensing technologies which make them useful in wetland and peatland applications are discussed below.

2.3.2 Optical Remote Sensing

2.3.2.1 Optical Remote Sensing Fundamentals

The first forms of optical remote sensing began back in 1858 (Lillesand and Kieffer 2000). Aerial photography, the earliest form of remote sensing, used the portion of the EMS that is visible to the human eye (0.4 to 0.7 μm). The optical portion of the EMS (Figure 2.8) extends from approximately 0.3 to 14 μm and includes and includes ultraviolet (UV), visible (0.4 to 0.7 μm), near-infrared (NIR) (0.7 to 1.3 μm), mid-

infrared (MIR) (1.3 to 3 µm), and thermal-infrared (TIR) (3 to 14 µm) wavelengths (Lillesand and Kieffer 2000). Traditionally, optical remote sensing systems have been more popular for earth resources remote sensing applications. Because the visible portion of the EMS allows users to delineate targets within an image without computer assistance, it is natural to be biased towards these technologies.

This thesis is concerned with the optical response of broad reservoir cover type targets. In general the project is concerned with the optical responses of water, vegetation types, and barren land or soil, all of which may be commonly associated with a subarctic reservoir. The spectral reflectance of a ground target, whether it is vegetation, soil or water, can be plotted as a function of wavelength to display it's spectral reflectance curve (Mather 2004). These spectral reflectance curves act as spectral signatures that allow us for discrimination between different earth targets in the optical portion of the EMS. Soil, water, and vegetation are often used to demonstrate typical spectral response curves of earth based materials (Lillesand and Kiefer 2000;Mather 2004). Spectral libraries are used to provide a reference of typical spectral response curves for different land cover types. Figure 2.9 illustrates an example of the response patterns of water, and different vegetation types in the VNIR portion of the EMS. With the exception of the visible range from 400 – 500 nm, all three cover types have distinctly different reflectance throughout the VNIR spectrum, indicating that an optical VNIR multispectral image would be able to discriminate between the three cover types. The characteristics that make water, vegetation, and soil, spectrally unique are discussed below.
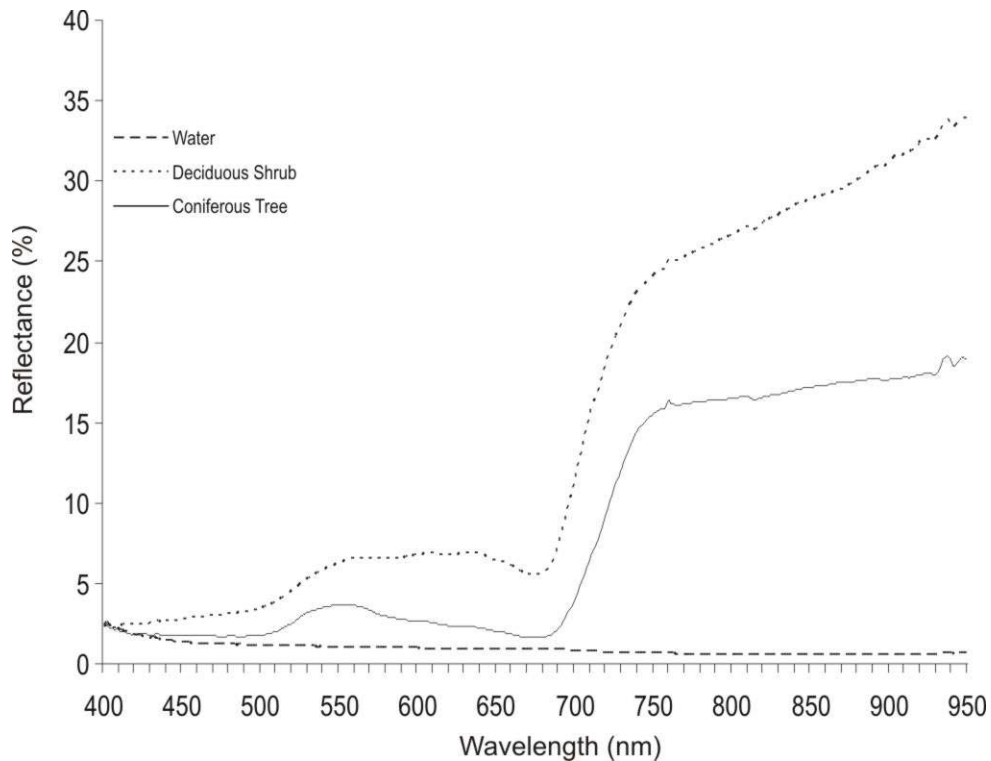
Figure 2.9. Example of spectral reflectance curves for selected water and vegetation cover types.

2.3.2.2 Land Cover Response in the Optical Spectrum

2.3.2.2.1 Water

Optical remote sensing technologies are often used in the study of water bodies (Vertucci & Likens 1989;Brezonik et al. 2005;Menken et al. 2006). The optical response properties of water are well known (Lillesand and Kieffer 2000; Mather 2004; Elachi and van Zyl 2006). In general, there is a reduction in the amount of reflected EMR with an increase in wavelength across the visible and near-infrared region of the EMS as water absorbs energy in these wavelengths, with deep clear water approaching 0 % reflectance in the near-infrared region of the EMS (Figure 2.9). This makes the near-infrared band an important tool in discriminating between land and water, as most land surfaces are highly reflective in the NIR spectrum. Surface reflectance, volume reflectance, and bottom

reflectance are the three main mechanisms affecting the amount of EMR that is returned to the sensor from a water body.

Depending on sensor angle and water body surface conditions, surface reflectance from the water body may be specular or result in sun glint due to a rough surface, angle of the sensor, and angle of the sun. Surface albedo is a common occurrence that should be accounted for when making detailed comparisons between water sediment concentrations and spectral reflectance. Correction algorithms have been applied to optical imagery where this type of reflectance occurs (Wolter et al. 2005). Bottom reflectance is a function of the depth and clarity of the water and the properties of the water body substrate. The amount of incident energy that is transmitted through the water body is reflected from the bottom back to the sensor. This property has been used to derive depth and substrate maps from high resolution optical imagery (Stumpf and Holderied 2003).

Volume reflectance is affected by the character and abundance of dissolved and suspended inorganic and organic material, including suspended mineral sediment, colored dissolved organic matter (CDOM), and chlorophyll. This property has been the basis of many water quality studies linking spectral response with suspended material concentrations(Vertucci & Likens 1989; Han 1997; Brezonik et al. 2005;Menken et al. 2006). Within the water column of the water body, EMR can be absorbed by the water and dissolved substances as well as backscattered by the suspended particles. Suspended solids scatter the down-welling radiation, where scattering is proportional to the concentration of the suspended particulates and can be affected by size and color of the sediments. A positive linear relationship exists between suspended matter concentration and reflectance in the VNIR region of the EMS, where concentrations are low to

moderate (Han 1997; Lodhi et al. 1997). This relationship becomes increasingly non-linear with increasing suspended sediment concentrations. Chlorophyll has absorption bands in the region below 500 nm and between 640 and 690 nm. Therefore an increase in chlorophyll concentration tends to result in decreased water reflectance in blue wavelengths and increased reflectance in green wavelengths.

2.3.2.2.2 Vegetation

Earth resource satellites operating in the optical spectrum have been used for vegetation mapping and monitoring studies since the early 1970s and the spectral reflectance properties of vegetation are well known (Lillesand and Kieffer 2000; Mather 2004; Elachi and van Zyl 2006). Photosynthetically active vegetation generally has low reflectance in the blue and red regions of the visible portion of the optical spectrum, attributed to the absorption of blue and red light by chlorophyll and other pigments, which absorb 70 – 90 % of this light to provide energy for the process of photosynthesis. A minor peak in reflectance occurs in the green portion (500 – 600 nm) of the EMS giving healthy vegetation its green appearance (Figure 2.9). There is a sharp rise in reflectance at approximately 700 nm, which remains high in the near-infrared region between 750 and 1350 nm due to interactions between internal leaf structure and the EMR. The position of the beginning of the steep rise in reflectance is known as the red edge point and is often used to characterize vegetation vigor. Reflectance is affected mainly by leaf-tissue water content in the 1350 to 2500 nm region, resulting in a minima reflectance recorded near 1450 and 1950 nm. Plant senescence is characterized by a decline in reflectance in the near-infrared region (750 – 1350 nm).

Combinations of optical bands have been used to create indices of vegetation health and vigor in order to enhance classification accuracy in wetland applications (Townshend and Walsh 2001). The normalized difference vegetation index (NDVI) uses the red visible (chlorophyll absorption band), and near infrared band (high reflectance in healthy vegetation) to create a new set of information that characterizes vegetation health and vigor. In addition it has also been used to aid in the discrimination of land and water, where water typically has an NDVI < 0 (Giglio et al. 2003). NDVI is expressed in the following equation

$$NDVI = (NIR - RED)/(NIR + RED) \qquad\qquad (2.2)$$

2.3.2.2.3 Soil

The spectral reflectance properties of soil are well known (Lillesand and Kieffer 2000; Mather 2004; Elachi and van Zyl 2006), and differ from that of vegetation and water. Generally soil will demonstrate increased reflectance across the optical portion of the EMS. This is in contrast to the behavior of water which shows a gradual decline approaching zero percent reflectance in the near-infrared (Figure 2.9). The reflectance properties of soil are mostly affected by the presence of organic matter, soil moisture content, soil texture, and the presence of iron oxide. The spectral region between 850 and 930 nm is a ferric iron absorption band. Iron oxide in soils appears red because it absorbs EMR in the wavelengths shorter and longer than the red visible band. Water absorption bands occur between 1300 and 1500 nm and 1750 and 1950 nm.

2.3.2.3 Optical Remote Sensing in Wetland and Peatland Applications

2.3.2.3.1 Field Spectroscopy

Validation studies for remote sensing applications have utilized field spectroscopy to take spectral reflectance readings of specific targets to coincide with satellite imagery of the study area (Harris et al. 2006). Field spectroradiometers provide users with a recording of reflectance from a target in many discrete narrow bands, usually in the optical range of 350 – 2500 nm, and are used to: 1) Aid in the analysis and interpretation of remotely sensed imagery; 2) Calibrate a sensor; and 3) Verify information extracted from remote sensing data (Lillesand and Kieffer 2000). Studies using spectroradiometers in the field have looked at the spectral characteristics of water bodies (Vertucci and Likens 1989; Lodhi et al. 1997; Han 1997), vegetation canopies (Nichol et al. 2000; Loechel et al. 1996) and even specific vegetation targets such as detecting moisture status of *Sphagnum spp.* (Vogelmann and Moss 1993; Harris et al. 2006). Some studies (Loechel et al. 1996; Schaepman et al. 1997; Nichol et al. 2000; Walthal et al. 2001) have looked at the use of field spectroradiometers mounted to an aerial vehicle such as a helicopter for greater accessibility to remote targets. At pre-selected altitudes the instantaneous field of view (IFOV) of the spectroradiometer can be used to mimic the IFOV resolution of an optical satellite platform. Nichol et al. (2000) used a 15 degree fore optic to produce an IFOV of 79 m at a helicopter altitude of 300 m over their ground targets. Schaepman et al. (1997) identify a number of spatial, spectral, and temporal inhomogeneities that may be encountered when taking spectral measurements from airborne platforms. One such issue that often arises is the adjacency effect, which results in spectral reflectance contributions from surrounding water and vegetation targets

entering into the IFOV of the intended target (Schaepman et al. 1997). In addition,

technical constraints often hinder the ability to collect sufficient spectral reference data

during a survey. Schaepman et al. (1997) collected reference data before, after and once

during the middle of a 2 hour helicopter flight due to technical limitations.

2.3.2.3.2 Medium Resolution Sensors

Landsat MSS, Landsat TM, SPOT, AVHRR and Indian Remote Sensing Satellite

(IRS) are all examples of optical satellite systems that have been used to study wetlands

(Ozesmi and Bauer 2002). The Boreal Ecosystem Atmosphere Study (BOREAS) used

multiple small, medium and large scale airborne remote sensing platforms in order to

map land cover including boreal peatlands in northern Manitoba in the early and mid

1990s as one of the multiple project objectives (Gamon et al. 2004). Mapping of

wetlands and their vegetation using optical satellite imagery has been studied at medium

scales using Landsat imagery (Dixon and Stewart 1984; Brook 2001;Townsend & Walsh

2001; Brook and Kenkel 2002; Poulin et al. 2002; Toyra and Pietroniro 2005; Li & Chen

2005). Dixon and Stewart (1984) used Landsat MSS to classify and map peatland

vegetation near The Pas, Manitoba at a scale of 1:250,000 with an overall accuracy of

75%.

Principle component analysis (PCA) is a multivariate statistical technique often

used in the field of remote sensing to reduce the dimensionality of a multi-band image

data set. Highly correlated image bands are combined and replaced with a lower number

of less correlated Eigen images accounting for most of the variance found within the

original multi-band data set. Munyati (2004) utilized PCA for a change detection analysis

of multi-date Landsat TM and MSS imagery of an African wetland. Brook and Kenkel (2002) used PCA and ordination analysis as part of a multivariate approach to identify the spectral bands of Landsat TM that would best separate peatland vegetation classes of Wapusk National Park, Manitoba in an image classification algorithm. Landsat TM bands 3, 4, 5, and 7, were identified as important bands in discriminating spectral differences between peatland vegetation classes, while the visible bands were determined to be highly correlated and not contributing to a significant discrimination of vegetation classes. Landsat TM bands 5 and 7 are in the mid infrared portion of the EMS and provide spectral reflectance information related to vegetation and soil moisture content, Landsat TM bands 3 and 4 are also commonly used to discriminate vegetation types (Lillesand and Kieffer 2000). Landsat TM bands 3, 4, and 5 have been found to be the most effective band combination for wetland classification applications (Ozesmi and Bauer 2002).

2.4.2.3.3 High-Spatial Resolution Sensors

In the past, one of the limitations of satellite remote sensing has been its lack of spatial resolution for interpretation of wetland features (Ozesmi and Bauer 2002). DigitalGlobe Inc. successfully launched their first Quickbird satellite on October 18, 2001. At the time of this project's inception, DigitalGlobe had the highest resolution commercially available imagery. The pixel resolution for the panchromatic band is 61cm at nadir, while the multispectral bands have a spatial resolution of 2.44 m at nadir. Classic multispectral sensors such as the Landsat series of satellites and now the ASTER series of sensors, sacrifice high spatial resolution for larger swath widths and greater spectral

resolution. The onset of commercially available high resolution satellite imagery has seen the image resolution approach that of large scale aerial photography. The advantage of high resolution satellite imagery in wetland mapping is the ability to create inventory maps at larger scales and with greater detail with the added discriminant capabilities of near-infrared channels.

A number of studies have utilized high resolution imagery to map wetlands and aquatic vegetation and have achieved positive results (Dechka et al. 2002; Sawaya et al. 2003; Laba et al. 2007; Wei and Chow-Fraser 2007). Sawaya et al. (2003) used IKONOS and Quickbird high-resolution satellite imagery to study three potential applications, one of which included aquatic vegetation surveys of emergent and submergent plant groups. The high spatial resolution of the imagery and the inclusion of multispectral bands allowed assessment of the aquatic vegetation variation within lakes and wetlands that could not otherwise be obtained through the use of Landsat imagery or aerial photography (Sawaya et al. 2003). Dechka et al. (2002) used IKONOS imagery to classify and map wetland vegetation communities. Final classification accuracies reached 84 %. Initial classifications resulted in low accuracies, as field validation did not cover the full spectral variability in the IKONOS images. Sawaya et al. (2003) reiterate the importance of validation data in successful classification of high-resolution satellite imagery. Point validation data collected in the field, which may be suitable for classification of moderate-resolution data, are often not sufficient to validate classification of high-resolution imagery, and therefore they suggest segmentation and object-based classification approaches (Sawaya et al. 2003). Wei and Chow-Fraser (2007) were able to achieve overall wetland classification accuracies of 90 % over 11 test

sites in eastern Georgian Bay. Likewise, Laba et al. (2007) found Quickbird to provide significant potential for the mapping of invasive plant species in estuarine environments. Andrefouet et al. (2003) report much improved accuracies of 15 -20 % when using IKONOS over Landsat when mapping coral reef habitats.

Studies that have used high-resolution in wetland related applications have achieved classification accuracies that at least meet or exceed that of moderate resolution sensors such as Landsat or conventional aerial photography. Wei and Chow-Fraser (2007) provide a cost benefit analysis of mapping sea grass using IKONOS, Landsat, and aerial photography. IKONOS provided the best classification accuracy followed by aerial photography and Landsat , with accuracies of 89%, 63%, and 59% respectively. IKONOS imagery is less costly than aerial photography, but much more expensive than Landsat. Mumby and Edwards (2002) (Mumby & Edwards 2002) indicate that IKONOS has a benefit over Landsat if the following three criteria are met: (1) adequate validation data are available to identify small habitat patches, (2) the area to be studied is less than 500 km^2, (3) the goal is to monitor small-scale (< 10m) habitat dynamics. The user has to determine the cost-benefit between required accuracies and the size of area to be studied at the outset of the project.

High resolution airborne spectrographic imagers such as the compact airborne spectrographic imager (CASI) have been used to discriminate spectral differences between peatland vegetation communities (Thomas et al. 2003). The benefit of a hyperspectral imaging system is the production of hundreds of narrow band images across the visible and infrared portions of the EMS, which can be used to discriminate

and map vegetation types at great detail. This type of system provides high spatial and spectral resolution from an airborne platform.

2.3.3 Microwave Remote Sensing

2.3.3.1 Microwave Remote Sensing Fundamentals

Radar is an acronym for Radio Detection and Ranging. Imaging radars operate in the 1mm to 1 metre range of the EMS. Because radar operates with larger wavelengths it is largely unaffected by atmospheric attenuation, and can be imaged in through cloud cover giving it a large advantage over optical systems. Such as in an optical system, microwave EMR is reflected, transmitted, and absorbed by ground targets, however the interaction of microwave EMR with the ground targets is different. There are some other notable differences between the two remote sensing systems. Where most optical sensors are passive, measuring reflected sun energy from ground based targets, imaging radars are mostly active, emitting their own pulse of microwave energy and measuring the time it takes to return or echo from ground based targets in order to determine object distance. This also allows an active microwave system to image 24 hours a day if required.

Synthetic aperture radar (SAR) is a type of remote sensing sensor that operates in the microwave region of the EMS. It is termed synthetic aperture radar because it mimics the effect of having a long radar antenna in order to achieve increased radar resolution. Brute force radar, otherwise known as a real aperture radar (RAR), is the parent of SAR and was used in many early aerial applications of imaging radar, however to achieve high resolutions from space the antennae would have to be much too large.

Within this microwave region there are a number of designated microwave bands, originating from military applications, of varying wavelength that have been used for remote sensing applications. Table 2.4 indicates the range that these various sensors operate in. RADARSAT-1, the C-band SAR platform used in this study operates at 5.3 GHz. C-band radar is considered to provide a well balanced response for a wide variety of earth resource applications (CCRS 2009).

Table 2.4. Various satellites using the multiple wavebands available in the microwave portion of the electromagnetic spectrum (EMS).

Band	Wavelength (cm)	Frequency (GHz)	Satellites/Sensors
K_a	0.75-1.1	40-26.5	-
K	1.1-1.67	26.5-18	-
K_u	1.67-2.4	18-12.5	ERS-1,2; Quickscat/Seawinds
X	2.4-3.75	12.5-8	SIR-C
C	3.75-7.5	8-4	Radarsat-1, 2; ERS-1,2; ENVISAT-1(ASAR)
S	7.5-15	4-2	Almaz-1
L	15-30	2-1	Seasat-1; JERS-1; ALOS (PALSAR)
P	30-100	1-0.3	AirSAR

2.3.3.1.1 Radar Reflectivity and Sigma Naught

The microwave pulses emitted from a radar return as echoes derived from one or more individual reflections from ground terrain (Raney 1998). In the literature the most common measure of radar reflectivity is sigma naught ($\sigma°$), which is also known as the backscattering coefficient (Ulaby et al. 1981) or the normalized radar cross-section. The backscattering coefficient represents the average reflectivity of a horizontal material sample, normalized with respect to a unit area on the horizontal ground plane, and it describes the amount of average backscattered power compared to the power of the incident field as a fraction (Raney 1998). Sigma nought is expressed as a power estimate

in decibels (dB). Other measures include gamma (γ), and beta nought (β°) and are described by Raney (1998).

2.3.3.1.2 Target Scattering

Ground targets may be point target or discrete scatterers, or targets whose physical size is smaller than the impulse response width of the radar. Corner reflection is an example of the discrete scatterer model at work (Raney 1998). Examples of corner reflectors in the environment include flooded trees next to open calm water, and icebergs next to a sea surface. Ground targets may also follow a distributed or diffuse scatterer model, where the signal return is a net average over a region of random individual scatterers (Raney 1998). An example of a diffuse scatterer would be a forest canopy.

Scattering occurs on both the surface of objects and within the volume of objects. Surface scattering is much more apparent in like-polarized and short wavelength radar imagery, whereas volume scattering is more prevalent in cross-polarized and large wavelength radar imagery (Lewis and Henderson 1998). Volume scattering takes place in a three-dimensional environment with multiple targets such as leaves, branches and trunks below a vegetation canopy.

Microwave scattering is influenced by both the parameters of the radar system and the nature and orientation of the ground targets as well as a combination of the two. The system parameters that influence reflectivity include wavelength, polarization, look angle, look direction, and resolution. The ground target parameters include surface roughness, local incident angle, and complex dielectric constant. All of these parameters affect whether scattering from a ground target is primarily surface scattering or scattering from within the volume.

2.3.3.1.3 Surface Roughness

Surface roughness of a ground target is an important parameter determining the appearance of a target in a radar image. Roughness can be defined on three different scales: (1) microscale roughness influences image tone and is related to roughness on the scale of a fraction of the system wavelength, (2) mesoscale roughness is considered to be the "gross roughness envelope" and relates to image texture, (3) macroscale roughness is determined by terrain effects, such as radar shadow (Lewis A.J. and Henderson F.M. 1998).

Microscale roughness has been defined in a number of ways. A very crude threshold of a rough surface is $\lambda/10$, where the roughness characteristics of a target are greater than 1/10 of the wavelength of the imaging system(Lewis A.J. and Henderson F.M. 1998). More complex estimates take into account the look angle (Φ) of the imaging system. The Rayleigh Criterion expresses surface irregularities as root mean square height variations (h_{rms}) and defines a surface as being rough if

$$h_{rms} > \lambda/8\cos\Phi \qquad\qquad (2.3)$$

More recently Woodhouse (2006) indicated the need for a stricter threshold between smooth and rough surfaces. The Fraunhoffer Criterion, which is said to be more appropriate for modeling microwave scattering from natural surfaces (Woodhouse 2006), defines a smooth surface as being the less than 1/ 32 of the wavelength times the cosine of the incident angle.

A smooth surface as defined by the above criterion will act as a specular reflector, where incident microwave energy is reflected away and not returned to the sensor. This is

why calm water appears dark in radar images. As the wavelength dependent roughness of the target increases, it begins to act as a diffuse scatterer, by which the backscattered component increases. Rough surfaces appear bright in radar images.

2.3.3.1.4 Local Incident Angle

The angle at which microwave energy interacts with a ground target affects the amount of energy returning to the sensor. The incident angle is defined as the angle between the sensor line-of-sight and the local vertical with respect to the geoid, whereas the 'local incident angle' takes into account the local slope angle of the target (Lewis and Henderson 1998). Generally, an increasing incident angle will result in decreased reflectivity from distributed scatterers (Lewis and Henderson 1998).

2.3.3.1.5 Complex Dielectric Constant

The complex dielectric constant affects the absorption and propagation of microwave energy within terrain surfaces. Moisture within target objects greatly affects the energy interaction within a target. In the microwave region most dry natural materials have a dielectric constant of 3 to 8, whereas water has a dielectric constant of 80 (Lewis and Henderson 1998). Simply put, a high dielectric constant implies a high moisture content, low signal penetration, high radar reflectivity and potentially a high signal return. In contrast, a low dielectric constant signifies low moisture content, potentially high signal penetration, and lower radar signal return (Lewis and Henderson 1998). The complex dielectric constant is expressed as

$$\epsilon = \epsilon' + i\epsilon'' \tag{2.4}$$

2.3.3.1.6 Speckle

Speckle is a product of the coherent processing of scattered signals and is sometimes known as coherent fading (Lee 1986; Ulaby et al. 1986; Raney 1998). Variation in the phase of signals returning to the SAR produces a random pattern of bright and dark pixels (Lillesand and Kiefer 2000). The result is a grainy 'salt and pepper' effect in the image. The ongoing debate is whether to accept speckle as important information or to try and eliminate it from the image. If the goal of the study is to suppress image speckle it can be dealt with in one of two methods.

The first method of speckle suppression makes adjustments for speckle prior to images being created. Multi-look processing averages several sub-images or looks formed during SAR processing in order to reduce noise or speckle variance (Lee 1986; Raney 1998). The downside to multi-look processing however is a loss in spatial resolution. For example MacDonald Dettwiler and Associates (MDA), offers a number of RADARSAT-1 image products that implement multi-look processing in order to reduce the effects of speckle (RADARSAT International 2000). They also offer a single-look fine-beam mode SAR georeferenced extra-fine resolution (SGX) product, which utilizes the full azimuth resolution capabilities of the SAR instrument at the expense of increased image speckle. The SGX image product is sampled with respect to range and azimuth cell resolution (approx 8m) using Nyquist criteria to achieve a pixel spacing of 3.125m at the expense of quadrupling the data volume (RSI 2000). Raney (1998) recommends avoiding this type of sampling if at all possible, however if no other option is necessary the sampling procedure must follow a reduction of the signal bandwidth.

The second method of image speckle suppression is known as adaptive filtering. Adaptive filtering is a post-processing technique employed in image processing software to reduce the effects of image speckle (Lee 1986). Adaptive filters build on conventional linear filters in that they improve image variation while preserving image resolution (Raney 1998). Examples of well known adaptive filtering algorithms developed for SAR speckle reduction include: the Lee filter (Lee 1986), the Frost filter (Frost 1981), and the Kuan filter (Kuan 1987).

2.3.3.2 Land Cover Response in the Microwave Spectrum

2.3.3.2.1 Water

Imaging radars typically see calm open water as a smooth surface and it therefore acts as a specular or forward scatterer of microwave energy. This is why water appears as a homogeneous area of dark tone on a radar image. It is possible for the surface of a water body to be roughened by wind driven surface waves. If this is the case, the backscattered radar component increases and the reflected radar component decreases. The presence of emergent aquatic vegetation may also lead to increased backscatter from lakes creating additional land/water interpretation confusion (Bryan 1981).

Liquid water exhibits a dielectric spectrum with a strong dependence on the microwave frequency and a relatively weak sensitivity to physical temperature. Frozen water (ice) has a dielectric constant that approaches that of dry soil (Dobson and Ulaby 1998). An increase in salinity increases the electrical conductivity and thereby increases dielectric constant and in return radar backscatter.

The look angle of the radar sensor can affect radar backscatter from water bodies. Lower look angles tend to have higher radar returns from water bodies, thereby reducing the tonal contrast between land and water (Lewis 1998).

2.3.3.2.2 Vegetation

Microwave energy is reflected, transmitted and absorbed when interacting with vegetation canopies. Surface scattering is related to the apparent surface roughness of the vegetation canopy, which in turn is dependent upon the wavelength and angle of the incident microwave (Leckie and Ranson 1998). If the forest or vegetation canopy appears rough to the radar the surface scattering or reflection increases, whereas the opposite effect is experienced with a smooth surface. Examples of rough surfaces may be an irregular open canopy coniferous forest, whereas a smooth surface may be a closed, consistent height deciduous canopy or a grass or sedge ground cover.

Transmission into a vegetation canopy results in volume scattering. This scattering is affected by gradual changes in dielectric constant, small inhomogeneities, and the size and density of objects or elements such as leaves, twigs, branches and trunks within the canopy (Leckie and Ranson 1998). Once in the volume of the media, the radar signal is either lost to attenuation or backscattered to the sensor. Scattering and absorption, or conductive loss within the media's volume, are the main causes of signal attenuation. Volume elements that are small in comparison to the wavelength, such as small leaves or twigs, act as attenuators, whereas elements that are larger, such as branches, will act as scatterers (Leckie and Ranson 1998).

Plant moisture content is directly related to dielectric constant of the vegetation. An increase in moisture content increases the dielectric constant of the vegetation elements. An increase in dielectric constant tends to increase both absorption and reflection within the vegetation's volume (Leckie and Ranson 1998). The amount of moisture within the plant media determines the depth to which the signal will penetrate the surface and volume of the target. Low moisture content will allow deeper penetration than high moisture content. Surface moisture related to precipitation, fog or dew will also increase the dielectric constant. Microwave behavior with a moist plant surface depends on the wavelength of the incoming radiation. Longer wavelengths will be less affected, whereas shorter wavelengths such as C-band would possibly show an increase in backscatter. Wet or rainy conditions may result in an overall contrast reduction in the resulting image (Leckie and Ranson 1998).

2.3.3.2.3 Soil

The interaction of microwave energy on bare soil is strongly influenced by the surface roughness, which affects the shape of scattering pattern, and the soil's dielectric properties, which controls the magnitude of reflection, absorption and transmission of the incident wave (Dobson and Ulaby 1998). The dielectric properties of the soil are influenced by soil moisture, density, particle-size distribution, mineralogy and fluid chemistry. Radar backscatter is influenced most strongly by moisture content which can drive the dielectric properties up from approximately 3 for dry bare soil, well into the range of 30-40 for very moist soils (Dobson and Ulaby 1998). Soil parameters such as salinity and organic matter content have been shown to have some effect on radar

74

backscatter, however to a much lesser extent then surface roughness and moisture content (Brisco and Brown 1998).

2.3.3.3 Microwave Remote Sensing in Wetland and Peatland Applications
2.3.3.3.1 Synthetic Aperture Radar

The use of radar imaging in hydrologic and wetland applications is wide spread and well documented. A number of studies have used SAR imagery for studying northern wetlands and peatlands (Toyra et al. 2001; Toyra and Pietroniro 2005; Li and Chen 2005; Grenier et al. 2007; Li et al. 2007). There have been a number of reviews that discuss the use of SAR in wetland and related remote sensing applications (Pietroniro and Leconte 2000; Ozesmi and Bauer 2002). The contrast in surface roughness between a calm smooth water body and a relatively rough vegetated land surface allows SAR to detect low radar return from water and higher radar returns from land (Lewis A.J. 1998). It is able to penetrate forest and vegetation canopies and provide a return from flooded ground surfaces (Barber et al. 1996; Townshend and Walsh 1998), detect open water extent (Bryan 1981; Toyra and Pietroniro 2005), detect soil moisture (Benallegue et al. 1995; Baghdadi et al. 2002), and aid in the delineation of wetland vegetation communities (Sokol et al. 2004). These characteristics make SAR ideal for applications in wetland environments potentially making it useful for peatland reservoir environments.

Water level fluctuation in wetlands and managed reservoirs is common, and shoreline vegetation is often flooded. Longer wavelengths such as L-band have been shown to penetrate tree canopies in flooded areas (Townshend and Walsh 1998). Long wavelengths are less prone to surface and immediate volume scattering and can penetrate

deep in to forest canopies. Signals are enhanced as a result of dihedral corner reflection, or a double bounce effect off the specular water surface and trunks of flooded trees. Flooded forests show up as bright tones in radar imagery as a result of this characteristic (Ozesmi and Bauer 2002). Townshend and Walsh (1998) utilized JERS-1 L-Band HH polarized and ERS-1 C-Band VV SAR imagery to discriminate between flooded and non-flooded areas in a forested wetland. They found that the JERS-1 imagery was able to distinguish flooded forest stands to a greater degree than ERS-1 imagery. Barber et al. (1996) found C-band HH SAR data was able to discriminate between flooded and non-flooded forest stands along the boundary of a floodplain much better than with ERS-1 C-Band VV imagery. Based on these results, polarization in addition to wavelength and look angle would appear to play a role in the ability of SAR to penetrate forest canopies in order to discriminate between flooded and non-flooded forest. Optical wavelength remote sensing systems often have difficulty discriminating between water laden wetlands and surrounding dry vegetation (Pietroniro and Leconte 2000). The characteristics of microwave systems help discriminate flooded forest and shrub from upland vegetation canopies which are often found along the shorelines of managed reservoirs.

A number of studies have relied on SAR's ability to discriminate open water from surrounding land in wetland or flooded areas (Bryan 1991; Barber et al. 1996; Toyra et al. 2001; Toyra and Pietroniro 2005). A calm water surface acts as a specular reflector of microwave EMR, and therefore there is little return of energy to the sensor. The resulting image will show water as dark homogenous areas, with surrounding land showing a

diffuse scattering response and appearing brighter. There are cases where a normally calm water body becomes roughened by winds thereby increasing radar backscatter.

Single co-polarized SAR images have not historically been successful in discriminating between vegetation communities Sokol et al. (2004) reviewed the study by the CCRS in which they used ERS-2 C-Band VV and RADARSAT-1 C-Band HH imagery to discriminate between bog and fen peatland communities in the Goose Bay, Labrador area of Canada. They found there to be no significant difference in the radar backscatter between bog and fen communities with either the RADARSAT-1 or ERS-2 data. Backscatter from peatland communities decreased with an increase in incidence angle of the RADARSAT-1 data, finding as much as an average 7 dB difference between S1 and S7 (20°-49°).

The use of texture statistics derived from the grey level co-occurrence matrix (GLCM) has shown to improve classification over a single-date tonal image (Barber and LeDrew 1991; Arzandeh and Wang 2002). The GLCM is a two dimensional array that provides the co-occurrence probability of pairs of grey-level pixels within a local window (Haralick et al. 1973). A number of texture measures have been produced with the GLCM they include: mean, variance (standard deviation), homogeneity, contrast, dissimilarity, entropy, angular second moment, and correlation. Arzandeh and Wang (2002) evaluated various combinations of these texture measures to improve classification for various applications with good results for improved discrimination of wetland classes.

In addition multi-polarized SAR data has shown much more promise in discriminating between different wetland vegetation communities. Baghdadi et al. (2001)

found that single HH polarized and cross polarized C-band data were better suited then

VV polarized data for classifying cover types (forested and non-forested peat bog, marsh,

open water, clearing and forest) throughout the growing season in the Mer Bleue region

of Ontario. The study produced overall classification accuracies of 74% for HH

polarization, 76% for cross-polarized and 59% for VV polarization.

CHAPTER 3 : REMOTE SENSING OF A DYNAMIC SUB-ARCTIC PEATLAND RESERVOIR USING OPTICAL DATA

3.1 INTRODUCTION

In this chapter I explore the potential of optical VNIR remote sensing technologies for discriminating floating peatlands in a sub-arctic peatland reservoir. In the past, mapping and monitoring of peatland inundation, upheaval, transport, and breakdown over time has been limited to manual interpretation of low level aerial photography and manual digitization (Ronka & Uusinoka 1976; Grondin and Ouzilleau 1980; Le Groupe Dryade 1984; Belanger et al. 1991; Robert 2000; Manitoba Hydro 2003; Asada et al. 2005; KHLP 2010). Since the first launch of commercially available high-resolution optical satellites, with IKONOS in 1999, mapping from satellite imagery has greatly improved. Objects < 1 m in size can now be accurately mapped through manual or computer assisted interpretation and classification techniques. In this study the QuickBird high-resolution optical satellite, provides broad multi-spectral VNIR image channels at high spatial resolutions. In addition field spectroradiometers can be used to provide detailed spectral information for selected ground targets in order to validate satellite-based remotely sensed imagery to discriminate and map land cover types. To date, no known studies have employed high-resolution optical satellite imagery for discriminating reservoir surface changes related to floating peatland uplift, transport and disintegration dynamics.

The primary objective of this chapter is to determine the visible and near-infrared (VNIR) spectral properties of land cover classes in Stephens Lake, Manitoba to support the development of a best practices approach for discriminating land (i.e. floating peatlands, forested land, and barren land) from water, using a high-resolution optical satellite VNIR imaging sensor. The specific research questions for this chapter are:

1) a) Using a helicopter mounted spectroradiometer can the general spectral VNIR properties of ground samples that comprise dominant land cover types in a sub-arctic peatland reservoir be described?

   b) Does a visual analysis of spectral validation data collected from a helicopter mounted spectroradiometer provide a good indication of whether or not QuickBird high-resolution optical imagery could potentially be used to discriminate reservoir land cover classes?

2) Can each individual band of QuickBird image data be used to detect significant spectral differences within and among the land and water classes?

3) a) Can QuickBird multispectral image data be used to effectively discriminate between the four dominant land cover classes in a sub-arctic peatland reservoir?

   b) Which combinations of QuickBird VNIR image band data are best able to discriminate among the studied land cover classes? Does the inclusion of a derived band ratio variable (NDVI) or a pre-processing multivariate analysis such as principal component analysis (PCA) enhance or limit the ability to discriminate between the four dominant sub-arctic peatland reservoir land cover classes?

3.2 METHODS

3.2.1 Site Specific Study Area

The process of peatland uplift in Stephens Lake began shortly after reservoir filling in the early 1970s (KHLP 2010). Today, the remaining peat island formations occur primarily in the protected back bays of the reservoir, where they are protected from surface wave erosion. Three areas on the west side of Stephens Lake contain large floating peat island formations (Figure 3.1). O'Neil Bay contains a peat island formation in the southeast corner protected by prevailing winds and water current. The islands are dominated by a homogeneous cover of *Carex* spp. (sedge) and small (< 1m) shrubs, primarily *Myrica gale*, with underlying dense carpets of *Sphagnum* spp (peat moss). The fringes of some islands are populated by *Typha* spp. (cattail). Surrounding shoreline areas are dominated by woody debris and willow (*Salix* spp.) and upland vegetation consists of open black spruce (*Picea mariana*) forest. The Ross Wright formation is a large remnant black spruce peat plateau mass that remains anchored to underlying organic and mineral soils. The peat islands are dominated by a homogeneous cover of graminoid species, *Carex* spp. and *Calamagrotis* spp., and ericaceous shrubs co-habiting with dense *Sphagnum* spp. carpets. The third study area, north of Boisvert Island is further out in the open lake, but bordered on three sides by mineral islands. This formation is slightly different than the latter two, showing the effects of water level variation throughout the central portion. It contains small floating bare peat mats upon which the vegetation has died off due to submersion. The living portions of the islands are dominated by *Carex* spp.(sedge) and tall shrub species, primarily *Salix* spp.(willow) and *Myrica gale* (sweet gale).
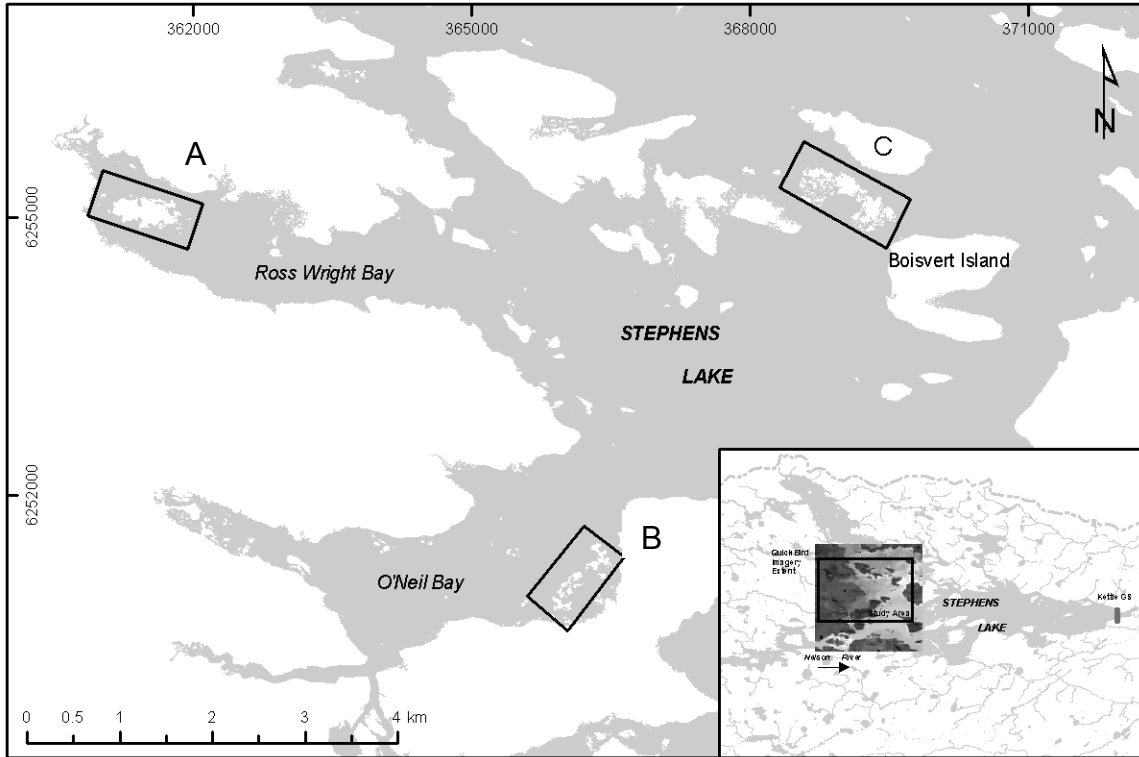
Figure.3.1. Location of the (A) Ross Wright Bay, (B) O'Neil Bay, and (C) North Boisvert Island floating peatland formation study areas in Stephens Lake (Spatial Data Source: Geogratis 1:50K NTDB, (C) Department of Natural Resources Canada).

3.2.2 Data Collection

Field surveys were conducted during 1-8 August 2005 and 2-15 August, 2006. An Analytical Spectral Device (ASD) FieldSpec® VNIR spectrometer was used to collect field relative reflectance spectra in the 350 to 1050 nm optical range of the electromagnetic spectrum (EMS), in wavebands approximately 1 nm in width. A Bell Jet Ranger helicopter was used to collect reflectance spectra at altitudes of ~5.5, 174, 208 metres above ground level (AGL) over selected sample sites. The bare fiber optic cable of the ASD spectrometer was attached vertically to the skid or 'J-Step' of the helicopter. The height variation above the targets was implemented in order to mimic the instantaneous field of view of different optical satellite sensors. At 18 feet AGL the ground field of view (GFOV) of the ASD instrument with a bare fiber optic cable (25°

FOV) is 2.44 m (Figure 3.2). This GFOV is comparable to that of the QuickBird sensor.

Data was collected at 11 different sites representative of water, forested land, and peat

islands. Measurements were taken by positioning the helicopter approximately

perpendicular to the sun's azimuth and maintaining a constant altitude. Each spectrum

consisted of 20 individual measurements taken consecutively and averaged by the

spectrometer. This process was repeated three times for each sample. Due to helicopter

blade rotation shadow and limited access to the helicopter skid/J-Step, it was decided that

white reference calibration using a white reference Spectralon panel would only be taken

prior to lift off and after grounding. Schaepman et al. (1997) used a similar approach.
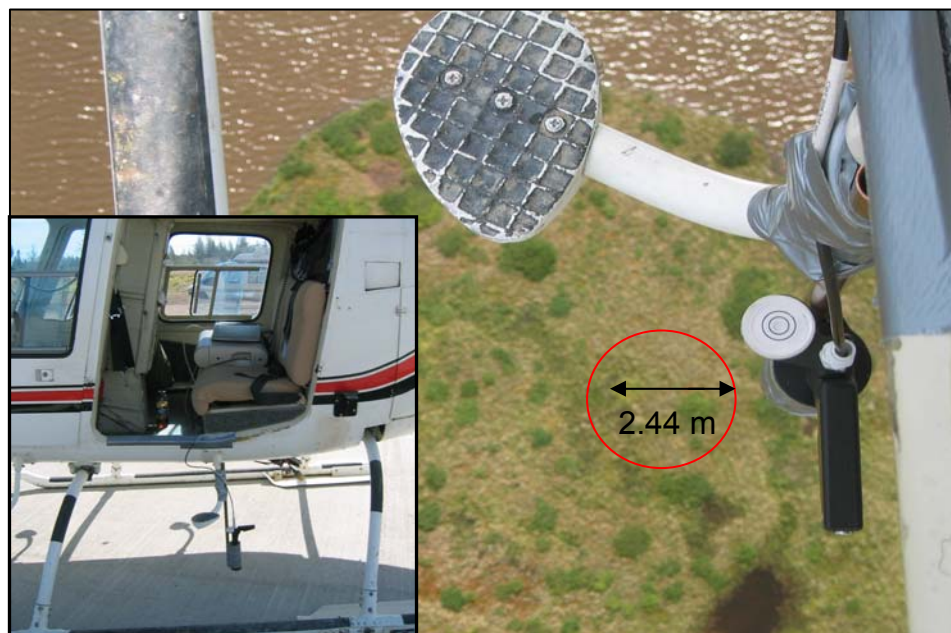
Figure 3.2. Photos of a spectroradiometer attached to J-Step of a Bell Jet Ranger helicopter (left), and a mimicked 2.44 GFOV over a peat island target (right). (Photo credit J. Larter 2006)

Oblique aerial photography and videography were acquired during the helicopter

surveys. A Redhen Systems Inc. GPS linked aerial video camera was mounted to the nose

of the helicopter. Remote controls allow the camera to be operated from within the

helicopter cabin during flight. The photo and video data sets were used to assist in the creation of cover type validation maps for selection of training and validation areas. Due to the variable position of floating peat islands, it was decided that detailed mapping of the study areas in the field, via the use of sub-metre GPS, would not be an advantage. Mapping in the field was completed by drawing on field photo maps and recording sampling locations with a handheld Garmin GPS. Dominant species cover was recorded and mapped in the field.

A 100 % cloud free Quick Bird image was acquired on September 2, 2006 (Figure 3.3) after 7 unsuccessful attempts in 2005 and early 2006.. The QuickBird satellite, launched in 2001, is a sun-synchronous high resolution multispectral optical satellite. It provides high spatial resolution (0.61 m pan and 2.44 m VNIR) combined with relatively broad visible (Blue 450-520 nm, Green 520–600 nm, Red 630-690 nm) and near-infrared (760 – 900 nm) spectral bands. Lake level at time of capture was 140.84 m ASL (Manitoba Hydro Unpublished Data). The image covered a 14 x 14 km area on the southwest corner of Stephens Lake. The image was free of haze and "sun glint" effects. Atmospheric and scene correction were not considered necessary for the purposes of the study as such raw digital numbers (DN) representing relative reflectance were used in the analysis.
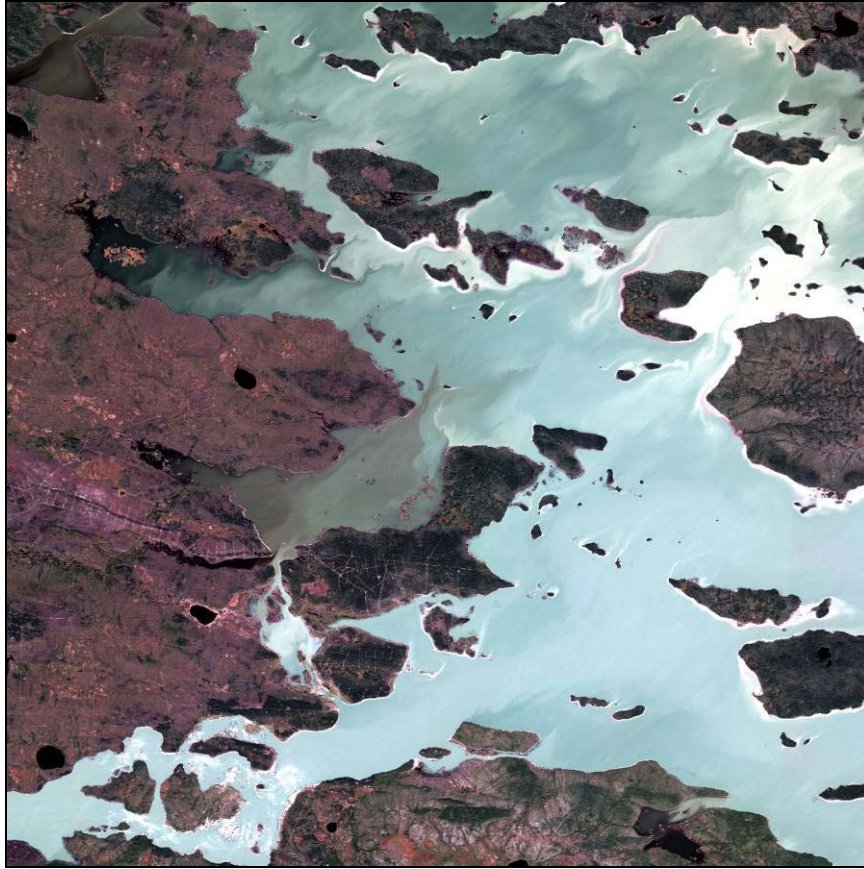
Figure 3.3. QuickBird. VNIR multispectral high resolution image acquired on September 2, 2006. True color image composite is shown. Copyright: DigitalGlobe 2006.

The QuickBird Standard imagery product was processed by Digital Globe to remove radiometric, sensor, and geometric errors. A coarse digital elevation model (DEM) was also applied to normalize for some topographic relief the resulting image was projected to universal transverse mercator (UTM) (WGS 84) with a horizontal precision of +/- 20 m. Terrain distortion was not considered to be a concern in the low relief study area. A geometric shift of 14 m to the west and 2 m to the north was completed so that the image would align with a 2006 panchromatic 0.25 m resolution digital ortho image (DOI) of Stephens Lake, which was provided by Manitoba Hydro. A normalized difference vegetation index (NDVI) band was derived from the ratio of the difference of the red band and the near-infrared band over the sum of the two bands. The NDVI band

was then added back to the original 4 band QuickBird image to make a 5 band image composite.

3.2.3 Land Cover Classes

In this thesis *land cover* refers to the type of features present on the surface of the earth (Lillesand and Kiefer 2000). This includes all land, wetland, and water cover types. A hierarchical classification framework adapted and modified from Anderson et al. (1976) and used by the United States Geological Service (USGS), is used to define the land cover types found in the study area (Table 3.1). Level 1 in the table is the most general classification level and serves as a land and water mask. Discrimination between these two classes is the primary objective of this thesis. Level 2 is derived from the Anderson et al. (1976) Level I classification and includes the 4 dominant reservoir land cover classes (peatland, forested land, barren land, and open water) treated in this research. Level 3 in the table mimics the Anderson et al. (1976) Level II classification. Level 4 in the table is user defined, as is prescribed by the Anderson et al. (1976) Level III classification. Table 3.2 defines the level 2 land cover classes, these classes are pictured in Figure 3.4. Note the variability in water colour (Figure 3.4c) resulting from high total suspended sediment (TSS) content, which forms a turbid water mass and high coloured dissolved organic matter (CDOM) content, which constitutes a brown or humic water mass. The classification structure and class definitions described are used throughout this thesis and form the basis of the GIS based validation map.

Table 3.1. Hierarchical classification of reservoir land cover classes developed for use in this thesis adapted from Anderson et al. 1976.

Level 1 Cover Type	Level 2 Cover Type	Level 3 Cover Type	Level 4 Cover Type
Land	Forested land	Evergreen forest land	Dense coniferous forest Open coniferous forest (upland and peat plateau) Mixed forest
		Transitional forest land	Forest fire regeneration
	Peatland (wetland)	Non-forested peatland	Shrub /typha peatland Graminoid/Ericaceous shrub/Moss peatland
	Barren land	Exposed Mineral Soil/Bedrock Mixed barren land Shore zone transition	Exposed Mineral Soil/Bedrock Woody shoreline debris Shore zone transition
Water	Open water	Reservoir	Brown water Transition mixing water Turbid water

Table 3.2. Definition of level 2 land cover classes used throughout this thesis.

Class	Definition
Forested Land	Forested mineral uplands can consist of jack pine or black spruce dominated stands, and may also contain small clusters of upland Aspen forest stands. Peatland plateau forests contain black spruce - Labrador Tea - lichen communities. Crown closure can be anywhere from closed to open. . Transitional and deciduous cover types are not included.
Peatland/ Peat island	Floating peat islands and aquatic peatlands tend to lack substantial tree cover. They can contain small stunted tamarack or black spruce, however most trees will die off shortly after inundation due to the consistently high water table. Peat islands are dominated by shrub, moss and graminoid species. Moss ranges from Sphagnum where small hummocks remain well above the water table to brown moss where fen communities have begun to dominate due to nutrient rich lake water flow.
Barren Land	Non-vegetated, exposed mineral soil, rock or woody debris shorelines. Tend to have high reflectance across the visible/near infrared spectrum.
Open Water	Water color/clarity ranges from brown (humic), high DOC in organic back bays to high TSS turbid water in the open lake.
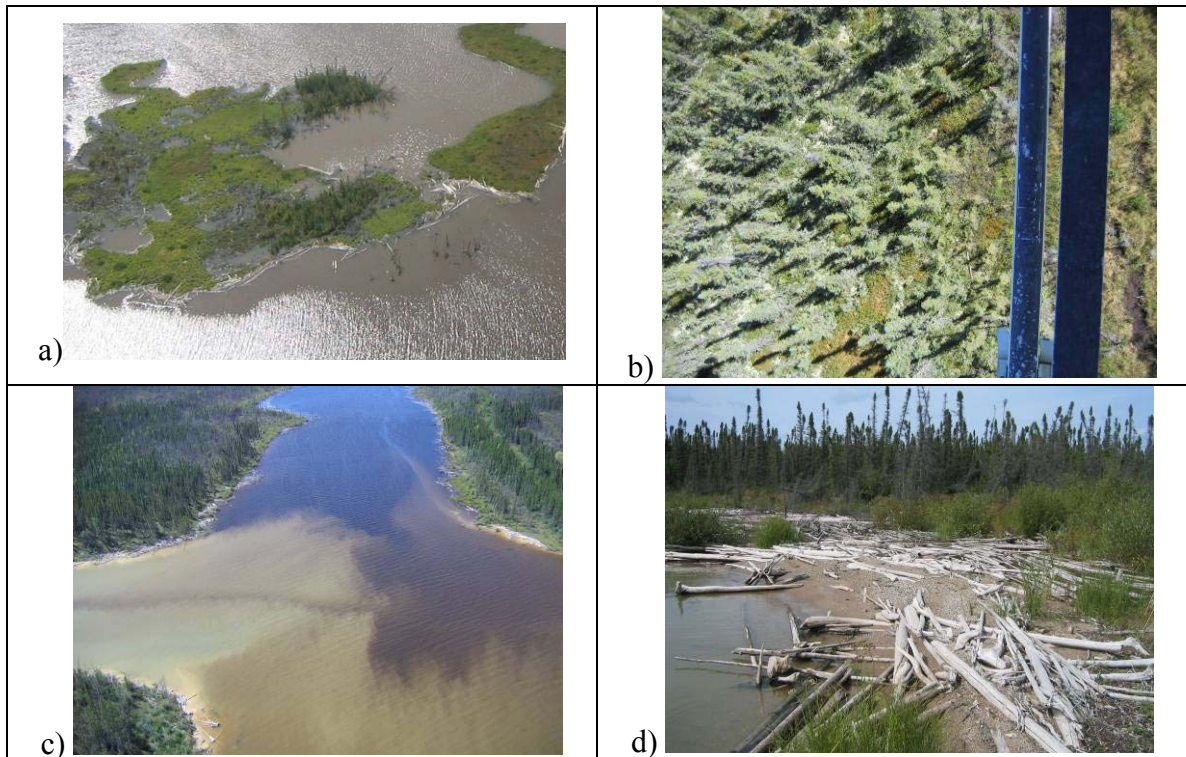
Figure 3.4. Level 2 land cover classes showing a) floating peatland/peat island class; b) forested land class; c) open water class; and d) barren land class.Photo Credit: J.Larter.

3.2.4 GIS Validation Map

In addition to managing all collected validation data, a geographic information system (GIS) was used to develop a validation map in order to select univariate and multivariate model and test sample groups for the QuickBird optical pixel data (Figure 3.5). Photo maps with broad peatland cover types hand drawn during field surveys were digitized using Environmental Research Systems Institute's (ESRI) ArcGIS® 9.2 GIS software. The polygons were manually refined through the interpretation of oblique air photos, geo-located video, and QuickBird optical satellite imagery itself using the panchromatic and combinations of true color and near-infrared false color composite digital images. A simple land and water mask was generated using an image segmentation approach in ENVI® 4.3 (ITT Visual Information Solutions) in order to

spectrally separate land from water in the near infrared band of the Quickbird multi-spectral imagery. The newly created 2 class image was imported into ArcGIS and converted from a raster to a vector GIS format. The land-water vector dataset was intersected with the digitized polygons. Once complete, the digitized and updated polygons were assigned the hierarchical classification structure (Table 3.1). A 2 metre internal buffer was applied to the validation polygons, in order to eliminate the spectral uncertainty between cover type classes where mixed pixels might have been mistakenly included.
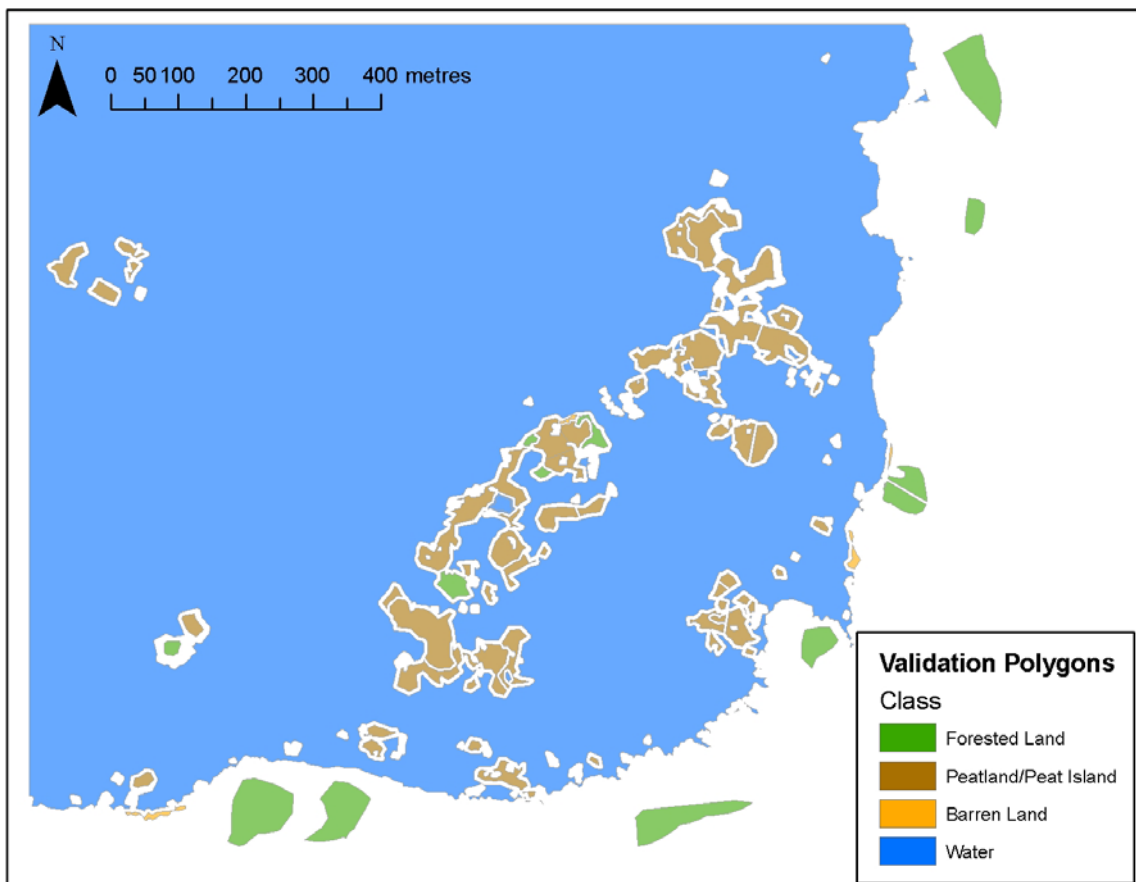
Figure 3.5. GIS-based validation map used for stratified random pixel sampling. The O'Neil Bay study area is shown.

3.2.5 Data Analysis

3.2.5.1 Spectral Reflectance Curve Comparisons

The ASD spectroradiometer averaged 20 samples per reading across the VNIR spectrum of 350 to 1000 nm. At each site 3 readings were taken. The average of the three readings for each class was plotted by percent reflectance, calculated between the target and the white reference, and spectral wavelength. Reflectance spectra collected at sample sites from the air were first plotted in ASD ViewSpecPro and then exported to Microsoft Excel in order to create spectral reflectance curves for comparison of spectral signatures between the broad peatland reservoir cover types. In total 9 different classification level 4 cover types in each of three of the four level 2 land cover classes were sampled. Barren land samples were not identified at the time of the aerial survey. Four peat island cover types included: grass and ericaceous cover, sedge and small shrub cover, sedge and brown moss cover, and tall shrub cover. Two forest samples were taken including: black spruce, and regenerating forest (recent burn). Three open water samples were taken, which included: visibly brown colored (humic) water, visibly turbid and brown mixing water, and visibly turbid water. Reflectance curves were generated by plotting reflectance on the y axis and wavelength on the x axis for selected targets in order to make direct comparisons of spectral signatures. A second relative comparison of spectral reflectance of the land cover classes was conducted by creating univariate box plot graphs of the ASD reflectance values for the spectral ranges of each of the four QuickBird multispectral bands. Direct visual comparisons were made between the different cover types as a precursor step in determining the ability of the relatively wide QuickBird optical bands to spectrally separate the land cover classes of interest.

3.2.5.2 Analysis of QuickBird Data within and Among Land Cover Classes

A stratified random approach to sampling was used to extract pixel DNs from the optical bands of the QuickBird image. ArcGIS was first used to create a regularly spaced grid of points (2.44 m) within the GIS based validation polygons. A per-pixel stratified random sampling approach was then used to select a maximum of 300 pixels for each of the four land cover classes from the three site specific validation areas (O'Neil Bay, Ross Wright Bay, North Boisvert Island) in the GIS. Raw 11-bit DN radiometric data was then extracted from each of the four QuickBird optical bands and derived NDVI band using ArcGIS® Spatial Analyst. The newly created data set was imported into Microsoft Excel ® 2003.

Exploratory statistical analysis was used to identify outliers in the raw optical variable DN samples, and to determine the nature and distribution of the underlying optical variable sample data. Data was analyzed with XLSTAT® (Addinsoft) visualization tools to create univariate box plots for each of the optical variables in order to identify and subsequently remove any outliers that may have been selected during the sampling process. Sites along boundaries between cover classes were eliminated where a mixed pixel effect would have caused confusion between classes.

A number of failed tests for normality (Shapiro-Wilk) and unsuccessful attempts at normalization (square root and log transformation) suggested that a non-parametric statistical technique would be used to test for differences in distributions between land cover classes, an approach consistent with Legendre and Legendre (1998). Remotely sensed data are discrete rather than continuous and are binomially or multinomially

distributed, generally not following a normal distribution (Congalton 1991). Most multivariate data analysis techniques were developed under the assumption that the variables are normally distributed, however most of these methods do not actually require full normality but may perform better with normally distributed data (Legendre and Legendre 1998).

Kruskal-Wallis' H test, similar to the parametric analysis of variance (ANOVA), allows for comparison of $k > 2$ multiple independent samples. In this study the test was used to determine whether or not there were significant differences between like classes from the three study areas for each of the optical variables. The Mann Whitney U test was selected to isolate the source of significant difference or similarity ($P < 0.05$) within classes between study areas. After this test, the predictive capability of a multivariate linear discriminant analysis (LDA) (described below) is used to determine how well each study area sub dataset is able to predict class membership for each of the other two study area's land cover classes.

Kruskal-Wallis' H test was also used to determine significant optical variable differences among the four level 2 land cover of the three study area data sets pooled together.. The Mann Whitney U test was used to make multiple pairwise comparisons between class samples of each optical variable to identify the source of significant difference or similarity ($P < 0.05$).

3.2.5.3 Multivariate Analysis and Classification

A multivariate principal component analysis (PCA) was used as a pre-processing analysis method. PCA acts to reduce dimensionality in the optical variable data, by

summarizing, in the first few dimensions most of the variability within the data set. PCA

does not actually reduce dimensionality in a data set, instead it optimally re-expresses

linear variation along derived (variable weighted) ordination axes (Kenkel 2006). PCA

scores can be used as variable inputs into a multivariate discriminant analysis to

maximally separate desired classes. Although PCA was intended for use with

multinormal data distributions, data with slightly skewed non-normal distributions do not

necessarily bias the result and are considered valid inputs to the analysis (Legendre and

Legendre 1998). PCA was used to reduce dimensionality to three sets of principal

component scores (PCA1-3) for both the 4 QuickBird and 5 QuickBird variable (VNIR +

NDVI) DN data sets.

Linear discriminant analysis (LDA), also known as canonical variate analysis

(CVA), was used with the optical variables to maximally separate the four reservoir

classes. LDA has two main functions, the first is to determine the relative contribution of

explanatory variables to distinction among the *a priori* model classes, and the second is

as a predictive model in order to allocate new objects without class membership to a

known class based on a predictive linear equation (Legendre and Legendre 1998). In this

analysis it is used for both purposes. First, LDA is used to determine the relative

contribution of each optical variable to distinguish among the four cover classes in each

of the three study areas. Secondly it is used as a predictive model to determine how well

each of the three study areas predicts the other. Finally, LDA is used to determine the

relative contribution of explanatory variables to the discrimination of the four level 2 land

cover classes after pooling the data sets. Multiple variable combinations using 33% of the

sample optical variables and computed PCA scores were used to develop the linear

models that maximally discriminate between the four classes. Classification accuracy is assessed with a test group using 66% of the data, which were randomly defined in the GIS based validation map.

Classification accuracy was assessed in all cases using a confusion matrix of producer and user classification errors. Assessment of each model's ability to maximally discriminate between the four broad reservoir classes was completed by comparing overall classification agreement. In addition a KAPPA (Cohen 1960) analysis was used to compute an overall KHAT (K) statistic for each confusion matrix as a secondary comparison of overall classification agreement to identify the combination of optical variables that best separate the four broad reservoir classes. KHAT accuracy, unlike overall accuracy, indirectly includes the off-diagonal elements or errors of omission and commission in the equation and is often seen as a stronger comparison of accuracy of remotely sensed data (Congalton 1991).

3.3 RESULTS

3.3.1 Spectral Comparison of Selected Peatland Reservoir Targets

The four peat island reflectance curves obtained from surface validation with the helicopter based spectroradiometer are visually similar (Figure 3.6a). Peat island class spectra peaked at 550 nm of the visible spectrum for all four samples, and at (900 – 950 nm) of the NIR portion of the spectrum. The sedge/ericaceous shrub sample had the highest relative reflectance (8 %) in the green visible portion of the EMS. The tall shrub peat island sample had the lowest reflectance (5 %) in the green visible portion of the EMS, which separates it from the other three peat samples, indicating spectral variability between islands with greater leaf area and islands that lack significant shrub cover.

The spectral samples of black spruce forest were noticeably different from recent forest fire samples. The spectral reflectance curves (Figure 3.6b) illustrate higher reflectance across the spectrum for the regenerating forest floor over black spruce forest cover, which may be attributed to the bare trunks of dead and fallen trees. The upland regenerating forest floor is dominated by small broadleaf shrubs, graminoids and moss and is more actively involved in photosynthesis than the surrounding mature black forest stands.

The three water classes sampled with the spectroradiometer yield the most variable results across the visible spectrum of the three level 2 classes (Figure 3.6c). The highly turbid water sample has a maximum of 16-17 % reflectance in the 540 – 600 nm range, while the brown water absorbs almost all incident VNIR EMR (< 2 % across the VNIR spectrum). The mixing zone (interface between brown and turbid water) water sample had a peak reflectance of 6-7 % in the 570 – 590 nm range.
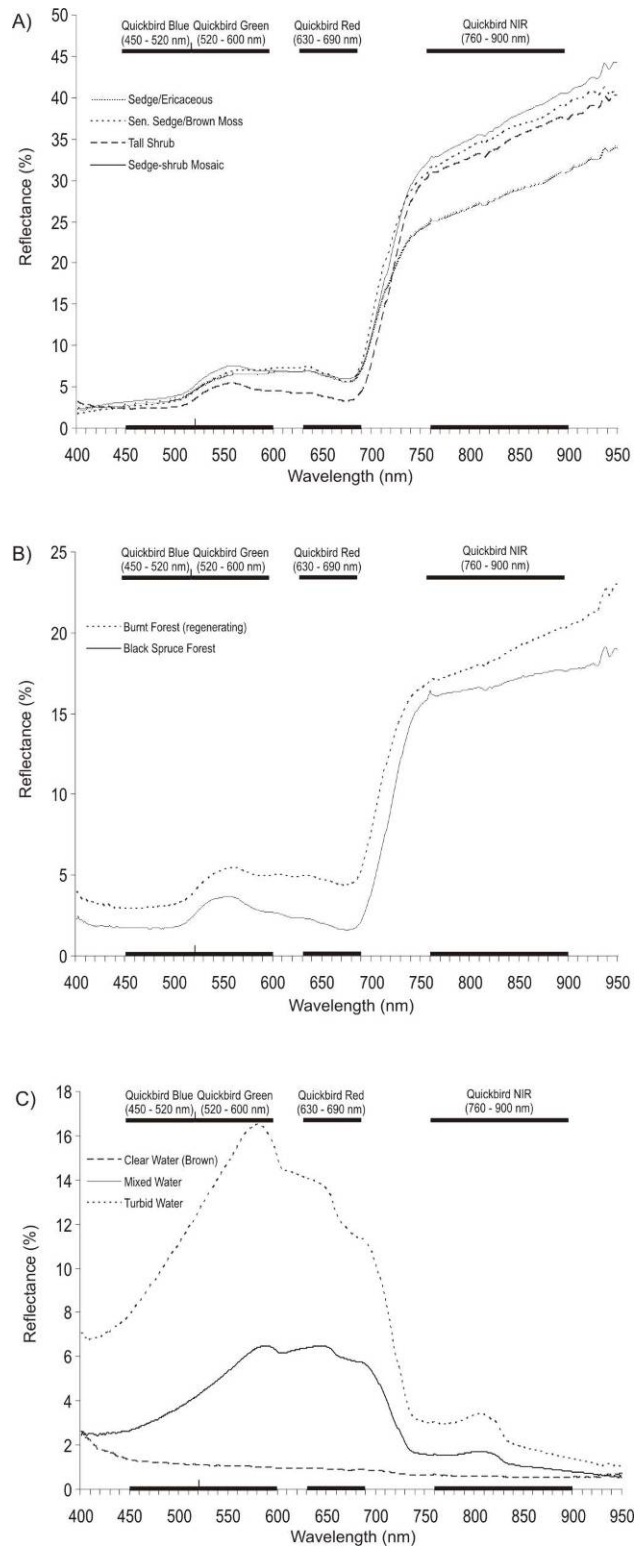
Figure 3.6. VNIR spectral reflectance curves for selected land cover types of A) Peat Island; B) Forested Land; C) Open Water.

Spectral samples from forested land, peat island, and water cover types show good separation in the green visible and NIR spectrum (Figure 3.7). The peat island spectral sample has higher spectral reflectance across the entire VNIR spectrum when compared to forested land and open water.
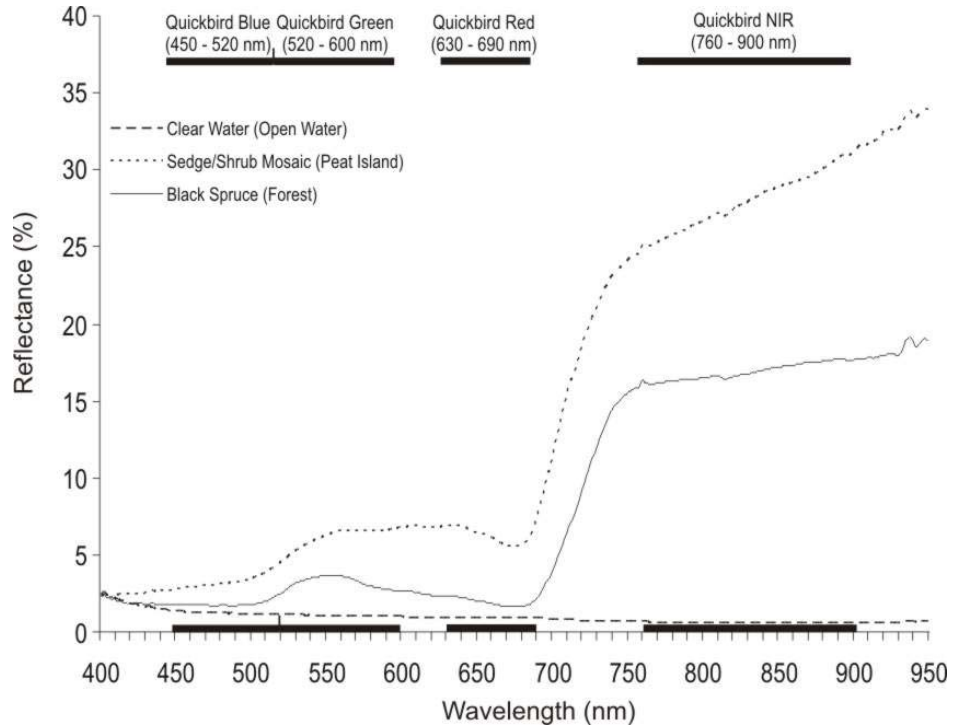
Figure 3.7. A comparison of spectral reflectance curves for typical water, peat island, and forested island land cover types on Stephens Lake.

The spectral samples for each class in the 450 – 520 nm range consistent with the QuickBird blue band are plotted in Figure 3.8a. Of the nine spectral samples taken in the field, only the turbid water class does not overlap with the other eight classes, indicating the visible blue portion is ineffective in separating the level 2 land cover classes of water, peat island and forested land from each other. The QuickBird green spectral range (520 – 600 nm) shows more separation between the classes (Figure 3.8b). The vegetated classes begin to show increased reflectance peaks due to chlorophyll activity, however the mixed
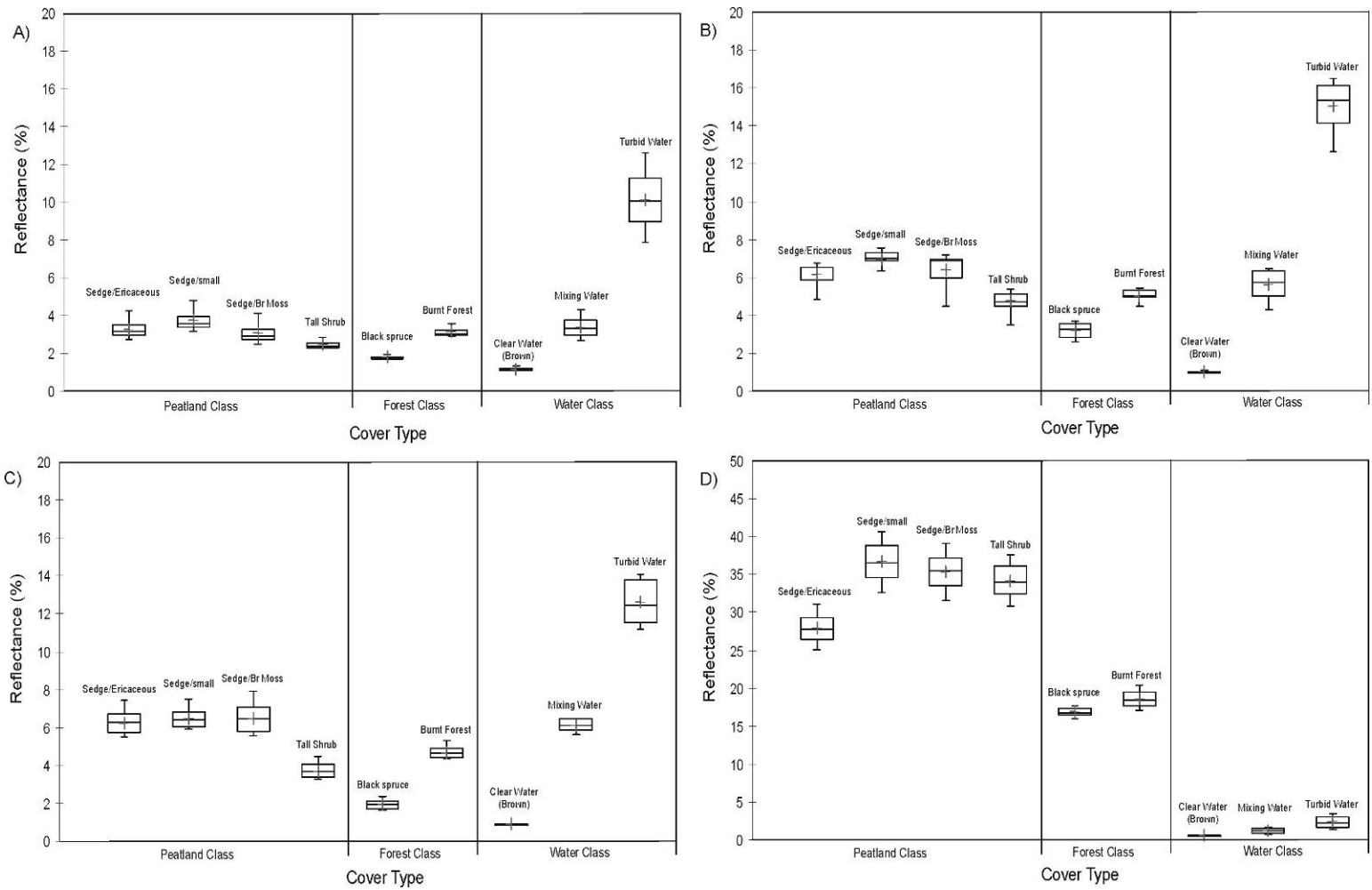
Figure 3.8. Spectral reflectance data of 9 selected cover types of water, peat island and forest land summarized by QuickBird spectral band widths in each of A) blue band (450 - 520 nm); B) green band (520 - 600 nm); C) red band (630 - 690 nm); and D) near-infrared band (760 - 900 nm).

98

water class still overlaps with the vegetated classes due to reflectance caused by suspended sediment in the water column. The red spectral range (630 – 690 nm) plot shows similar results as the green visible band (Figure 3.8c). The red band, a chlorophyll absorption band, shows a small decrease in the overall spectral reflectance for the vegetated samples of the forest and peat island classes. The water classes remain consistent across the three visible bands, with an apparent spectral separation between the three classes in all three visible bands. The NIR spectral range (760 – 900 nm) shows the greatest potential for spectral separation between the three level 2 land cover classes (Figure 3.8d). The red edge effect, NIR EMR interaction with internal leaf structure, causes a significant increase (~ 30 %) in reflectance in the peat island cover classes, while all three water classes absorb almost all incident EMR in the near-infrared portion. The two forest classes fall in the 15 – 20 % reflectance range in the near-infrared portion of the EMR.

Research question 1a was successfully answered, the general spectral VNIR signatures, obtained from a helicopter mounted spectroradiometer, of ground cover types that comprise three of the four land cover types were determined. Peat island spectra, although somewhat variable based on the dominant vegetation cover type, have higher relative reflectance than typical forested land and open water cover types across the entire VNIR spectrum

Research question 1b was answered by determining that when reference spectra are grouped by QuickBird visible band spectral ranges considerable spectral overlap is shown to exist between all peat island and forested land samples as well as the mixed turbid and brown water samples (Figure 3.8a-c). Only the turbid water sample is clearly

separable from the other samples using the visible QuickBird bands. There are clear differences between the three level 2 cover types in the QuickBird NIR (760 – 900 nm) spectral range (Figure 3.7d). The analysis of the helicopter based validation spectra grouped by broad QuickBird spectral band ranges indicates that QuickBird high-resolution optical imagery can potentially be used to successfully discriminate between the broad reservoir classes.

3.3.2 Analysis of QuickBird Data Within and Among Land Cover Classes

Differences in QuickBird band spectral responses within classes were assessed by study area. A non-parametric Kruskal Wallis' *H* test, similar to the parametric one-way analysis of variance (ANOVA), and the Mann Whitney U test (used for post-hoc multiple pairwise comparisons) were used to determine significant QuickBird VNIR spectral data differences within classes across the three study areas. With the exception of the water class, which appears to be highly variable across the visible QuickBird bands, classes appear to be similar across the three study areas in each of the five optical bands (QuickBird 1-4 + NDVI) (Figure 3.9). Results of the statistical tests, however, show significant (Kruskal-Wallis' H test: p = 0.000) within class differences across the three study areas for each of the QuickBird bands (Table 3.3). The exceptions include: forested land between Ross Wright Bay and North Boisvert Island in the red visible band (Mann Whitney: p = 0.436); the peat island class between O'Neil Bay and Ross Wright Bay in the blue band (Mann Whitney U test: p = 0.225) and between O'Neil Bay and North Boisvert Island in the NIR band (Mann Whitney U test: p = 0.506); and the barren land class between O'Neil Bay and North Boisvert Island in the red band (Mann Whitney U test: p = 0.135). This indicates that the QuickBird sensor is detecting subtle differences

related to dominant vegetation (forested land, peat island) or shore zone (barren land)

cover of the land-based cover types between the study areas. The differences in the water

cover class in the visible bands among the three study areas are both visually apparent

and statistically significant (Mann Whitney: $p = 0.000$). These differences are less

distinguishable in the NIR and derived NDVI bands. There is a noticeable gradient of

water color change from Ross Wright, brown (humic) colored water, to North Boisvert,

turbid high TSS open water. Recall that the turbid spectral sample (Figure 3.6c) had the

highest visible spectrum reflectance compared to all other cover type samples. Likewise

Figure 3.9a-c indicates that the North Boisvert open water QuickBird visible DN data has

the highest mean DN.
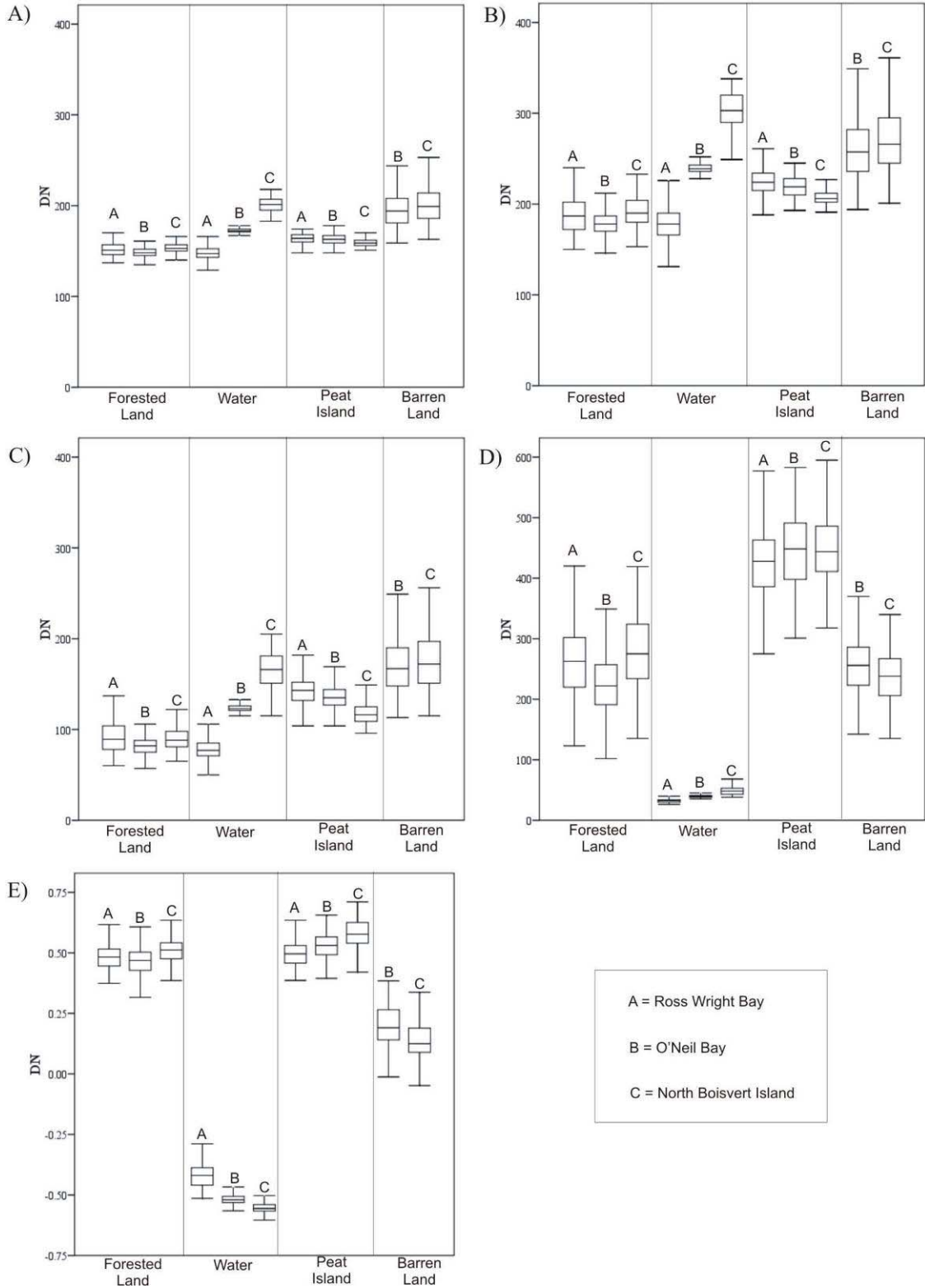
Figure 3.9. Univariate box plot diagrams of the four land cover classes in each of the three study areas showing spectral (DN values) distributions in each of A) QuickBird blue band; B) QuickBird green band; C) QuickBird red band; D) QuickBird NIR band; and E) QuickBird derived NDVI band (Note: DN range different for D) and E)).

102

Table 3.3. Results of statistical comparisons of class distributions within land cover classes between study areas using Kruskal-Wallis' H test, and the Mann Whitney U test non-parametric statistical tests.

| | | | | QuickBird Optical Variables | | | | | | | | | | |
| | | | | Blue | | Green | | Red | | NIR | | NDVI | |
Class	Statistic	Study Area	n	P	Different? (P < 0.05)	P	Different? (P < 0.05)	P	Different? (P < 0.05)	P	Different? (P < 0.05)	P	Different? (P < 0.05)
Forested Land	Kruskal -Wallis'*H*	All	871	0.000	yes	0.000	yes	0.000	yes	0.000	yes	0.000	yes
	Mann-Whitney	ON, RW		0.000	yes	0.000	yes	0.000	yes	0.000	yes	0.001	yes
	Mann-Whitney	ON, NB		0.000	yes	0.000	yes	0.000	yes	0.000	yes	0.000	yes
	Mann-Whitney	RW,NB		0.000	yes	0.009	yes	0.436	**no**	0.004	yes	0.000	yes
Open Water	Kruskal -Wallis'*H*	All	849	0.000	yes	0.000	yes	0.000	yes	0.000	yes	0.000	yes
	Mann-Whitney	ON, RW		0.000	yes	0.000	yes	0.000	yes	0.000	yes	0.000	yes
	Mann-Whitney	ON, NB		0.000	yes	0.000	yes	0.000	yes	0.000	yes	0.000	yes
	Mann-Whitney	RW,NB		0.000	yes	0.000	yes	0.000	yes	0.000	yes	0.000	yes
Peat Island	Kruskal -Wallis'*H*	All	835	0.000	yes	0.000	yes	0.000	yes	0.000	yes	0.000	yes
	Mann-Whitney	ON, RW		0.225	**no**	0.000	yes	0.000	yes	0.003	yes	0.000	yes
	Mann-Whitney	ON, NB		0.000	yes	0.000	yes	0.000	yes	0.506	**no**	0.000	yes
	Mann-Whitney	RW,NB		0.000	yes	0.000	yes	0.000	yes	0.000	yes	0.000	yes
Barren Land	Mann-Whitney	ON, NB	355	0.032	yes	0.025	yes	0.135	**no**	0.000	yes	0.000	yes

With the understanding that there are both subtle spectral differences within the land-based cover classes and large spectral differences within the water cover class, a multivariate LDA (QuickBird bands 1-3 + NDVI) was used to determine the ability of one study area data set to predict the classes in each of the other two study area data sets. Each model was significant (Wilk's λ: p = 0.000) in discriminating among the four classes. The O'Neil Bay LDA model had the lowest predictive capability producing overall classification accuracies of 74.0% (KHAT = 0.607) and 88.5 % (KHAT = 0.847) for Ross Wright Bay and North Boisvert Island respectively. The models built from the Ross Wright Bay and North Boisvert Island study areas, both perform significantly better when predicting the other study area cover type class memberships (Ross Wright KHAT > 0.950 and North Boisvert > 0.90). This would indicate that the O'Neil Bay cover type optical sample set does not account for all of the variability found between the three study areas.

Table 3.4. Overall classification accuracies and KHAT values for each individual study area LDA model predicting the remaining two study area data sets.

LDA Model	Predicted Data Set	Overall Accuracy	KHAT
O'Neil Bay	Ross Wright	74.0	0.607
	North Boisvert	88.5	0.847
Ross Wright	O'Neil Bay	98.0	0.970
	North Boisvert	97.7	0.966
North Boisvert	O'Neil Bay	95.9	0.945
	Ross Wright	95.3	0.929

Results of the pooled study area data show significant differences between the four level 2 land and water classes (Kruskal Wallis' H : p = 0.000; Mann Whitney: p = 0.000) (Figure 3.10, Table 3.5). Spectral overlap clearly exists between the land and water classes in the visible spectrum. The NIR and NDVI band plots show a distinct separation between the land-based and water class, again indicating that they play an important role in discriminating between land and water classes.
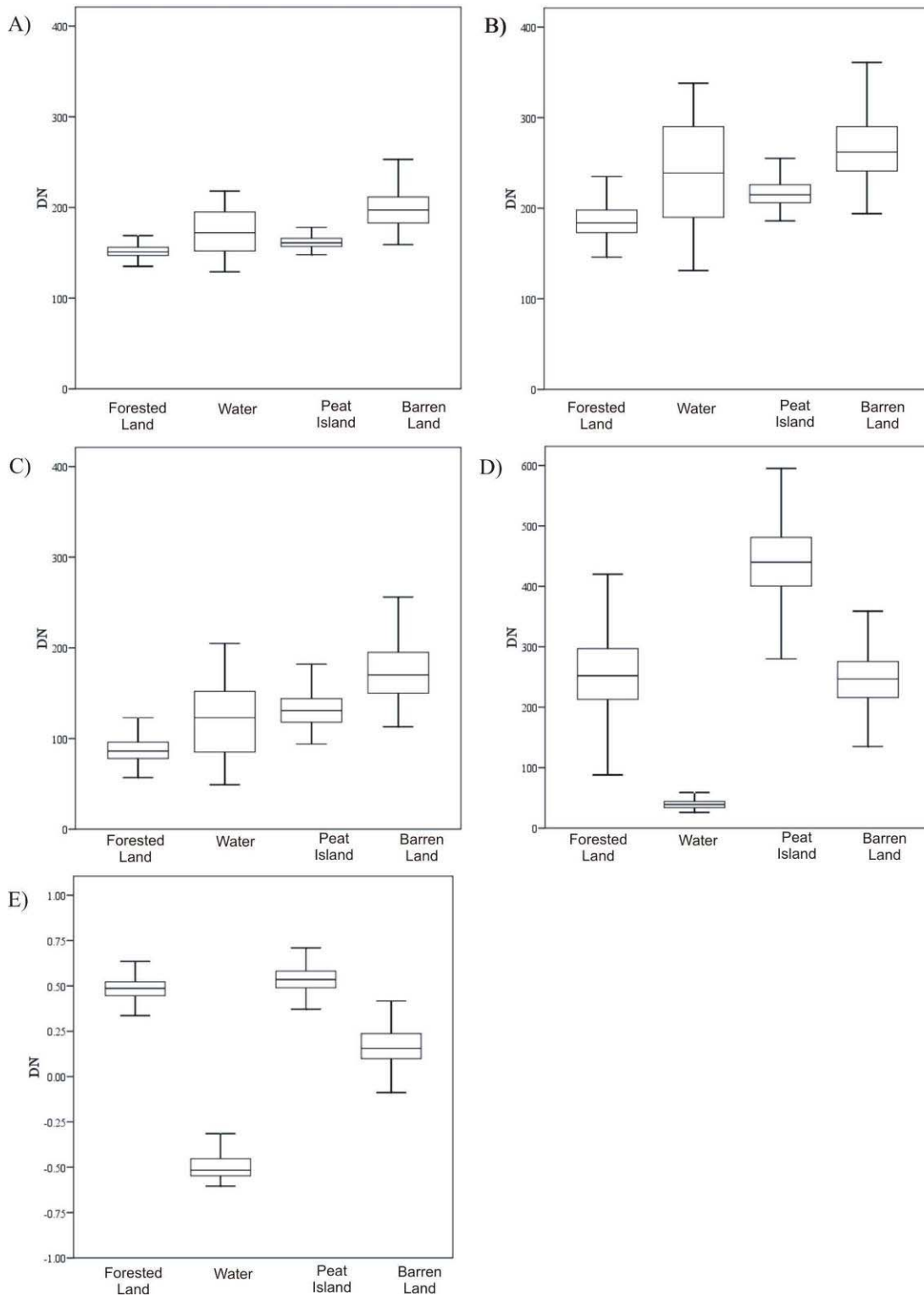
Figure 3.10. Univariate box plot diagrams of the pooled (n =2912) QuickBird spectral pixel data in each of the three study areas for A) QuickBird blue band; B) QuickBird green band; C) QuickBird red band; D) QuickBird NIR band; and E) QuickBird derived NDVI band (Note: DN range different for D) and E)).

106

Table 3.5. Results of statistical tests of QuickBird spectral band differences among the four pooled (n=2912) land cover classes using Kruskal-Wallis' H test, and the Mann Whitney U test.

			QuickBird Optical Variables									
			QB1		QB2		QB3		QB4		NDVI	
				Different?		Different?		Different?		Different?		Different?
Statistic	Class	n	P	(P < 0.05)	P	(P < 0.05)	P	(P < 0.05)	P	(P < 0.05)	P	(P < 0.05)
Kruskal -Wallis' *H*	All	2912	0.000	yes	0.000	yes	0.000	yes	0.000	yes	0.000	yes
Mann-Whitney	Forest, Water		0.000	yes	0.000	yes	0.000	yes	0.000	yes	0.000	yes
Mann-Whitney	Forest, Peat		0.000	yes	0.000	yes	0.000	yes	0.000	yes	0.000	yes
Mann-Whitney	Forest, Barren		0.000	yes	0.000	yes	0.000	yes	0.018	yes	0.000	yes
Mann-Whitney	Water, Barren		0.000	yes	0.000	yes	0.000	yes	0.000	yes	0.000	yes
Mann-Whitney	Peat, Barren		0.000	yes	0.000	yes	0.000	yes	0.000	yes	0.000	yes
Mann-Whitney	Peat, Water		0.000	yes	0.000	yes	0.000	yes	0.000	yes	0.000	yes

Research question 2 was successfully answered by demonstrating that on an individual band basis, QuickBird VNIR data can be used to discriminate between land and water cover types in a sub-arctic peatland reservoir. Subtle within-class differences exist between study areas of the land-based cover classes. It should be noted that the large sample sizes used for the univariate statistical analysis may lead to an overly sensitive result, which indicate these subtle within class differences that might not be experienced with a smaller class size. In some cases the resulting box plot appears to contradict the statistical result. Future studies may use statistical trials with a reduced sample size. High spectral variability was found in the water class (visible bands) related to increased reflectance likely from suspended sediments (turbid water masses) in the open areas of the lake and increased absorption from CDOM and DOC content (humic water masses) in the brown water back bays.

Using the predictive capabilities of LDA, each study area data set was able to predict the class membership of the classes of each of the other two study areas, indicating that the sample sizes adequately represent the spectral variability found in the studied reservoir classes. The QuickBird sensor was able to detect differences across the four land cover classes when they were pooled together, which is apparent when comparing spectral response in the NIR and NDVI bands.

3.3.3 Multivariate Discrimination and Classification

Multiple trials of LDA with different combinations of the pooled optical variables including the derived NDVI and PCA scores all provided significant (Wilk's λ: p = 0.000) discrimination among forested land, peat island, barren land, and water (model n =

933; test n = 1979). By reviewing the absolute value of the standardized canonical

discriminant function coefficients (Table 3.5), we can gain an understanding of the

relative contribution of each individual optical variable to each discriminant axis. The

first LDA trial uses only visible QuickBird bands (QB 1-3). The first discriminant axis is

dominated by the green and red bands, which describes 57.2% of the variance in the

optical data. The second discriminant axis is dominated by the blue visible band. The

next trial (QB 2-4) dropped the blue visible band and added the NIR band. The first

discriminant axis explains 89.4 % of the variance in the optical data, while the green and

blue bands still dominate and the contribution of the NIR band is much greater than the

blue band was in the first trial. This is reiterated in the next trial (QB 1-4), where the blue

band is added back in to the LDA and its contribution remains low on the first axis,

which explains 83.7% of the variance within the optical data. In general all three visible

bands are correlated, with band 1 and 2 being highly positively correlated. The addition

of the NIR band greatly increases the explained variance in the model. The NDVI derived

band is substituted for the NIR band in the next trial (QB 1-3 +NDVI). The first axis

explains 94.4 % of the variance which again is dominated by the green and red visible

bands, with significant contribution from the NDVI band. The scatter plot of scores for

the first two discriminant axes for the LDA of the QuickBird visible bands with the

NDVI band is illustrated in Figure 3.11. The scatter plot shows good separation for this

trial. Removing the blue band and adding the NIR band (QB 2-4 + NDVI) again slightly

increases the variance explained in the first axis (94.5%). By first performing a PCA on

the four QuickBird variables and using the first three resulting scores as inputs to the

LDA, the second PCA variable dominates the first axis, while the first and third PCA

variables describe the remaining 13.1% of the variance on the second discriminant axis. The second PCA score variable trial is a result of a PCA performed on the four QuickBird variables and the NDVI derived band variable. The first and second PCA variables account for 89.2 % of the variance on the first discriminant analysis, while PCA 3 dominates the second discriminant axis.

Table.3.5. Standardized canonical discriminant function coefficients for various band combinations, including the derived NDVI band and PCA scores, of the pooled data set LDA models.

Discriminant Axis	QB 1-3		QB 2-4		QB 1-4		QB 1-3 + NDVI		QB 2-4 + NDVI		QB PCA 1-3 (4 variable)		QB PCA 1-3 (5 variable)	
	1	2	1	2	1	2	1	2	1	2	1	2	1	2
QB1	-0.312	3.209	-	-	0.145	2.224	0.178	1.865	-	-	-	-	-	-
QB2	3.385	-1.355	1.749	1.722	-1.860	-3.117	-1.309	-3.177	-0.947	1.860	-	-	-	-
QB3	-3.374	-1.296	-1.405	-2.543	1.376	1.572	1.631	1.929	2.223	-1.386	-	-	-	-
QB4	-	-	-0.977	0.241	0.982	-0.127	-	-	-1.187	-1.334	-	-	-	-
NDVI	-	-	-	-	-	-	1.147	-0.077	2.017	0.718	-	-	-	-
PCA 1 (4 Var)	-	-	-	-	-	-	-	-	-	-	0.496	0.914	-	-
PCA 2 (4 Var)	-	-	-	-	-	-	-	-	-	-	-1.194	0.024	-	-
PCA 3 (4 Var)	-	-	-	-	-	-	-	-	-	-	0.392	-0.854	-	-
PCA 1 (5 Var)	-	-	-	-	-	-	-	-	-	-	-	-	2.019	-0.061
PCA 2 (5 Var)	-	-	-	-	-	-	-	-	-	-	-	-	-1.994	-0.292
PCA 3 (5 Var)	-	-	-	-	-	-	-	-	-	-	-	-	-0.754	0.952
% Variance	57.2	33.7	89.6	10.2	83.7	12.6	94.4	3.8	94.5	4.1	85.6	13.1	89.2	8.6
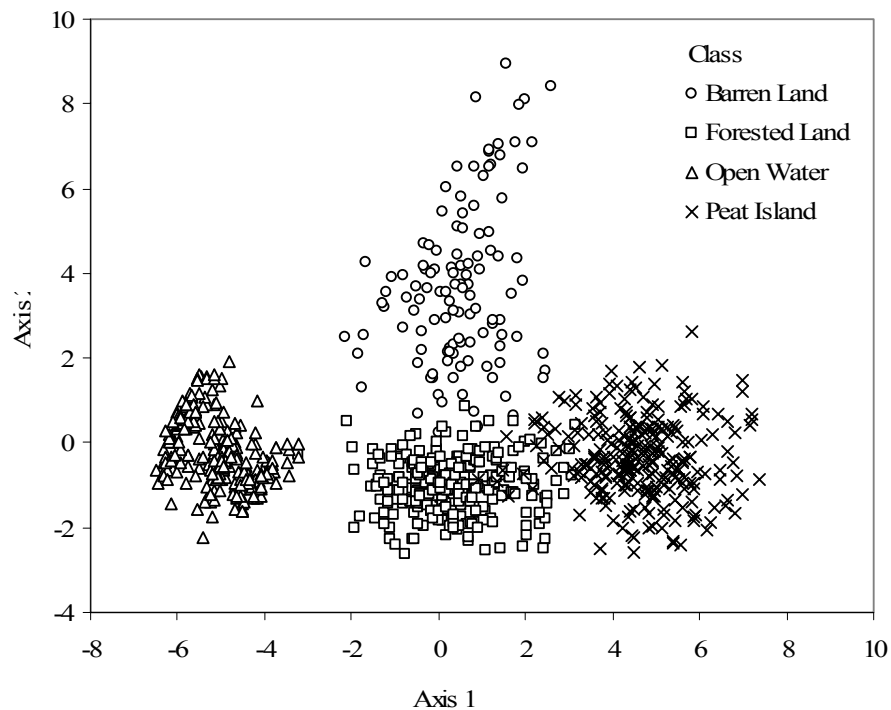
Figure 3.11. Scatter plot of discriminant axis scores of the pooled data set LDA model of the visible and NDVI variable combination.

110

With the exception of the LDA using only the visible QuickBird bands (Overall = 84.4

%; KHAT = 0.786) all LDA trials had excellent classification agreement (Overall > 96.9

%; KHAT > 0.936) (Table 3.6). Test group KHAT results were close (within 0.016) to

the model's KHAT, indicating the sample size (33% of the data) was sufficient in

accounting for the majority of variance within the entire sample set. The addition of the

NIR QuickBird band illustrates the importance of having at least one pair of non-

correlated variables in the LDA. Open water is misclassified when a NIR band does not

exist. This is likely due to areas where suspended sediments are reflecting high amounts

of visible light back to the sensor, whereas the NIR wavelengths are heavily absorbed by

water and reflected by vegetation. Recall Figure 3.8, which showed that brown coloured

water has similar spectral properties to black spruce forest stands in the visible spectrum.

Water, regardless of its suspended sediment content, absorbs almost 100 % of NIR EMR.

Conversely healthy vegetation reflects large amounts of NIR light. These properties make

the NIR band invaluable in discriminant models. The inclusion of the NDVI derived band

has a similar effect to the NIR band, which results in excellent discrimination (Overall =

98.1 %, KHAT = 0.974). The NDVI band accentuates the large vegetation reflection

difference between the red visible band (primarily absorbed due to photosynthetic

activity) and the NIR band (internal leaf structure reflectance). The introduction of the

NDVI band works well when only visible bands are present in the discriminant model;

however the NDVI band has a similar effect to adding the NIR band to the discriminant

model. When the NDVI band is added to a combination of the green, red and NIR bands,

classification agreement is reduced. The QuickBird visible (bands 1-3) and NDVI

combination had a marginally better classification result. This resulted in the least

amount of spectral confusion between cover type classes (Table 3.7). A minimal amount

of misclassification occurred between peat island and forested land cover types, which is

visually evident in the scatter plot of discriminant function scores (Figure 3.11). The PCA

score variable trials also perform well and have high accuracies (4 variable PCA: 97.8%,

K = 0.970). However there was no increase in classification agreement over other trials

by first subjecting the QuickBird VNIR spectral data to a PCA. Reduction of

dimensionality in a data set is likely more useful in an optical remote sensing system that

has a greater number of spectral bands.

Table.3.6. Classification and accuracy assessment results for the combinations of QuickBird band LDA models.

Study Area/ Data Set	LDA QuickBird Variables	# of Variables	Overall Model/Test Agreement (%)				Test Class Agreement (%)				Test Samples
			Model Overall	Model KHAT	Test Overall	Test KHAT	Forested Land	Open Water	Peat Island	Barren Land	
Pooled	Bands 1 - 3	3	85.5	80.1	84.4	78.6	88.4	71.8	88.9	94.5	1979
	Bands 1 - 4	4	98.4	97.8	98.1	97.4	96.6	99.5	97.9	98.7	1979
	Bands 1 - 3 + NDVI	4	97.9	97.1	98.1	97.4	96.3	100.0	97.9	98.7	1979
	Bands 2 - 4	3	97.8	96.9	98.0	97.2	96.6	99.5	98.1	97.5	1979
	Bands 2 - 4 + NDVI	4	97.1	96.0	97.3	96.3	93.6	100.0	97.7	98.7	1979
	4 Var PCA 1-3	3	97.3	96.3	97.8	97.0	95.4	99.8	98.1	98.3	1979
	5 Var PCA 1-3	3	97.2	96.2	96.9	95.8	93.9	99.8	96.3	98.7	1979

Table 3.7. Complete confusion matrix for the LDA model using the combination of the QuickBird visible and NDVI bands.

	Barren Land	Forested Land	Open Water	Peat Island	Row Total
Barren Land	235	2	0	1	238
Forested Land	3	571	0	19	593
Open Water	0	0	579	0	579
Peat Island	1	11	0	557	569
Column Total	239	584	579	577	1979

Producer's Accuracy
Barren Land = 235 / 239 = 98.3%
Forested Land = 571 / 584 = 97.8%
Open Water = 579 / 579 = 100.0%
Peat Island = 557 / 577 = 96.5 %

User's Accuracy
Barren Land = 235 / 238 = 98.7%
Forested Land = 571 / 593 = 96.3%
Open Water = 579 / 579 = 100.0%
Peat Island = 557 / 569 = 97.9%

Overall Accuracy
= 1942 / 1979 = 98.1%

KHAT
= 0.974

Research question 3a was answered by demonstrating that QuickBird high-resolution optical VNIR imagery provides excellent classification results, when peat islands are discriminated from the other level 2 land cover classes in using LDA.

Research question 3b found that the combinations of QuickBird image bands that best discriminate among the four level 2 classes are the combination of the 4 VNIR QuickBird bands, and the combination of the QuickBird visible bands (1-3) plus the derived NDVI band (Overall = 98.1 %; KHAT = 0.974). Secondly, the inclusion of a derived NDVI band to enhance discrimination is most effective when added to correlated visible bands, however no increase in classification accuracy, when compared to a classification using the 4 QuickBird VNIR variables alone was observed. The effect of the NDVI band is similar to that of the NIR band, as it is derived from the red and NIR bands. Performing a PCA data reduction of the QuickBird VNIR bands prior to LDA, did not improve nor substantially hinder classification accuracy.

3.4 DISCUSSION

This study demonstrated that the distinct spectral characteristics of vegetation communities of floating peat islands allow for optical discrimination from other broad land cover classes. A distinguishing feature of floating peat islands is the noticeable lack of living tree cover. Initial flooding will tend to cause almost all tree species to become chlorotic and die (Asada et al. 2005). The consistently high water table ensures that most tree species are unable to reestablish themselves. Vegetation communities eventually adjust to the water level changes and transform from bog communities to fen and marsh communities (Asada et al. 2005). In boreal and subarctic eco-zones this characteristic makes floating peat islands distinguishable from a forested mineral and anchored peat plateau bog islands. The unique spectral characteristics of the surrounding open water allow peat islands to be distinguished from water in addition to surrounding mineral and peatland forest.

The spectral variability of water becomes an important consideration when using an optical remote sensing system to discriminate between land and water features in a reservoir. Some reservoirs are susceptible to extensive mineral shoreline erosion (Saint-Laurent et al. 2001). Mineral erosion leads to increased suspended sediments of clay and silt shoreline materials in the water column. Terrestrial inputs from local peatland watersheds can result in increased colored dissolved organic matter (CDOM), resulting in brown colored humic water. Fluctuations in the concentrations of CDOM, total suspended sediments (TSS), and chlorophyll, can cause water bodies to reflect and or absorb varying amounts of VNIR electromagnetic energy (Vertucci & Likens 1989; Han 1997; Doxaran et al. 2002; Karaska et al. 2004).

The color and clarity of water range greatly within Stephens Lake. The back-bay inlets to O'Neil and Ross Wright Bays contain higher concentrations of DOC and CDOM, resulting in a brown humic water mass that absorbs large amounts of VNIR EMR (Cooley et al. 2009). As you move east towards the middle of the bays you can see a distinct mixing of high DOC brown water and moderately high TSS turbid water of primarily suspended silt sediment. As TSS increases in these mixing zones so does the amount of scattered incident visible and near-infrared EMR. Lodhi et al. (1997) and Han (1997) found a distinct increase in reflected visible light with increase in the amount of suspended soil content under experimental conditions. Han (1997) noted that the linear relationship between reflectance and suspended sediment concentration increased with wavelength between 400 and 900 nm and a near linear relationship was found between 720 and 900 nm. Lodhi et al. (1997) determined differences in soil size (clay vs. silt) equated to an approximately 10 % reflectance increase in silt sediments versus clay sediments. They equated a peak reflectance of approximately 14 % at around 680 nm (red/near-infrared interface). Han (1997) measured a peak reflectance of 23 % at approximately 620 nm. In this study peak reflectance for turbid waters reached 16 % at 580 nm. Whereas humic or high CDOM back bay inlets showed no more than 2 % reflectance across the VNIR spectrum. In this study, the water class was found to have high within-class variability in the visible bands between the three study areas. The helicopter based validation spectra confirmed this high degree of variability. Moderately turbid water can be confused with peat island and forested land spectra within the visible spectrum. The addition of the NIR band allows even highly turbid water to be well separated from land-based classes. Even after pooling the highly variable water classes,

the separation in the NIR band was evident. The problem of visible spectral confusion between turbid water masses and some land-based cover classes should be considered when applying a multispectral land cover classification to reservoirs with turbid waters.

This study employed the use of a helicopter-mounted spectroradiometer to gather large amounts of spectral validation data quickly over the reservoir. Helicopters have been used in past studies to take spectral measurements over forest canopies and water bodies (Loechel et al. 1996; Schaepman et al. 1997; Nichol et al. 2000; Walthal et al. 2001). Reflectance measured from forest sites may vary with solar illumination angle, viewing angle, under storey or background reflectance and atmospheric effects, as well as intrinsic canopy parameters such as phytomass and leaf area index (LAI) of the dominant species (Nichol et al. 2000). Schaepman et al. (1997) have identified the culmination of these factors as contributing to the adjacency effect. This study did not account for these parameters, and instead compared spectral reflectance in a relative sense to determine separation land and water classes throughout the VNIR EMS. Due to the variable nature of sediment plumes and water masses in the reservoir, future studies may want to consider collecting spectral measurements in tandem with water chemistry samples in order to link airborne spectral reflectance with sediment concentrations.

In this study VNIR spectral data from a spectroradiometer or a high-resolution optical sensor, to readily separate land from water. This provides insight into the use of optical VNIR data for the mapping and monitoring of land and water boundary changes over time in a dynamic peatland reservoir.

3.5 CONCLUSION

Spectral VNIR data collected from a helicopter-mounted spectroradiometer was successful in determining the relative reflectance properties of selected water, floating peatland, and forested land cover types (question 1a). The ability to validate several, normally inaccessible, cover types in a short period of time was important to gaining an understanding of their VNIR spectral properties. The spectral properties of peat islands were found to be sufficiently unique across the VNIR spectrum compared to other dominant land cover types in Stephens Lake. A visual assessment of selected cover type validation spectral reflectance curves collected from the helicopter-mounted spectroradiometer provided a good indication of potential land and water discrimination using broad spectral channels of high resolution optical imagery (question 1b).

Research question 2 demonstrated that QuickBird VNIR data can be used to discriminate between land and water cover types in a sub-arctic peatland reservoir on a band by band basis. The NIR band and derived NDVI band appeared to be the most adept at separating the land and water classes. Spectral VNIR differences within the land-based classes of forested land, peat island and barren land among the three study areas, were found to be statistically significant., However, visual comparisons of within-class spectral VNIR distributions were found to be similar and warranted, pooling of the data across the three study areas. Subtle spectral differences were found to exist in both the peat island class, likely attributable to variable vegetation composition (i.e. fen vs. bog community), and the forested land class, likely attributable to stand density variability (i.e. dense vs. open canopy). High spectral variability was found within the water class between study areas, which can likely be explained by the variability of water masses within Stephens

Lake (turbid vs. brown). To illustrate that each study area data set included enough samples to cover the spectral variability within the reservoir an LDA model was used to demonstrate whether or not the spectral samples of land cover classes in one of the three study areas could successfully predict the class membership of the other two study areas with some degree accuracy. The O'Neil Bay data set had the lowest classification accuracies for the other two study areas.

Research question 3a and 3b addressed the potential of the QuickBird multispectral variables to discriminate the four cover classes in an LDA for the three study areas pooled together, including the derived NDVI variable and transformed PCA score variables. All combinations of QuickBird VNIR variables with the exception of the visible bands alone (KHAT = 0.786) had excellent (KHAT > 0.958) classification results. The combination of the four VNIR QuickBird bands and the visible bands with the NDVI band both performed slightly better (KHAT = 0.974) than the other combinations. The inclusion of the derived band ratio variable (NDVI) had a similar result to leaving the NIR band in the model. The PCA score LDA models performed well (KHAT = 0.970 and 0.958), however slightly better results were achieved with the untransformed QuickBird bands.

This chapter has achieved the overall objective of successfully determining the ability of a high resolution optical sensor (QuickBird) to discriminate between land (i.e. forested land, floating peatland, and barren land) and water in a sub-arctic peatland reservoir.

CHAPTER 4 : REMOTE SENSING OF A DYNAMIC SUB-ARCTIC PEATLAND RESERVOIR USING SYNTHETIC APERTURE RADAR DATA

4.1 INTRODUCTION

In this chapter I explore the use of synthetic aperture radar (SAR) as a tool for discriminating land (forested land, peat islands, barren land) from water in a sub-arctic peatland reservoir. Specifically I look at microwave scattering properties of peat islands, forested land, open water and barren land with respect to variable environmental conditions during data acquisition, imaging parameters, and the effects of coherent fading. I look at the implementation of SAR image texture statistics to improve single-date imagery target discrimination. Imaging radars have an advantage over more frequently used optical systems. They are active systems, providing their own source of electromagnetic radiation (EMR) allowing acquisition day or night. The longer wavelengths in the microwave portion of the spectrum can penetrate cloud cover, enabling a flexible image acquisition schedule.

Local incidence angle, surface roughness, and dielectric constant are the three primary factors influencing radar return to the sensor (Raney 1998). These are different considerations than the EMR interactions with optical sensors. Generally, an increasing sensor incident angle will result in decreased reflectivity from distributed scatterers (Lewis and Henderson 1998). Water surface waves are known to increase backscatter thereby decreasing scene contrast in the subsequent image (Bryan 1981). Rainfall events during data acquisition, known as rain shadow, can cause increased backscatter (Raney

1998). Surface materials dampened from recent rainfall increase the dielectric properties of materials, resulting in increased backscatter (Leckie and Ranson 1998).

Active and passive sensors operate in different ways. Single-polarized SAR images only have one image channel and lack the spectral variability that multi-band optical images possess, which can make discrimination of land cover targets difficult. The use of image texture for land cover discrimination relies on spatial heterogeneity in the absence of spectral variability. This study employs the use of texture statistic bands derived from the Grey Level Co-occurrence Matrix (GLCM), in order to improve discrimination of land and water classes.

The primary objective of this chapter is to describe the microwave scattering characteristics of land cover classes in a hydroelectric reservoir with respect to the considerations above, in order to aid in the development of a best practices approach to discriminating land including forested land, floating peatlands, and barren land, from water in a dynamic reservoir using a SAR imaging sensor. The specific research questions for this chapter are:

1) What are the radar backscattering characteristics of land (forested land, floating peatland, barren land) and what factors may influence radar reflectivity?

    a) Are there significant differences in within-class radar reflectivity between the three floating peatland formation study areas?

    b) Are there significant differences in within-class radar reflectivity related to varying weather conditions between RADARSAT-1 image acquisitions?

    c) What effect does sensor incident angle have on within-class radar reflectivity?

d) Are the radar returns from each of the four studied classes (after pooling between study areas) sufficiently different to discriminate among them?

2) Does the use of texture statistics derived from the GLCM aid in the discrimination of land and water cover classes in single band imagery?

a) Do individual texture statistics derived from a RADARSAT-1 SGX image provide sufficient information to discriminate between peat island, forested land, open water and barren land cover classes in a sub-arctic reservoir?

b) What combinations of texture statistics derived from the GLCM provide the best discrimination between peat island, forested land, open water, and barren land cover classes in a sub-arctic reservoir? Does the use of PCA scores derived from the texture statistics provide a better classification result?

3) Is classification improved when discriminating between land and water only? Would RADARSAT-1 fine beam mode SAR imagery make an effective land and water masking tool?

4.2 METHODS

4.2.1 Data Collection and Processing

RADARSAT-1 C-band, HH polarized fine beam mode single look SGX data was acquired for the study area from RADARSAT International (RSI) during the summer (July-August) months in 2005 and 2006 (Table 4.1). In total four images covering the range of available incident angles (F1N-F5F) were acquired. The image data covered the O'Neil Bay, Ross Wright Bay and North Boisvert Island study areas defined in Chapter 3 (Section 3.2.1, Figure 3.1). Due to the scale at which boundaries needed to be discriminated it was decided that the fine beam data, with a 3.125 m pixel size (8 m radar resolution), would be the most suitable. The fine beam data is processed using Nyquist sampling criteria, in order to achieve the increased pixel resolution. The fine beam SGX image product retains all of the information of the fine beam SGF (6.25m) image product, however the volume of data is quadrupled (RSI 2000).

Table 4.1. RADARSAT-1 fine beam SGX data acquisition date, time, and weather conditions during acquisition, acquired for the study. Source: National Climate Archive, Environment Canada (www.climate.weatheroffice.ec.gc.ca).

								Environment Canada Data (Gillam Airport)	
Beam Mode	Orbit	Date	Time CST	Water Level (m ASL)	Weather Conditions	Precipitation 24hr (mm)	Wind Speed (km/h)	Wind Direction (deg)	Wind Direction	Observed Lake Conditions
F2N	Desc	8/4/2005	7:32 AM	141.10	Cloudy, Drizzle, Fog	<1	22	270	W	Rough, white capping, gusts to 35
F2N	Desc	7/30/2006	7:31 AM	141.03	Mainly clear	0	5	340	NNW	Calm water
F5F	Desc	8/13/2006	7:23 AM	140.96	Mainly clear	3	17	210	SSW	Mostly calm, small waves
F1N	Desc	8/16/2006	7:35 AM	140.94	Mainly clear	0	19	200	SSW	Mostly calm, small waves

The Environment Canada weather station at Gillam airport (30 km east) was used to provide accurate weather readings during the times of image acquisition. Field notes were also taken for local water conditions during the times of image capture. During the

acquisition of the first RADARSAT-1 image (August 4, 2005), poor weather conditions were noted (Table 4.1) and confirmed by Environment Canada data (2005). The water surface on Stephens Lake was rough with white caps in open areas, and light rain had preceded image capture. The other three image acquisitions had relatively calm weather conditions in comparison to the August 4, 2005 image.

Radar backscatter coefficient (σ°), the most common measure of SAR reflectivity and expressed in decibels (dB), was calculated from the raw CEOS format DN amplitude images in the ENVI 4.3 (ITT 2008) environment. Relative (within image) calibration is said to be on the order of +/- 1 dB, while absolute calibration (between images) has been said to be on the order of +/- 2 dB (Vachon et al. 1997). These calibration values were used for comparison between multi-date SAR fine beam images (Cooley and Barber 2003).

A bilinear 3rd order polynomial transformation model was used to warp each of the RADARSAT-1 fine beam SGX image subsets to a common Universal Transverse Mercator (UTM) (NAD 83) zone 15 projection using ENVI 4.3. Forty well spaced ground control points (GCPs) were used to transform the RADARSAT-1 fine beam images. The Root Mean Square Error (RMSE) of the models for the 4 SAR images fell below 1.00 ranging from 0.84 to 0.99 of a pixel unit. The bilinear interpolation technique uses a distance weighted average of the digital numbers (DNs) of the four nearest pixels (Mather 2004). Raney (1998) advises against the use of a nearest neighbor interpolation when geometric correction of SAR imagery is deemed necessary, as this routine leads to image artifacts and distorted image statistics. A bilinear or cubic convolution interpolation is considered more applicable for applications that utilize SAR data.

A per-pixel stratified random sampling method was utilized to select representative samples of floating peatland, forested land, open water, and barren land cover classes. A regularly spaced grid of points at a distance of 3.125 m was generated for each of the three study areas using ArcGIS® 9.2. The GIS based validation map developed in Chapter 3 (Section 3.2.4) was used to select a maximum of 300 well spaced random sample sites for each of the four broad cover classes in each of the three study areas. SAR backscatter ($\sigma°$) data was extracted from each of the four fine beam images and placed into a database managed with Microsoft Excel. Exploratory statistical analyses were conducted with XL Stat 2006 (Addinsoft) and SPSS 15.0 to determine class distributions for selection of appropriate statistical measures.

4.2.1.1 Adaptive Filtering

Speckle, or coherent fading, is a consequence of coherent illumination of a SAR imaging system (Raney 1998). Speckle is evident in image data as a salt and pepper effect in areas which should otherwise appear to be visually homogenous. It is tempting for users of SAR imagery to remove the effects of speckle from the image. Speckle suppression techniques have been well studied (Frost 1981; Lee 1986; Kuan 1987; Hirose et al. 1989). The tradeoff to the removal of speckle is a loss of scene texture, which is thought to be an important component of scene information. There are two categories of speckle suppression techniques. The first involves multi-look processing on board the instrument, the second involves filtering techniques performed using image processing software (Lee 1986). This study uses the latter method by applying adaptive filters available in the image processing software package ENVI 4.3 to suppress speckle while

preserving the texture of relatively homogeneous land cover classes of peat island, open water, forested land, barren land and their edges, within the SAR image. For comparison purposes, a filter size of 3x3 was used for all filtering techniques. The six adaptive filters used include the Lee, Enhanced Lee, Frost, Enhanced Frost, Gamma, and Local Sigma. In order to evaluate the effectiveness of the six filters for this study a measure of speckle suppression performance had to be selected. The *Speckle Suppression Factor* (Xie et al. 1999) is used to measure SAR speckle suppression in homogeneous areas (Equation 4.1):

$$F = \left(\frac{S}{S_F} \right)^2 \qquad\qquad (4.1)$$

Where F is the SAR suppression factor calculated by dividing the normalized standard deviation (ratio of standard deviation to mean) of the homogeneous pixels in the original image S, by the normalized standard deviation of the homogeneous pixels in the filtered image S_F. The higher the suppression factor value the greater the performance or ability of the adaptive filter to suppress speckle. The RADARSAT-1 F2N image acquired July 30, 2006 was used to test the performance of the adaptive filters. A random sample of 90 3x3 pixel (n=810) neighborhoods for each of the four broad land cover types across the three study areas was used to evaluate the performance of each of the 6 adaptive filters. Descriptive statistics were then generated for each of the four classes for each trial. The SAR speckle suppression equation is then applied, to compare speckle in the original image and each of the six filters. The adaptive filter that best suppresses speckle, while retaining image texture, is then used throughout the remainder of the study.

The generated SAR speckle suppression factors for each adaptive filter are listed in Table 4.2.The resulting SAR speckle suppression factors (F) indicate that the Gamma, Frost, Enhanced Frost, and Enhanced Lee provide similar speckle suppression. The Local

Sigma adaptive filter had the least effective speckle suppression. The Enhanced Lee and Enhanced Frost filters provided almost identical speckle suppression results. Either filter would be useful for applications that require the resolution of small feature cover classes in a reservoir setting. The Enhanced Lee filter preserved mean σ° within 0.25 dB and reduced standard deviation for each of the four classes. This Enhanced Lee filtering technique was carried forward for the remainder of the study.

Table 4.2. SAR backscatter statistics and speckle suppression factors for unfiltered and adaptively filtered data sets for each of the four broad cover classes.

Filter	Cover Type	Mean	Stdev	S	S_F	F
Unfiltered July 30 F2N	Forested	-10.5729	4.9638	-0.4695	-	-
	Water	-22.9121	4.9713	-0.2170	-	-
	Peat Island	-12.6349	4.8745	-0.3858	-	-
	Barren Land	-9.3861	5.3890	-0.5742	-	-
Lee	Forested	-10.5068	3.0943	-	-0.2945	2.5413
	Water	-22.757	2.9452	-	-0.1294	2.8107
	Peat Island	-12.6809	2.9851	-	-0.2354	2.6860
	Barren Land	-9.27359	3.6155	-	-0.3899	2.1688
Enhanced Lee	Forested	-10.5555	2.6407	-	-0.2502	3.5217
	Water	-22.692	2.5514	-	-0.1124	3.7239
	Peat Island	-12.7123	2.5841	-	-0.2033	3.6020
	Barren Land	-9.3129	3.1147	-	-0.3345	2.9470
Frost	Forested	-10.4871	2.8262	-	-0.2695	3.0348
	Water	-22.6916	2.5536	-	-0.1125	3.7174
	Peat Island	-12.7022	2.5970	-	-0.2044	3.5608
	Barren Land	-9.1953	3.3190	-	-0.3609	2.5303
Enhanced Frost	Forested	-10.5555	2.6407	-	-0.2502	3.5217
	Water	-22.692	2.5514	-	-0.1124	3.7239
	Peat Island	-12.7123	2.5841	-	-0.2033	3.6020
	Barren Land	-9.31596	3.1068	-	-0.3335	2.9640
Local Sigma	Forested	-10.1738	4.6048	-	-0.4526	1.0759
	Water	-22.5088	4.5535	-	-0.2023	1.1504
	Peat Island	-12.3011	4.4567	-	-0.3623	1.1339
	Barren Land	-8.92765	5.0679	-	-0.5677	1.0230
Gamma	Forested	-10.4425	2.9699	-	-0.2844	2.7249
	Water	-22.692	2.5514	-	-0.1124	3.7239
	Peat Island	-12.7123	2.5841	-	-0.2033	3.6020
	Barren Land	-9.00525	3.6041	-	-0.4002	2.0580

4.2.2 Data Analysis

4.2.2.1 Univariate Analysis of SAR Backscatter

Research question 1 determines the radar backscattering characteristics of each land class (i.e. forested land, peat island, barren island) and water cover classes, and identifies factors that may increase or decrease backscatter from these targets. A series of three univariate analyses are used to address the three research sub-questions.

SAR $\sigma°$ land cover class data are first analyzed between the three study areas to determine if there are any significant differences between each of the four cover types between each study area. This step is also employed to determine if pooling data for each class in the three study areas is valid. Data for each land cover class in each of the three study areas were first merged and an equal number of samples from each study area for each land cover class was selected from the main database (n = 2225). After tests for normality and heterogeneity of variance, a parametric one way Analysis of Variance (ANOVA) was selected to determine significant within-class radar backscatter differences between the three study areas. A Scheffe's test matrix of pairwise comparison probabilities was used to isolate the source of significantly ($P < 0.05$) different radar returns between study areas for each the four image data sets. Data for the three study areas were to be pooled following this statistical procedure if class means were statistically similar or mean differences were within the between image Radarsat-1 calibration limit of +/- 2 dB.

A Student's t test was used to determine significant differences ($P < 0.05$) in $\sigma°$ within the four land cover classes between two dates of identical imagery (RADARSAT-1 F2N) to determine whether prevailing weather conditions during image acquisition

have an effect on radar backscatter . Weather conditions during the August 4, 2005 F2N fine beam SGX image acquisition were cloudy and slightly rainy, with high winds (Table 4.1). There had been slight (<1 mm) precipitation in the form of fog and fine mist the night before, leaving a small amount of moisture on surrounding vegetation. Wind was 22 km/h with gusts to 30 km/h. The high wind speeds created 1 to 2 foot swells and white-capping in open water areas, which was more noticeable in open water areas. The weather conditions during the acquisition of the F2N image on July 30 2006 were in direct contrast to the year before. Wind speeds were negligible and no precipitation had occurred in the preceding 24 hours and water surface conditions were calm.

Data from three of the RADARSAT-1 fine beam images were used to determine the effect of incident angle on σ° from each of the four land cover classes. The F1N, F2N, and F5F fine beam mode viewing angles, range between 37 and 47°. ANOVA was used to test the effect of incident angle on the σ° from each of the four land and water classes. A Scheffe's test matrix of pairwise comparisons was used to isolate the source of significantly ($P < 0.05$) different radar returns by incident angle.

In the final univariate analysis, ANOVA was used to determine the ability of SAR backscatter to discriminate between floating peatland, forested land, barren land, and open water cover classes for each of the four RADARSAT-1 fine beam images. A Scheffe's test matrix of pairwise comparisons was used to isolate the source of significantly different radar returns between land cover classes.

4.2.2.2 SAR Texture Statistics

Texture information inherent in SAR images has been used to enhance automatic image interpretation of wetland types (Arzandeh and Wang 2002) and may be more

useful than image tone for interpreting radar data (Ulaby et al. 1986). The Grey Level

Co-occurrence Matrix (GLCM), first defined by Haralick et al. (1973) for classifying

imagery is the most popular statistical algorithm for texture measurement (Arzandeh and

Wang 2002). Studies have shown that texture statistics derived from the GLCM

outperform other approaches (Barber et al. 1993). The GLCM is a two-dimensional array

that provides the co-occurrence probability of pairs of grey values within a defined

window (Haralick et al. 1973). Inter-pixel angle (α) or orientation and inter-pixel

distance (δ) are considered when generating a GLCM. The GLCM is expressed

algebraically following Haralick et al. (1973) in Equation 4.1 and where *Cij* is defined in

Equation 4.2:

$$Pr(x) = \{C_{ij} | \delta, \alpha\} \tag{4.1}$$

$$C_{ij} = \frac{P_{ij}}{\sum_{ij=1}^{n} P_{ij}} \tag{4.2}$$

In this study I select 8 texture statistics first proposed by Haralick et al. (1973) to

discriminate floating peatlands from other broad land cover types (Table 4.3).

Table 4.3. A summary of texture statistics derived from the GLCM used in this study.

Texture Statistic	Equation	Description
mean	$\sum\limits_{i=1}^{n}\sum\limits_{j=1}^{n} i \cdot C_{ij}$	Measure of both tone and texture. A measure of the mean grey level of each row.
variance	$\sum\limits_{i=1}^{n}\sum\limits_{j=1}^{n} (i - \mu)^2\, C_{ij}$	Measure of heterogeneity. Variance increases when the grey-level values differ more from their mean.
Homogeneity (inverse difference moment)	$\sum\limits_{i=1}^{n}\sum\limits_{j=1}^{n} \dfrac{C_{ij}}{1 + (i - j)^2}$	Measure of image homogeneity. A large homogeneity value indicates smaller differences in pairs of grey levels.
contrast	$\sum\limits_{i=1}^{n}\sum\limits_{j=1}^{n} C_{ij}\,(i\text{-}j)^2$	Measure of the amount of local variation present in the image.
dissimilarity	$\sum\limits_{i=1}^{n}\sum\limits_{j=1}^{n} C_{ij}/(i\text{-}j)/$	Measure similar to contrast. The response to off-diagonal values is linear, therefore not as sensitive to large values as with contrast.
entropy	$\sum\limits_{i=1}^{n}\sum\limits_{j=1}^{n} C_{ij} \log C_{ij}$	Measure of image disorder. A texturally non-uniform image will have very small values, implying entropy is large.
angular 2nd moment (energy)	$\sum\limits_{i=1}^{n}\sum\limits_{j=1}^{n} C_{ij}^2$	Measure of textural uniformity (repetitions of pixel pairs). Large values are incurred where there is less local texture variation.
correlation	$\sum\limits_{i=1}^{n}\sum\limits_{j=1}^{n} \dfrac{(i - \mu_x)\,(j - \mu_y)\, C_{ij}}{\sigma_x\, \sigma_y}$	Measure of grey tone linear dependencies. High correlation values imply a linear relationship between the grey levels of pixel pairs.

The August 16, 2006 F1N RADARSAT-1 image was selected for the analysis of texture statistics derived from the GLCM. This image was selected due to the proximity of it's acquisition date relative to the QuickBird optical image, in order to allow for direct comparisons in future analyses. Prior to analysis the image was subset, to reduce processing time, and subjected to the GLCM texture analysis algorithm in ENVI 4.3. The algorithm requires four user defined parameters in order to execute the analysis. Parameters implemented in this analysis included a 5 x 5 moving neighborhood window, 64 bit quantization level, an inter-pixel distance of 1 and an inter-pixel angle of 0°, which

equates to a horizontal look direction. Some studies (Barber and LeDrew 1991; Arzandeh and Wang 2002) have evaluated the effect of variations to these parameters to improve classification for applications of sea ice discrimination and wetland discrimination. The resulting data set was an 8 band texture statistic composite image of the study area. Texture statistic data was then extracted from the 8 band texture statistic image set using the same stratified random sampling sites previously generated (Section 4.2.1) and placed in a Microsoft® Excel database for further statistical analysis.

Research question 2 addresses whether the use of texture statistics derived from the grey-level co-occurrence matrix (GLCM) aid in the discrimination of the reservoir land and water cover classes. The selected texture statistics are first analyzed for their individual (univariate) ability to detect differences in land cover classes. This analysis is followed by a multivariate discrimination and classification using combinations of the selected texture statistics.

4.2.2.3 Univariate Analysis of SAR Texture Statistics

Texture statistic sample data were analyzed first to determine the nature of the data distributions for the selection of appropriate statistical measures. Entropy and Second Angular Moment were excluded from further analysis due to highly skewed non-normal sample distributions. Each texture statistic was then tested for its ability to discriminate between the four broad land cover classes in order to address research question 2a. The non-parametric Kruskal-Wallis' H test, followed by Dunn's procedure for multiple pairwise comparisons were selected as appropriate tests to determine sources

of significant texture variable differences between the four broad land cover classes to determine each texture statistic's ability to discriminate.

4.2.3.4 Multivariate Analysis of Single Date SAR Texture Statistics

LDA was first used to discriminate between the four broad land cover classes using arbitrarily selected combinations of texture statistic explanatory variables derived from filtered and non-filtered SAR image data in order to address research question 2c. The results of the multivariate classifications were then assessed to determine the best overall classification accuracies between the original filtered and non-filtered images. This step was taken to determine whether or not important texture information is lost during the pre-processing adaptive filtering step.

Research question 2b is addressed through a series of multivariate analyses. A PCA was used to generate a new set of linearly transformed texture statistic variables to be used as explanatory variables within the LDA to determine whether this step provided an improved classification. A second set of discriminant analyses was run to assess the ability and contribution of combinations of SAR texture statistics derived from the GLCM and the transformed texture statistic PCA scores, to the discrimination of peat islands from the other broad land cover classes.

In each LDA trial 33 % of the sample texture variables and computed PCA scores were used to develop the linear models that maximally discriminate between the four classes. Classification accuracy for the model is assessed with a test group using the remaining data (67 %). Classification accuracy was assessed in all cases using a confusion matrix of producer and user classification errors. Assessment of each model's ability to maximally discriminate between the four broad reservoir classes was completed

by comparing overall classification agreement of the test data set. In addition a Kappa coefficient (Cohen 1960) analysis was used to compute an overall KHAT (K) statistic for each confusion matrix as a secondary indicator of classification agreement in order to identify the combination of texture statistic variables that best separate the four broad reservoir classes.

4.3 RESULTS

4.3.1 Univariate Analysis of SAR Backscatter within Classes between Study Areas

Radar returns σ° of the four fine beam mode image radar returns in each of the three study areas (O'Neil Bay, Ross Wright Bay, North Boisvert Island) are Gaussian with the exception of barren land (Shapiro-Wilk; forest p range = 0.06 to 0.97, df = 250; floating peatland p range = 0.05 to 0.69, df = 175; water p range = 0.16 to 0.96, df = 250) and have equal variance (Levene; forest p range = 0.09 to 0.45; floating peatland p range = 0.06 to 0.44; water p range = 0.74 to 0.96). A non-parametric Mann-Whitney U test was used to determine significant differences between the distributions between study areas A (O'Neil Bay) and C (North Boisvert Island) where the barren land class occurs.

Differences in σ° for the open water class between study areas shows that the August 4 2005 F2N image is significantly (ANOVA; P = 0.006) different from water between O'Neil Bay and Ross Wright Bay and Ross Wright Bay and North Boisvert Island (Table 4.4). These differences, however, fall within the 1 dB within-image calibration limit. The July 30, 2006 F2N image shows significant (P = 0.000) difference in radar return outside of calibration limits (mean difference = 1.628 dB) between O'Neil Bay and Ross Wright Bay. The F1N and F5F images show no significant differences in σ° for open water between each of the three study areas.

The floating peatland class is not significantly different (ANOVA; p = 0.534, p = 0.456, and p = 0.659) between the August 2005, and July 30 2006 F2N and F1N images respectively (Table 4.4). ANOVA revealed significant (p=0.038) differences between study areas, although Scheffe pairwise comparison of the F5F image showed differences are not significant and are within sensor calibration limits.

Radar returns from forested land class indicates all images but the July 30, 2006 F2N have sources of significant differences (ANOVA: $p < 0.001$) between study areas. The small difference (0.176 dB) in $\sigma°$ between O'Neil Bay and North Boisvert Island in the F5F image is well within the calibration limit. The August 4, 2005 F2N and the F1N image show sources of significant differences in $\sigma°$ that are slightly outside of the 1 dB calibration limit.

The Mann-Whitney U test for sources of significantly different radar returns from barren land revealed no significant differences between study areas in the August 4, 2005 F2N and F5F images. The July 30, F2N image shows significantly different (Mann-Whitney U; $p = 0.000$) $\sigma°$ outside of image calibration limits at 2.4 dB. The F1N image shows a small difference in $\sigma°$, but is within calibration limits.

Table 4.4. Within-class (water (n=750), peat island (=525), forested land (n=750), and barren land (n=200) differences in backscatter between study areas (A =O'Neil Bay, B=Ross Wright Bay, C=North Boisvert Island) for each of fourRADARSAT-1 fine beam SGX images.

Class	Image	Statistic	Study Area	n	P-value	Different?	Mean Diff	Within Limit[1]
Water	F2N(Aug2005)	Anova	All	750	0.001	yes	-	-
		Scheffe	A, B	750	0.006	yes	0.744	yes
		Scheffe	A, C	750	1.000	no	0.001	-
		Scheffe	B, C	750	0.006	yes	-0.743	yes
	F2N (July 2006)	Anova	All	750	0.000	yes	-	-
		Scheffe	A, B	750	0.000	yes	-1.628	yes
		Scheffe	A, C	750	0.001	yes	-0.732	yes
		Scheffe	B, C	750	0.000	yes	0.896	yes
	F5F	Anova	All	750	0.682	no	-	-
	F1N	Anova	All	750	0.632	no	-	-
Peat Island	F2N(Aug2005)	Anova	All	525	0.534	no	-	-
	F2N (July 2006)	Anova	All	525	0.456	no	-	-
	F5F	Anova	All	525	0.038	yes	-	-
		Scheffe	A, B	525	0.996	no	-0.023	-
		Scheffe	A, C	525	0.079	no	-0.603	-
		Scheffe	B, C	525	0.095	no	-0.580	-
	F1N	Anova	All	525	0.659	no	-	-
Forest	F2N(Aug2005)	Anova	All	750	0.000	yes	-	-
		Scheffe	A, B	750	0.018	yes	-0.564	yes
		Scheffe	A, C	750	0.000	yes	-1.037	yes
		Scheffe	B, C	750	0.058	no	-0.474	-
	F2N (July 2006)	Anova	All	750	0.463	no	-	-
	F5F	Anova	All	750	0.001	yes	-	-
		Scheffe	A, B	750	0.024	yes	0.612	-
		Scheffe	A, C	750	0.735	no	-0.176	yes
		Scheffe	B, C	750	0.002	no	-0.788	yes
	F1N	Anova	All	750	0.000	yes	-	-
		Scheffe	A, B	750	0.838	no	0.135	-
		Scheffe	A, C	750	0.000	yes	-0.932	yes
		Scheffe	B, C	750	0.000	yes	-1.067	yes
Barren Land	F2N(Aug2005)	Mann-Whitney U	A, C	200	0.276	no	-	-
	F2N (July 2006)	Mann-Whitney U	A, C	200	0.000	yes	2.4	no
	F5F	Mann-Whitney U	A, C	200	0.944	no	-	-
	F1N	Mann-Whitney U	A, C	200	0.008	yes	0.97	yes

Research question 1a demonstrates there are small within-class differences in $\sigma°$ between study areas for each of the four RADARSAT-1 fine beam images. There were

only two occurrences where σ° differed between like cover types outside of within-image calibration limits (July 30 F2N: open water and Barren Land). Most of the cover types between study areas are not significantly different in σ° when calibration are considered. Pooling of the cover type σ° data for each study area into one data set for further univariate and multivariate analyses is therefore recommended and is applied for the remainder of the analyses.

4.3.2 Effects of Weather Conditions on SAR Backscatter

The tonal differences between the August 5, 2005 and July 30, 2006 RADARSAT-1 F2N images captured on days with contrasting weather conditions are illustrated in Figure 4.1. The open water area in the centre of the August 5, 2005 F2N image appears to be brighter, having increased σ°, compared to the July 30, 2006 F2N image. Conditions during the August 2005 F2N were adverse, with winds out of the west steady at 22 km/hr and gusting well above 35 km/hr. On the eastern shores of islands and the mainland in the August 2005 F2N image there appears to be areas of homogeneous dark tone. These areas of water are shielded by the westerly winds, and therefore their surfaces are free from large waves that typically develop in open areas as a result of wave energy and increased fetch distance.
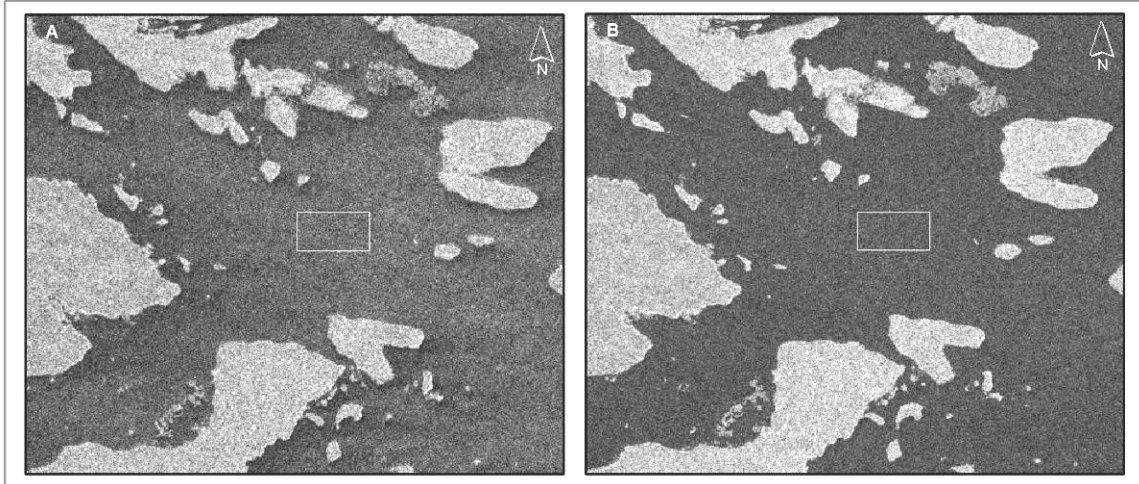
Figure 4.1. RADARSAT-1 F2N fine beam SGX imagery collected on August 5, 2005 (left) during adverse wind and wave conditions, and on July 30, 2006 (right) during calm weather conditions. The winds out of the west appear to create shadows on the east sides of some islands in the image on the left. Copyright: Canadian Space Agency 2006

The results of the Student's t test showing significant differences in radar return by land cover types between the two images is summarized in Table 4.5. Open water and barren land both have significantly different (Student's t: $p < 0.015$) $\sigma°$ returns between the two F2N images. The open water class however is well beyond the inter-image calibration limit of +/- 2 dB. This potentially indicates that radar backscatter has been increased by the rough surface conditions. It appears that radar return is slightly higher for all land cover classes in the August 2005 F2N image. Early morning rain, fog, and dew, deposited on the surfaces of the forested lands and peat islands may be contributing to increases in the dielectric constant of the vegetation surface, thereby causing a slight increase in returned $\sigma°$ to the sensor.

Table 4.5. Comparison of differences in backscatter between August 5, 2005 and July 30, 2006 RADARSAT-1 F2N data collected during contrasting weather conditions.

Class	Aug. 5 2005 Mean σ°	July 30, 2006 Mean σ°	Mean Diff	t-value	P-value	Different (P < 0.05)
Water	-19.256	-22.145	2.888	11.913	0.000	yes
Peat Island	-12.279	-12.706	0.427	1.596	0.111	no
Forest	-9.68	-10.07	0.388	1.638	0.102	no
Barren	-10.553	-9.885	-0.668	-2.436	0.015	yes

Research question 1b demonstrates that weather conditions creating wind roughened water surfaces can create increased backscatter to the SAR sensor. Antecedent precipitation can also lead to increased radar reflectivity from vegetated peat island and forested land surfaces.

4.3.3 Sensor Incident Angle and SAR Backscatter

The mean radar reflectivity from the four broad land cover classes from each of the three varying incident angle images is shown in Figure 4.2. As incident angle increases (F1N to F5F) there is a noticeable decrease in radar reflectivity from each land cover class. The results of the ANOVA identifying differences in σ° for each incident angle image are summarized in Table 4.6. The barren land class has statistically similar (Scheffe: $p = 0.115$) radar returns between the F2N and F5F images, with a mean difference of 0.577 dB. Peat island and forested land also have comparable mean radar returns between the two images however they are still significantly (Scheffe: $p = 0.024$ and $p = 0.014$) different. The greatest mean differences in backscatter consistently occur between the F1N and F5F images, which account for a difference in sensor incident angle

of 10°. The open water and peat island land cover classes have mean backscatter

differences outside the between-image calibration limit (2 dB).
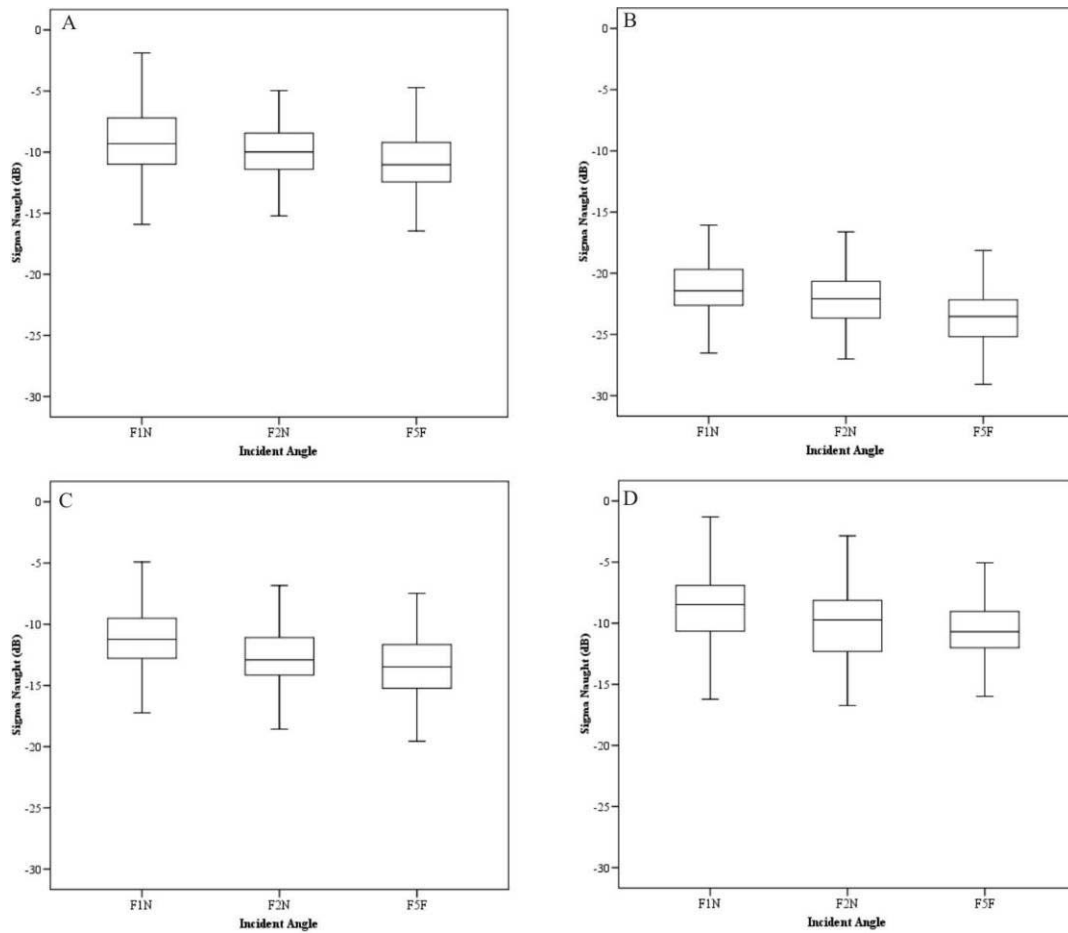
Figure 4.2. Box plots showing differences in backscatter across F1N, F2N, and F5F incident angle images for (A) forested land, (B) open water, (C) floating peatland, and (D) barren land

Table 4.6. Within-class backscatter differences among three different RADARSAT-1 fine beam incident angle images (water n=800, peat island n=700, forested land n=860, barren land n=218).

Class	Statistic	Image	Mean Diff	P-value	Different
Water	ANOVA	All	-	0.000	yes
	Scheffe	F2N, F5F	1.4582	0.000	yes
	Scheffe	F2N, F1N	-0.8833	0.000	yes
	Scheffe	F5F, F1N	-2.3415	0.000	yes
Peat Island	ANOVA	All	-	0.000	yes
	Scheffe	F2N, F5F	0.7094	0.024	yes
	Scheffe	F2N, F1N	-1.4442	0.000	yes
	Scheffe	F5F, F1N	-2.1537	0.000	yes
Forest	ANOVA	All	-	0.000	yes
	Scheffe	F2N, F5F	0.7282	0.014	yes
	Scheffe	F2N, F1N	-0.9344	0.001	yes
	Scheffe	F5F, F1N	-1.6626	0.000	yes
Barren	ANOVA	All	-	0.000	yes
	Scheffe	F2N, F5F	0.5768	0.115	no
	Scheffe	F2N, F1N	-1.2985	0.000	yes
	Scheffe	F5F, F1N	-1.8753	0.000	yes

Research question 1c demonstrates that the incident angle of the propagated microwave has an effect on the amount of $\sigma°$ returned to the sensor. An increase in incident angle across three RADARSAT-1 fine beam images showed a decrease in the amount of backscatter returned to the sensor for each of the four broad land cover classes. It should be noted that large class sizes may have the effect of generating an overly sensitive statistical result. Visual interpretation of the box plots would indicate that cover classes in images that are close in incident angle (i.e. F2N and F1N), should actually be statistically similar. Additional studies may consider running these statistics with smaller sample sizes. In the end, differences within land cover classes across incident angle images tend to be within calibration limits.

4.3.4 Univariate Analysis of SAR Backscatter Between Classes

Mean SAR backscatter from each land cover class in each of the four fine beam RADARSAT-1 SGX images is illustrated in Figure 4.3. The results of the ANOVA showing significant differences between broad land cover classes in each of the four SAR images are summarized in Table 4.7. With the exception of the forested land and barren land cover classes, each class has significantly different $\sigma°$ for each of the four images. Forested land and barren land have statistically similar radar returns in the July 30 2006 F2N (Scheffe: $p = 0.913$), F5F (Scheffe: $p = 0.567$) and F1N (Scheffe: $p = 0.232$) images. The mean $\sigma°$ difference between the two classes is close (0.87 dB) in the August 4, 2005 F2N image. In each image the other classes have mean $\sigma°$ differences greater than the image calibration limit (1 dB). Open water has the greatest difference in mean $\sigma°$ from the other three land based classes in each of the four images. However, this is less pronounced in the August 4, 2005 F2N image, likely do to the increased backscatter resulting from waves, which acts to reduce overall class tonal contrast.
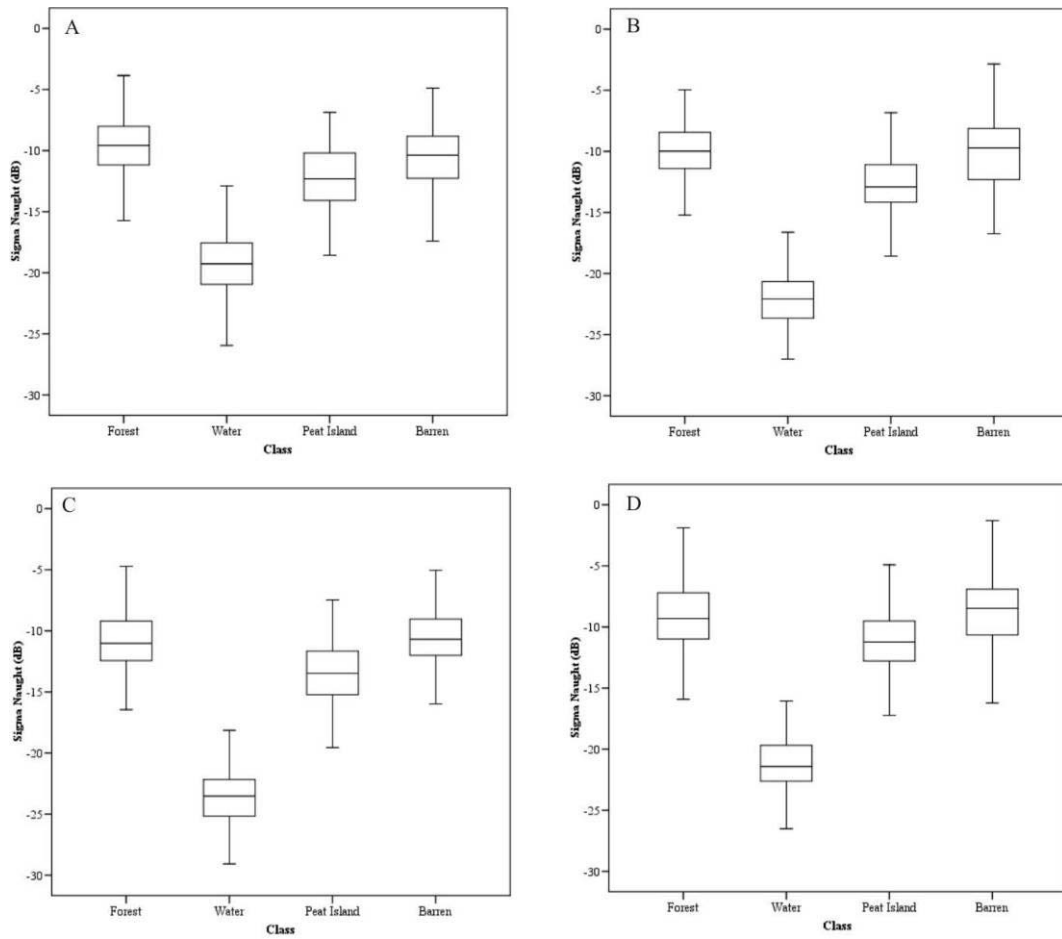
Figure 4.3.Box plots showing differences in backscatter among the four broad land cover classes for each of the four fine beam images (A) August 5, 2005 F2N, (B) July 30, 2006 F2N, (C) August 13, 2006 F5F, and (D) August 16, 2006, F1N.

Table 4.7. Statistical comparison (ANOVA) of backscatter differences between each broad land cover class for each acquired RADARSAT-1 fine beam SGX image.

Image	Statistic	Class	Mean Diff	P-value	Different
Aug 4, F2N	ANOVA	All	-	0.000	yes
	Scheffe	Forest, Water	9.5741	0.000	yes
	Scheffe	Forest, Peat	2.5968	0.000	yes
	Scheffe	Forest, Barren	0.8711	0.010	yes
	Scheffe	Water, Peat	-6.9773	0.000	yes
	Scheffe	Water, Barren	-8.7029	0.000	yes
	Scheffe	Peat, Barren	-1.7256	0.000	yes
July 30, F2N	ANOVA	All	-	0.000	yes
	Scheffe	Forest, Water	12.0745	0.000	yes
	Scheffe	Forest, Peat	2.6361	0.000	yes
	Scheffe	Forest, Barren	-0.1849	0.913	no
	Scheffe	Water, Peat	-9.4384	0.000	yes
	Scheffe	Water, Barren	-12.2594	0.000	yes
	Scheffe	Peat, Barren	-2.8209	0.000	yes
Aug 13, F5F	ANOVA	All	-	0.000	yes
	Scheffe	Forest, Water	12.8044	0.000	yes
	Scheffe	Forest, Peat	2.6173	0.000	yes
	Scheffe	Forest, Barren	-0.3364	0.567	no
	Scheffe	Water, Peat	-10.1872	0.000	yes
	Scheffe	Water, Barren	-13.1408	0.000	yes
	Scheffe	Peat, Barren	-2.9536	0.000	yes
August 16, F1N	ANOVA	All	-	0.000	yes
	Scheffe	Forest, Water	12.1256	0.000	yes
	Scheffe	Forest, Peat	2.1262	0.000	yes
	Scheffe	Forest, Barren	-0.5490	0.232	no
	Scheffe	Water, Peat	-12.1256	0.000	yes
	Scheffe	Water, Barren	-9.9994	0.000	yes
	Scheffe	Peat, Barren	-2.6752	0.000	yes

In answering research question 1d, we find that with the exception of the forested land and barren land classes, each RADARSAT-1 image provides significantly different radar returns between the land and water cover classes. These two classes appear as heterogeneous areas with higher mean $\sigma°$ in the imagery, compared to the floating peatland and open water classes. From a univariate perspective RADARSAT-1 fine beam SGX imagery is able to effectively discriminate between floating peatlands, forested land, and water.

4.3.4 Univariate Analysis of SAR Image Texture Statistics

Exploratory statistical analysis of SAR texture statistic data distributions of the F1N image revealed non-Gaussian distributions and normalization techniques were unsuccessful. A non-parametric Kruskal-Wallis' H test was used to test for differences in texture statistic data between the four land cover classes.

The results of the Kruskal-Wallis' H test and subsequent Dunn's procedure for pairwise comparisons are summarized in Table 4.8. The six texture statistics analyzed consistently show no significant difference between the forested land and barren land cover classes. Variance, contrast and dissimilarity show significant difference between the remaining class pairwise comparisons. Mean, homogeneity, and correlation show statistically significant similarities between forested land, floating peatland, and barren land.

In answering research question 2a it was discovered that the texture statistics: variance, contrast, and dissimilarity, are each successful in discriminating between all cover types with the exception of barren land and forested land. Mean, homogeneity, and correlation are unable to discriminate between the three land-based cover classes; however it appears that they are able to discriminate between land and water cover types.

Table 4.8. Statistical comparison of differences in SAR image texture statistic between the four broad land cover classes (water n=800, peat island n=700, forested land n=860, barren land n=218)

Texture	Statistic	Class	Pairwise Difference [1]	P-value	Different? (P < 0.05) [2]
Mean	Kruskall-Wallis H	All	-	0.000	yes
	Dunn's Procedure	Forest, Water	2302.06	-	yes
	Dunn's Procedure	Forest, Peat	267.69	-	no
	Dunn's Procedure	Forest, Barren	-35.88	-	no
	Dunn's Procedure	Water, Peat	-2034.37	-	yes
	Dunn's Procedure	Water, Barren	-2337.93	-	yes
	Dunn's Procedure	Peat, Barren	-303.56	-	no
Variance	Kruskall-Wallis H	All	-	0.000	yes
	Dunn's Procedure	Forest, Water	3008.15	-	yes
	Dunn's Procedure	Forest, Peat	555.50	-	yes
	Dunn's Procedure	Forest, Barren	-67.06	-	no
	Dunn's Procedure	Water, Peat	-2452.65	-	yes
	Dunn's Procedure	Water, Barren	-3075.21	-	yes
	Dunn's Procedure	Peat, Barren	-622.56	-	yes
Homogeneity	Kruskall-Wallis H	All	-	0.000	yes
	Dunn's Procedure	Forest, Water	-839.19	-	yes
	Dunn's Procedure	Forest, Peat	-221.50	-	no
	Dunn's Procedure	Forest, Barren	-35.17	-	no
	Dunn's Procedure	Water, Peat	617.70	-	yes
	Dunn's Procedure	Water, Barren	804.02	-	yes
	Dunn's Procedure	Peat, Barren	186.33	-	no

Texture	Statistic	Class	Pairwise Difference [1]	P-value	Different? (P < 0.05) [2]
Contrast	Kruskall-Wallis H	All	-	0.000	yes
	Dunn's Procedure	Forest, Water	2895.52	-	yes
	Dunn's Procedure	Forest, Peat	413.43	-	yes
	Dunn's Procedure	Forest, Barren	-87.92	-	no
	Dunn's Procedure	Water, Peat	-2482.09	-	yes
	Dunn's Procedure	Water, Barren	-2983.45	-	yes
	Dunn's Procedure	Peat, Barren	-501.36	-	yes
Dissimilarity	Kruskall-Wallis H	All	-	0.000	yes
	Dunn's Procedure	Forest, Water	1712.01	-	yes
	Dunn's Procedure	Forest, Peat	371.60	-	yes
	Dunn's Procedure	Forest, Barren	-96.18	-	no
	Dunn's Procedure	Water, Peat	-1340.41	-	yes
	Dunn's Procedure	Water, Barren	-1808.19	-	yes
	Dunn's Procedure	Peat, Barren	-467.78	-	yes
Correlation	Kruskall-Wallis H	All	-	0.000	yes
	Dunn's Procedure	Forest, Water	-970.47	-	yes
	Dunn's Procedure	Forest, Peat	75.56	-	no
	Dunn's Procedure	Forest, Barren	-9.53	-	no
	Dunn's Procedure	Water, Peat	1046.03	-	yes
	Dunn's Procedure	Water, Barren	960.95	-	yes
	Dunn's Procedure	Peat, Barren	-85.09	-	no

[1] Critical Difference of 362.1357

[2] Bonferroni corrected significance level: 0.0001

4.3.5 Multivariate Discrimination and Classification Using SAR Texture Statistics

All 11 discriminant models provide statistically significant discrimination (Wilk's λ: p = 0.000) and are comparable in their result, with overall test agreement accuracy ranging between 60.54 and 63.32 % (K = 0.443 to 0.482) (Table 4.9). Most misclassification occurs with the barren land and forested land cover classes. The 5 variable combination of mean, variance, homogeneity, contrast and dissimilarity performs slightly better (Overall = 63.32%, K = 0.482) than the other linear discriminant models. The combination of contrast, dissimilarity and correlation had the lowest test classification accuracy (Overall = 60.54%, K = 0.443).

Table 4.9. LDA classification accuracy results for selected combinations and numbers of SAR image texture statistics including mean, variance (Var), homogeneity (Hom), contrast (Con), dissimilarity (Dis), correlation (Cor).

		Model/Test Agreement				Test Class Agreement (%)				
LDA Texture Variables	# of Variables	Model Overall (%)	Model KHAT	Test Overall (%)	Test KHAT	Barren Land	Forested Land	Peat Island	Open Water	Test Samples
Mean-Var-Hom	3	64.79	0.502	62.70	0.473	13.91	39.35	68.83	95.80	1764
Mean-Var-Hom-Con	4	65.02	0.507	62.53	0.472	17.22	38.16	71.13	93.61	1764
Var-Hom-Con	3	63.06	0.481	60.83	0.450	17.88	32.03	73.43	92.52	1764
Var-Hom-Con-Dis	4	64.79	0.504	61.11	0.452	13.91	31.86	72.80	95.26	1764
Hom-Con-Dis	3	62.60	0.470	61.56	0.455	11.26	38.33	67.15	95.44	1764
Hom-Con-Dis-Corr	4	64.10	0.491	60.94	0.448	12.58	36.12	67.57	95.07	1764
Con-Dis-Corr	3	63.06	0.477	60.54	0.443	13.25	35.09	68.83	93.61	1764
Mean-Var-Hom-Con-Dis	5	66.05	0.520	63.32	0.482	14.57	38.16	72.59	95.62	1764
Mean-Var-Hom-Con-Cor	5	65.02	0.507	62.53	0.472	17.22	38.16	71.13	93.61	1764
Mean-Var-Hom-Con-Dis-Corr	6	65.59	0.514	62.76	0.476	17.22	36.97	71.55	95.26	1764
PCA1-PCA2-PCA3	3	66.17	0.524	62.47	0.471	15.23	37.14	71.34	94.89	1764

The first discriminant axis for the five variable texture statistic model is dominated by homogeneity (Table 4.10), with some contribution from contrast, and accounts for 95 % of the variance in the data set. The major trend in the first discriminant axis shows a gradient between land and water and is likely dominated by an increase in surface roughness. Forested land and barren land cover classes, generally having high surface roughness are pulled to the left, with the floating peatland class being

homogeneously smoother, and calm water, generally acting as a specular reflector of

microwave EMR, on the right, which is reflective of their relative surface roughness.

Barren land is scattered about the peat island and forested land cover classes. It is evident

that the first discriminant axis is unable to effectively discriminate between barren land,

and forested land cover classes (Figure 4.4). The second discriminant axis is ineffective

in separating barren land from the floating peatland and forested land cover classes. The

confusion matrix (Table 4.11) of the five texture statistic LDA classification model

further indicates the misclassification of the barren land and forested land cover classes

which are most often confused with the open water class.

A PCA transformation of the six texture variable model prior to a performing a

discriminant analysis on the newly transformed PCA scores had moderate results

(Overall = 62.47%, K=0.471), which was slightly better in comparison to some of the

other texture statistic combination discriminant models. The preprocessing step did not,

however, enhance the classification accuracy result over the use of texture statistics alone

in any significant way. The first discriminant axis is dominated by PCA 1 which retains

over 90 % of the variance found in the original six untransformed texture variables (Table

4.9).
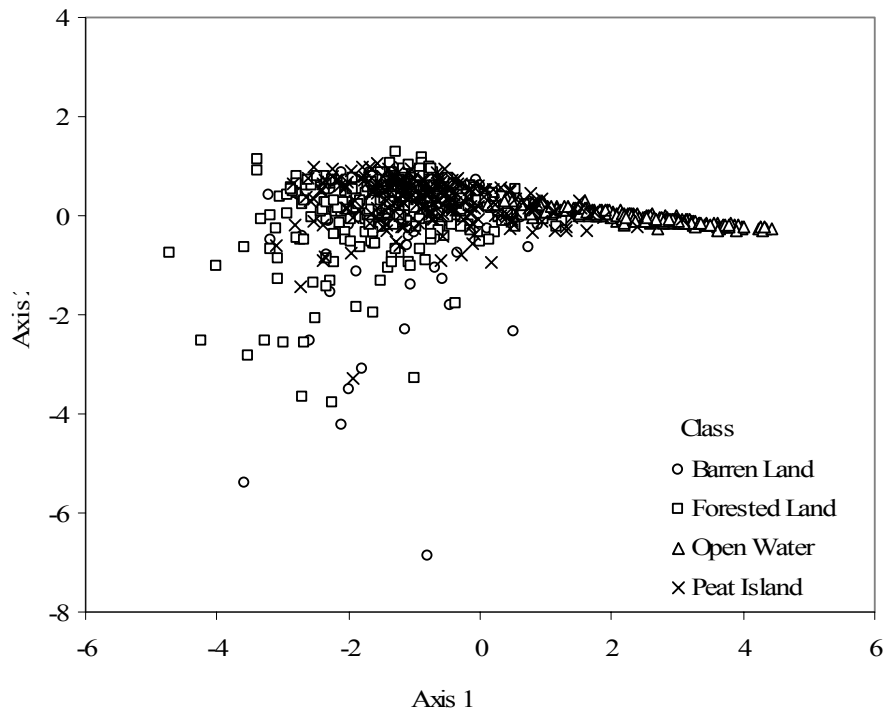
Figure 4.4. Discriminant axis score scatter plot for the LDA texture statistic combination of mean, variance, homogeneity, contrast, and dissimilarity.

Table 4.10. Standardized discriminant function coefficients derived from the 5 texture statistic discriminant analysis and the PCA transformed six texture statistic discriminant analysis (M=mean, V=variance, H=homogeneity, C =contrast, D =dissimilarity).

	LDA -M-V-H-C-D		LDA-PCA - 6 Variable	
Discriminant Axis	1	2	1	2
Mean	-0.536	-0.041	-	-
Variance	-0.065	-0.703	-	-
Homogeneity	0.810	0.277	-	-
Contrast	0.632	-1.703	-	-
Dissimilarity	-0.242	1.831	-	-
PCA 1	-	-	-1.038	0.333
PCA 2	-	-	0.576	0.460
PCA 3	-	-	0.523	0.728
% Variance	95.0	4.0	95.0	5.0

Table 4.11. Full error matrix of the five texture statistic discriminant analysis.

	Barren Land	Forested Land	Open Water	Peat Island	Row Total
Barren Land	22	48	81	0	151
Forested Land	24	224	337	2	587
Open Water	0	1	23	524	548
Peat Island	3	105	347	23	478
Column Total	49	378	788	549	1764

Producers's Accuracy
Barren Land = 22 / 49 = 44.9 %
Forested Land = 224 / 378 = 59.3%
Open Water = 524 / 549 = 95.4%
Peat Island = 347 / 788 = 44.0%

User's Accuracy
Barren Land = 22 / 151 = 14.6%
Forested Land = 224 / 587 = 38.2%
Open Water = 524 / 548 = 95.6%
Peat Island = 347 / 478 = 72.6%

Overall Accuracy
 = 1117 / 1764 = 63.3%

KHAT
 = 0.482

Research question 2b demonstrated that a five texture statistic discriminant model combination (mean, variance, homogeneity, contrast, and dissimilarity) provides a slightly improved classification of the four broad land cover classes compared to other texture statistic combinations. Homogeneity and contrast play a significant role in the discriminant model. A PCA transformation of the six texture statistics prior to discriminant analysis does not significantly improve classification.

In a final comparison, the four broad land cover classes were grouped into land (forested land, peatland, barren land) and water classes prior to analysis. The classification results comparing model performance for the four broad land cover classes versus the land cover classes collapsed down to land and water are summarized in Table 4.12. Overall classification accuracies improve by almost 50 % for each of the three texture statistic LDA models tested. Classification accuracy is excellent with the

combination of mean, variance, homogeneity, and contrast (Overall = 97.39%: K= 0.939).

Table 4.9. Classification accuracy for the three texture statistic discriminant analysis combinations of the four broad land cover classes and the land and water classes.

		4 Class				2 Class (Land/Water Mask)			
LDA Texture Variables	# of Variables	Model Overall (%)	Model KHAT	Test Overall (%)	Test KHAT	Model Overall (%)	Model KHAT	Test Overall (%)	Test KHAT
Mean-Var-Hom-Con	4	65.02	0.507	62.53	0.472	97.58	0.944	97.39	0.939
Mean-Var-Hom-Con-Cor	5	65.02	0.507	62.53	0.472	97.58	0.944	97.39	0.939
Mean-Var-Hom-Con-Dis-Cor	6	65.59	0.514	62.76	0.476	97.93	0.952	96.83	0.926

Research question 3 demonstrates that while overall classification accuracies involving multiple broad land cover classes remain low (< 65 %), classification models involving aggregated land and water cover classes show marked improvement (> 95 %). It is apparent that the single RADARSAT-1 SGX image texture statistics generated from the GLCM are better suited for discriminating between land and water than among multiple vegetated and non-vegetated broad land cover classes.

4.4 DISCUSSION

SAR has the ability to image day or night, and through cloud cover, giving it a distinct advantage over optical systems when discriminating between land and water cover types in a dynamic peatland reservoir. However, unlike optical data, SAR data is difficult to visually interpret without an intimate knowledge of its interaction with the surface and volumes of intended ground targets. The use of SAR in land cover mapping and monitoring applications is dependent on an understanding of factors including the inherent scattering characteristics of the intended targets, the effect of variable imaging parameters, and the influence of prevailing weather conditions during data acquisition. In this study SAR was examined for its ability to discriminate specific land cover types in under a wide range of aquatic and terrestrial conditions. An understanding of the unique microwave interactions that SAR has with terrain features is paramount to using SAR as a tool for discriminating, mapping and eventually monitoring peatland disintegration in a sub-arctic reservoir.

Calm water normally appears as a smooth surface to the SAR sensor (Figure 4.5: 2). Microwave energy will tend to scatter in a forward direction as a result of the specular reflection that tends to occur at the surface of a calm water body. This is why water appears as a dark homogeneous area in SAR imagery. Bryan (1981) found that windy weather conditions can lead to the formation of rough water surface conditions. These conditions are then relayed in the SAR backscatter image as areas of increased backscatter in what would normally appear as a dark homogeneous area in the imagery, as was revealed in this study. These conditions can occur with rough ocean surfaces as well as rough inland water body surfaces such as lakes and reservoirs and have been

described (Bryan 1981; Mouchot and Garello 1998; Pietroniro and Leconte 2000; Woodhouse 2006). Figure 4.5 (1) illustrates this as an increased component of the incident microwave being returned to the sensor. The water becomes a diffuse reflector as the SAR now sees the rough surface, according to Raleigh criterion.
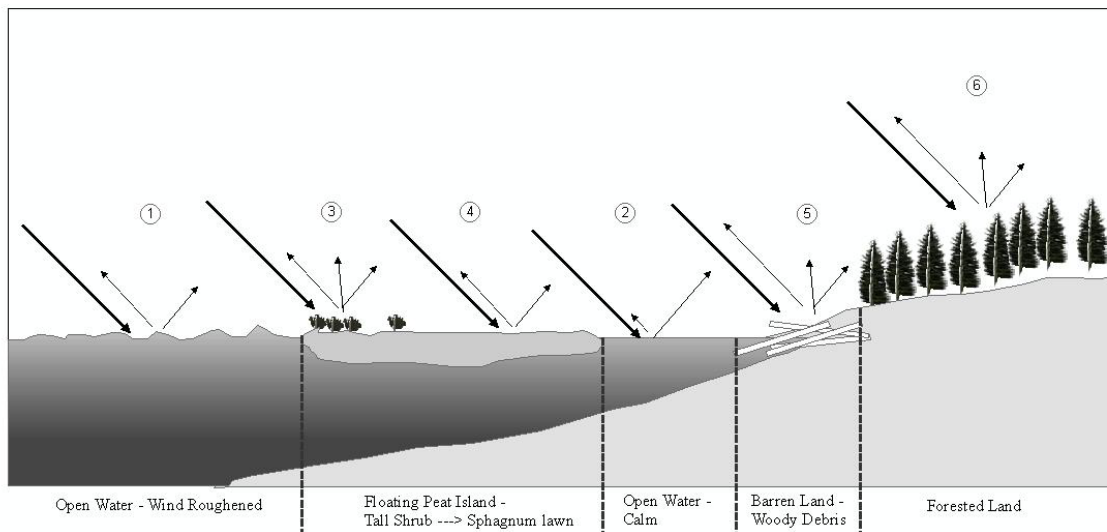
Figure 4.5. Theoretical microwave interaction with four broad land cover classes considered in this thesis.

The mean backscatter from open water areas in the RADARSAT-1 August 4, 2005 F2N image was significantly higher and above the 2 dB between image calibration limit than the RADARSAT-1 July 30, 2006 image under calm weather conditions. Differences within each of the other three classes remained within the 2 dB calibration limit. Increased backscatter over water areas therefore reduces the tonal contrast between land and water in SAR imagery making discrimination of land and water areas in SAR imagery difficult for visual interpretation and quantitative statistical discrimination. In this study I also demonstrated a decrease in SAR $\sigma°$ from open water with increasing sensor incident angle. Generally, an increasing incident angle will result in decreased reflectivity from distributed scatterers (Lewis and Henderson 1998). This pattern

however, was shown for each of the four broad land cover classes, and should be considered when utilizing different incident angle images in comparison applications. The importance of sensor wavelength, polarization, and look angle, should not be overlooked in land cover mapping applications.

SAR interaction with vegetation is much different than that of water and is influenced by a number of factors, including surface roughness, volume scattering, and the dielectric properties related to moisture content of the vegetation. There is greater interaction within the volume of vegetation when compared to water. The apparent surface roughness of the vegetation determines surface scattering, (i.e. the rougher a vegetation canopy appears to the SAR the greater the amount of energy scattered back to the SAR). The vegetation community on a floating peatland can range from tall shrub (sweet gale and willow) and cattail, 1 m in height, to low lying fine peat mat carpets dominated by moss and ericaceous shrubs that hug the hummocky peatland terrain. Floating peatlands can therefore appear somewhat rough to mainly smooth surfaces to the SAR sensor. Figure 4.5 (3 and 4) illustrate the interaction of microwaves with floating peatland vegetation, where the volume scattering that may occur within the canopy of tall shrub may lead to increased backscatter, or increased attenuation. Backscatter from the forested land class was slightly elevated over the peat island class. The irregular surface (surface roughness) and extensive larger branch system of a black spruce canopy (volume scattering), results in increased backscatter compared to the floating peatland cover class (Figure 4.5 (6)). It is also well known that moisture on the surface and within vegetation can lead to increased backscatter (Leckie and Ranson 1998). The high dielectric constant of water leads to increased backscatter from the surface of the vegetation. The August 4,

154

2005 RADARSAT-1 F2N data, in which acquisition followed increased ground surface moisture levels (light rain, fog, dew), had slightly higher σ° returns for the peat island and forested land cover classes compared to the July 30, 2006 image with the same imaging parameters in which there was no antecedent precipitation.

This study made use of scene texture statistics derived from the GLCM. The use of texture statistics over the use of image tone by itself has been shown to improve classification of wetland land cover types (Arzandeh and Wang 2002). The interaction of SAR with land cover targets is largely dependent on surface roughness (Lewis and Henderson 1998). Microscale roughness is the result of roughness on the scale of a fraction of the system wavelength (Rayleigh Criterion), which in turn dictates image tone. Mesoscale roughness is the result of the "gross roughness envelope", which is the spatial dependency of image tone, known as image texture.

The overall classification accuracy of floating peatlands, forested land, open water, and barren land cover classes was found to be low relative to the optical study results in Chapter 3. Scene texture variation between adjacent broad vegetation types in the sub-arctic peatland environment was not found to be different enough to successfully discriminate between all four cover classes. However, this study did demonstrate that SAR can be very successful in discriminating between land and water classes only. Classification accuracies were greatly improved when discriminating strictly between these two cover types.

4.5 CONCLUSION

The overarching objective of this chapter was to describe the SAR scattering characteristics of land (forested land, peat islands, barren land) and water in order to determine the ability of SAR to discriminate between land and water. A number of conclusions can be drawn from the results that were obtained while answering the specific research questions.

It was determined that various factors (i.e. sensor incident angle, weather conditions) may influence the amount of $\sigma°$ returned from floating peatland, forested land, open water and barren land cover classes between subsequent SAR images. Differences in $\sigma°$ were found within land cover classes between the three peat island study areas, but generally they were within the image calibration limits, and so class data was pooled.

Rough water surfaces, related to high winds, can experience increased $\sigma°$ and antecedent precipitation prior to image acquisition can also lead to increased $\sigma°$ from vegetated peat island and forested land surfaces. Although these weather conditions work to reduce the overall contrast between land and water in a SAR image, the $\sigma°$ variability between the two will remain high enough to successfully discriminate them. The ability of SAR to penetrate cloud cover and unfavorable weather makes it a valuable tool for time-sensitive applications.

The incident angle of the propagated microwave has a small effect on the amount of $\sigma°$ returned to the sensor. An increase in incident angle showed a decrease in the amount of backscatter returned to the sensor for each of the four broad land cover classes. The ability of RADARSAT-1 to image the same location multiple instances in short

periods of time relies on its ability to angle its SAR instrument in order to capture a scene, which is again why it is a valuable asset for time-sensitive applications.

RADARSAT-1 images showed significantly different σ° between three of the four studied land cover classes. Univariate analyses demonstrated that RADARSAT-1 fine beam SGX imagery can discriminate between floating peat islands, forested land, and water. Multivariate discrimination and classification using derived image texture statistic data resulted in considerable misclassification between the land-based classes. However, when the classes were generalized to land and water only excellent (>90%) classification results were achieved, demonstrating the sensor's ability to discriminate between changing land and water boundaries.

In summary, I have demonstrated that certain factors will influence σ° returned from the studied reservoir classes. The researcher needs be aware of these differences which are related to incident angle, prevailing weather conditions, and the inherent reflectivity characteristics of the intended targets of study. However it is not likely that the slight variability incurred would inhibit any applications that require the discrimination of the boundaries between land and water, as their σ° contrast will remain high, which allows for excellent discrimination by the sensor.

CHAPTER 5 : AN INTEGRATION OF OPTICAL AND MICROWAVE TECHNOLOGIES FOR THE REMOTE SENSING OF A DYNAMIC SUB-ARCTIC PEATLAND RESERVOIR

5.1 INTRODUCTION

I've explored the use of high resolution optical remote sensing technologies for the discrimination of land (forested land, peat islands, barren land) from water cover classes in a sub-arctic peatland reservoir. I've looked at the potential of SAR backscatter data and derived image texture statistics for achieving the same objective. This chapter compares, contrasts, and considers an integration of the two technologies.

In 2005, optical image acquisitions were unsuccessful six times. In 2006 two SAR images were acquired under cloudy conditions. Optical images are much easier to visually discriminate land and water cover types without the use of computer based image classification algorithms, however SAR images are almost always guaranteed, despite prevailing weather conditions during acquisitions. This characteristic becomes important for time sensitive applications.

The primary objective of this chapter is to determine if optical or SAR or an integration of image data from both satellites provide a better method of discriminating land and water cover types. The specific research questions in this chapter are:

> 1) Given three data availability scenarios, does a synthesis of the two remote sensing approaches provide a better method of discriminating land, including floating peatlands, forested land, and barren land, from water than one sensor by itself?
>
> > a) SAR texture statistic data enhanced with visible, near-infrared, or NDVI QuickBird data?

b) QuickBird visible band data enhanced with SAR σ° or texture statistic data?

c) QuickBird VNIR data enhanced with SAR σ° or texture statistic data?

2) Does an optical, SAR, or integrated remote sensing approach provide a more robust discrimination of land (i.e. floating peatlands, forested land, and barren land) and water?

Given the results of the first objective, the second objective of this chapter is to develop an image classification model that can be used to map and monitor land and water changes related to the unique processes that can occur in a peatland reservoir.

5.2 METHODS

5.2.1 Study Area and Imagery

The RADARSAT-1 F1N fine beam SGX image was captured on August 16, 2006 (water level = 140.94 m ASL) and the QuickBird high resolution optical image was acquired on September 2, 2006 (water level = 140.81 m ASL) (Figure 5.1). These two images were selected because of their close acquisition dates and relatively similar water levels.
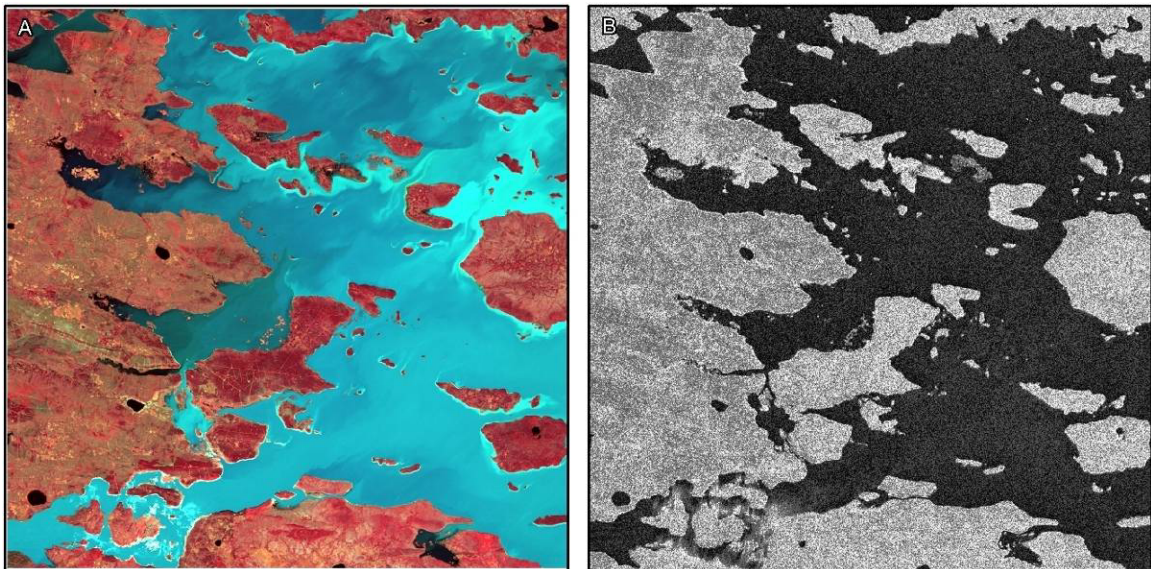
Figure 5.1. High resolution optical VNIR QuickBird imagery (false color infrared composite) (left), and RADARSAT-1 F1N imagery (right) acquired for this study. Copyright: Digital Globe 2006 and Canadian Space Agency 2006.

5.2.2 Data Processing and Sampling

SAR image texture statistics were derived from the GLCM consistent with the parameters and methods utilized in Chapter 4. Texture statistics used in this study included mean, homogeneity, and variance. DNs representing the QuickBird blue band

160

(450 – 520 nm), green band (520 – 600 nm), red band (630 – 690 nm) and near-infrared

(760 – 900 nm) were used as the optical data variables.

A 3.125 m spaced grid of points was generated for the three floating peatland

formation study areas was used to account for the pixel spacing of RADARSAT-1 fine

beam SGX image data. Optical and SAR texture data were extracted via stratified random

sampling of the GIS based vector validation map. A maximum of 300 sample sites per

class for each study area were selected. The SAR texture statistic and optical variables

were then extracted to each site in the GIS. The data were then randomly selected and

coded as being model (33 %) or test (67 %) data and stored in Microsoft$^{®}$ Excel.

5.2.3 Multivariate Discrimination and Classification

The SAR and high resolution optical data are analyzed using Linear Discriminant

Analysis (LDA). Linear combinations of SAR texture statistics and optical variables are

used to determine the best combination for discriminating classes of peat island, forested

land, open water, and barren land. Three scenarios are investigated: the first has SAR

texture data being the primary data source. Optical data (NIR, NDVI, and QuickBird

visible bands) are added to determine if classification is enhanced. The second scenario

has visible optical data as the primary data source and SAR backscatter data is added to

determine if there is an improvement in classification. The third scenario has VNIR

optical data as the primary data source and SAR data added to see if an improvement is

gained. In all cases LDA is first used to demonstrate the relative importance of the SAR

texture statistic and optical variables in discriminating among the four broad cover

classes by comparing the standardized discriminant function coefficients for each

variable in the models. This will provide information regarding the relative contribution

of SAR and optical variables to a given discriminant model. The models are then analyzed for their ability to best discriminate between classes of peat island, forested land, open water, and barren land.

LDA is used for multivariate discrimination and classification of the multiple SAR and optical data combinations. Class discrimination in all three scenarios uses the model data set and is assessed with the test data set. The agreement between predicted class membership and the validated classes was assessed using cross validation. Classification accuracy is assessed with overall accuracy and Kappa coefficients generated from confusion matrices for each model.

5.2.4 Image Classification and Accuracy Assessment

The land cover classification model was achieved using three general processing steps which were: 1) development of a reservoir and 100 m shore zone mask; 2) QuickBird image processing; 3) image classification (Figure 5.2). All processing steps were completed using ArcGIS® 9.2 Spatial Analyst (ESRI). A shore zone mask consisting of the area of Stephens Lake contained in the September 2, 2006 QuickBird image and 100 m of land area was created. Band thresholding is a common data analysis technique whereby one cover class is separated by another based on a separating value. A simple NDVI band value threshold was used to slice the NDVI band into a binary land and water image. A general rule for NDVI is that water is typically found between -1 and 0 and land between 0 and 1, but this may vary slightly from scene to scene. Other masking techniques are also commonly used and can be found in the literature (Lillesand and Kieffer 2000; Mather 2004). The binary raster was then converted to vector data set, at which point the large open water area of Stephens Lake was queried out by spatial

query. A 100 m buffer was then applied to the shoreline to create an area of land

extending inland 100 m along the shoreline. The buffer was then merged with the

reservoir water body and used to mask the optical PCA image created in the next

processing step. A PCA transformation was used to reduce the QuickBird optical and

derived NDVI band to three uncorrelated PCA image bands contributing 99.95 % of the

variance within the original 5 band image data set. An unsupervised hierarchical

clustering algorithm was chosen to ensure exhaustive inclusion of all pixel data in the

classification model. An iterative self organizing data analysis technique (ISODATA) of

unsupervised classification was selected for this purpose (Duda and Hart 1973; Tou and

Gonzales 1974; Mather 2004). This type of clustering uses a process in which, during

each iteration, all pixel samples are assigned to existing cluster centers based on

Euclidean distances and new means are recalculated for every class. A conservatively

high number of specified classes is usually recommended as the optimal number of

classes is usually unknown. In this analysis 100 classes with 20 iterations are selected as

inputs. A total of 95 natural class signatures were produced in this analysis, which are

also illustrated in a dendrogram or hierarchical classification graph. The generated

signature file was then used as the training input to a maximum likelihood algorithm for

final classification of the image. Maximum likelihood classification, not unlike Linear

Discriminant Analysis (LDA), calculates for each class the probability of the cell

belonging to that class given its attribute values. The pixel cell is then assigned to the

class with the highest probability. The dendrogram is used with the GIS to provide user

input labels of each natural class identified in the Iso cluster algorithm, based on

validation maps of the study area. The labeled classes can then be collapsed or grouped

together in the hierarchy to a general classification to represent broad land cover classes, in this case, peatland, forested land, open water, and barren land.

Shore Zone Mask	Image Processing	Classification

NDVI L&W Threshold

Simple Land/Water Mask

Reservoir Extraction

100 m shore buffer

Reservoir and Shore zone Mask

Band Masking

2006 QuickBird Image

NDVI Band Calculation

Merge Bands 1-4 with NDVI

5 Band QuickBird Image

PCA Band Transformation

3 Band PCA Image (masked)

ISOCluster (100 classes)

Maximum Likelihood

95 land cover class image

Dendrogram/ Class Labels

5 Class Broad Land Cover Image

Figure 5.2. Flow diagram of the methodology used to classify QuickBird high resolution imagery into the four broad peatland reservoir land cover classes developed in this thesis.

Validation data used in the multivariate discriminant models is used to assess classification accuracy of the unsupervised classification described above. A total of 2624 randomly selected validation pixels (polygon validation map) from peat island (n=850), forested land (n=583), open water (n=850), and barren land (n=355) were used to assess the classification accuracy of the unsupervised image classification model. A confusion matrix of unsupervised and validation class discrepancies was generated. Overall accuracy and KHAT were calculated from the confusion matrix to describe the classification accuracy of the model.

5.3 RESULTS AND DISCUSSION

5.3.1 SAR Texture Data Enhanced with Visible Optical Data

In this first scenario each of the four discriminant models provided statistically significant discrimination of the four land cover classes (Wilk's λ: p = 0.000)(Table 5.1). In the SAR texture (mean, homogeneity, and variance) LDA homogeneity dominates the first discriminant axis, accounting for 96.2 % of the variability in the data set, variance dominates the second discriminant axis (Table 5.2). Overall classification agreement of the test data was low at 62.7 % (KHAT = 0.473). Class confusion is high with barren and forested land classes. The addition of the NIR optical band to the SAR model shifts the dominance of the discriminant variable from homogeneity to the NIR band in the first discriminant axis (93.1 % variance). Overall classification agreement is improved by ~20 % (overall classification = 84.41, KHAT = 0.777). In this model barren land is still largely misclassified. The addition of the derived NDVI variable to the SAR texture model has a similar but less effective result to the addition of the NIR optical variable. The NDVI variable dominates the first discriminant axis. The texture variables have less of a contribution to the discrimination of the four classes, resulting in a lower overall classification accuracy (75.57%).

Table 5.1. Standardized discriminant function coefficients for each LDA SAR texture statistics + optical trial.(Note: hom = homogeneity, var = variance)

	Mean-Hom-Var		Mean-Hom-Var + QB NIR		Mean-Hom-Var + QB NDVI		Mean-Hom-Var + QB VIS	
Discriminant Axis	1	2	1	2	1	2	1	2
Mean	-0.533	0.014	0.225	-0.500	0.115	-0.437	-0.333	-0.236
Homogeneity	0.806	0.436	-0.427	0.545	-0.211	0.375	0.564	0.348
Variance	0.227	1.064	-0.149	-0.071	-0.066	-0.440	0.207	0.239
QB1	-	-	-	-	-	-	0.263	2.022
QB2	-	-	-	-	-	-	2.223	-2.470
QB3	-	-	-	-	-	-	-2.500	1.145
QB4	-	-	0.895	0.424	-	-	-	-
NDVI	-	-	-	-	0.974	0.178	-	-
% Variance	96.2	3.8	93.1	6.5	99.4	0.6	56.6	25.5

Table 5.2. LDA classification accuracy for each trial of SAR texture statistics + optical data for scenario 1. .(Note: hom = homogeneity, var = variance)

		Model/Test Agreement				Test Class Agreement (%)				
LDA Variables	# of Variables	Model Overall (%)	Model KHAT	Test Overall (%)	Test KHAT	Barren Land	Forested Land	Peat Island	Open Water	Test Samples
Mean-Hom-Var	3	64.79	0.502	62.70	0.473	13.91	39.35	68.83	95.80	1764
Mean-Hom-Var + QB NIR	4	85.39	0.791	84.41	0.777	13.91	85.35	90.17	97.81	1764
Mean-Hom-Var + QB NDVI	4	76.75	0.676	75.57	0.660	88.08	50.43	76.57	98.18	1764
Mean-Hom-Var + QB VIS	6	93.10	0.903	93.20	0.905	90.73	91.14	91.63	97.45	1764

The fourth discriminant model of the first scenario, in which visible QuickBird bands are added to the SAR texture statistic model results in the best overall classification accuracy (93.2%)(Table 5.2). In this model the green and red visible bands dominate the first discriminant axis, which accounts for 56.6 % of the overall variance in the data set. The second discriminant axis is dominated by the green and blue bands and accounts for 25.5% of the variance found in the data set. The second discriminant axis provides separation of the barren land class from the forested and peat island classes (Figure 5.3). The classification for the barren land class is improved to 90.73 % over the 13.91 % in the SAR texture statistic discriminant model by itself. The barren land class is most frequently confused with the peat island class in this model.
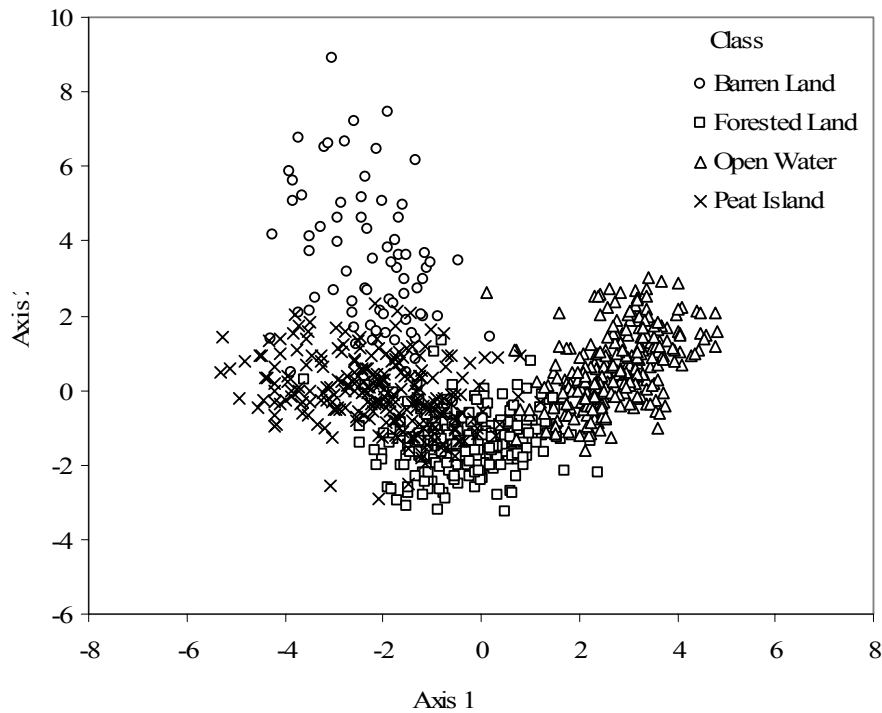
Figure 5.3. Discriminant axis scores scatter plot for the discriminant model in which optical visible bands (1-3) are added to SAR texture statistic data.

5.3.2 Optical Visible Data Enhanced with SAR Texture Data

In scenario 2, each of the five models provided statistically significant discrimination of the four broad land cover classes (Wilk's λ: p = 0.000). The stand alone QuickBird visible band discriminant model is dominated by the green and red visible bands in the first discriminant axis, which accounts for 60 % of the variance in the model. The second discriminant axis is dominated by the blue visible band and accounts for 31.4 % of the variance within the model (Table 5.3). The overall classification accuracy is 84.69 % (KHAT = 0.784), open water is the most commonly misclassified class at 72.63% (KHAT = 0.784) (Table 5.4). The addition of SAR $\sigma°$ data to the visible band discriminant model (QB 1-3) increased the overall classification accuracy (94.67 %,

KHAT= 0.925). The classification accuracy of open water improved to 99.09 %with the addition of the SAR σ° data to the visible band model. The first discriminant axis is dominated by the green and red visible bands with some contribution from the σ° variable, and accounts for 63.1% of the variance in the dataset. The models with the addition of one, two, and three SAR texture statistic variables to the visible discriminant model account for the remainder of the discriminant models. Overall classification accuracies do not significantly improve over the model in which σ° is added to the visible model, with overall accuracies of 93.71 (K = 0.912), 93.76 (KHAT = 0.912), and 93.20 % (KHAT = 0.905), respectively. In each of these three models the first discriminant axis is dominated by the green and red visible band variables, which accounts for between 54.5 and 56.6 % of the variance within the data set. Homogeneity has the greatest contribution to the discriminant axis of the three texture statistic variables.

Table 5.3. Standardized discriminant function coefficients for each LDA optical visible data + SAR backscatter and texture statistic data trial.

	QB 1-3		QB 1-3 + $\sigma°$		QB 1-3 + Mean		QB 1-3 + Mean-Hom		QB 1-3 + Mean Hom	
Discriminant Axis	1	2	1	2	1	2	1	2	1	2
QB1	-0.019	3.237	-0.103	0.793	-0.048	2.913	0.153	1.830	0.263	2.022
QB2	3.062	-1.828	1.860	-2.429	2.928	-1.894	2.329	-2.305	2.223	-2.470
QB3	-3.295	-0.834	-1.717	2.282	-3.039	-0.347	-2.512	1.191	-2.500	1.145
$\sigma°$	-	-	-0.827	-0.391	-	-	-	-	-	-
Mean	-	-	-	-	-0.357	-0.218	-0.236	-0.161	-0.333	-0.236
Homogeneity	-	-	-	-	-	-	0.524	0.356	0.564	0.348
Variance	-	-	-	-	-	-	-	-	0.207	0.239
% Variance	60.0	31.4	63.1	21.6	54.5	26.5	56.7	25.2	56.6	25.5

Table 5.4. LDA classification accuracy for each LDA optical visible data + SAR backscatter and texture statistic data trial.

		Model/Test Agreement				Test Class Agreement (%)				
LDA Variables	# of Variables	Model Overall (%)	Model KHAT	Test Overall (%)	Test KHAT	Barren Land	Forested Land	Peat Island	Open Water	Test Samples
QB 1-3	3	85.96	0.802	84.69	0.784	94.70	88.59	90.59	72.63	1764
QB 1-3 + $\sigma°$	4	94.59	0.924	94.67	0.925	96.03	92.67	91.63	99.09	1764
QB 1-3 + Mean	4	93.21	0.905	93.71	0.912	94.04	92.16	91.63	97.08	1764
QB 1-3 + Mean-Hom	5	94.02	0.916	93.76	0.912	94.04	92.67	91.63	96.72	1764
QB 1-3 + Mean-Hom-Var	6	93.10	0.903	93.20	0.905	90.73	91.14	91.63	97.45	1764

The visible band model enhanced with σ° performs the best for the second scenario in which SAR tone and texture data is added to visible optical data (94.7%, KHAT = 0.925). Figure 5.4 illustrates the separation of the four broad land cover classes. Open water is well separated from the other classes and is misclassified the least.
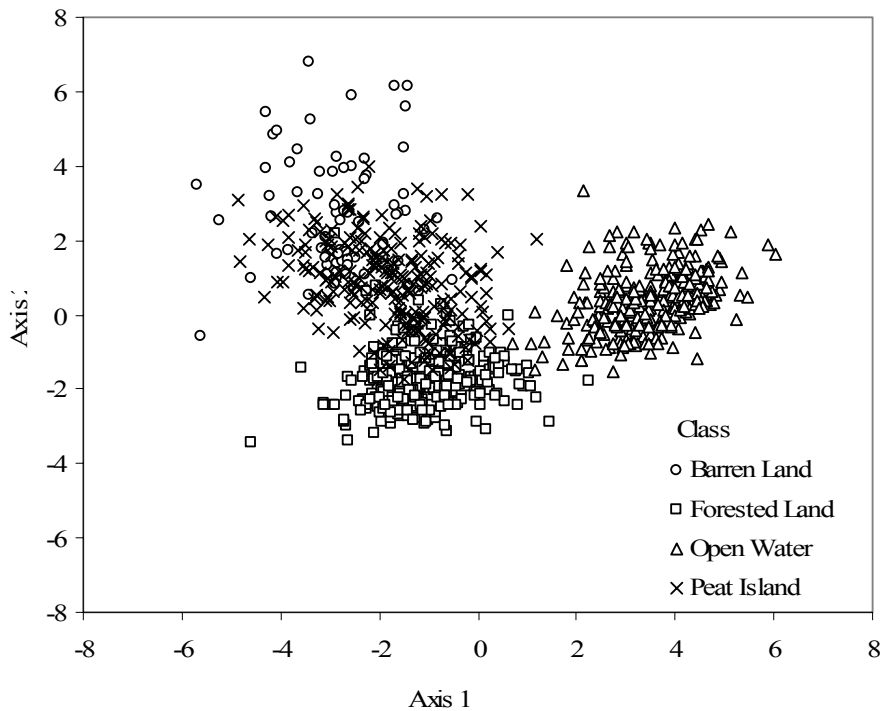

Figure 5.4. Scatter plot of discriminant axis scores for the LDA trial of SAR backscatter data added to optical visible data.

5.3.3 Optical VNIR Enhanced with SAR Texture Data

In scenario 3 the standalone VNIR optical model (QB 1-4) was found to have an excellent overall classification accuracy without the addition of SAR variables. The first discriminant axis is dominated by the green and red visible bands, with a contribution from the NIR band and accounts for 82.1 % of the variability in the data set (Table 5.5). The second discriminant axis is dominated by the blue and green visible QuickBird bands and accounts for 13.1 % of the variability within the data set. The addition of SAR $\sigma°$ to the VNIR model slightly increases the overall classification accuracy to 97.79% (KHAT = 0.969)(Table 5.6). In this model $\sigma°$ has a greater role in the second discriminant axis than in the first which is dominated primarily by the QuickBird green and red visible band variables (Table 5.5). The addition of the SAR texture statistics to the VNIR model does not improve classification over the model in which $\sigma°$ is added to the VNIR model.

Table 5.5. Standardized discriminant function coefficients for LDA trials in which SAR backscatter and texture statistic data are added to optical visible data.

	QB 1-4		QB 1-4 + $\sigma°$		QB 1-4 + Mean		QB 1-4 + Mean-Hom		QB 1-4 + Mean Hom	
Discriminant Axis	1	2	1	2	1	2	1	2	1	2
QB1	0.692	2.032	0.754	0.702	0.707	1.982	0.667	1.812	0.638	1.897
QB2	-2.406	-2.889	-2.149	-2.356	-2.332	-2.884	-2.201	-2.885	-2.181	-2.921
QB3	1.387	1.566	1.101	2.288	1.303	1.616	1.227	1.782	1.237	1.714
QB4	0.998	-0.176	0.886	0.015	0.976	-0.171	0.942	-0.133	0.937	-0.117
$\sigma°$	-	-	0.475	-0.418	-	-	-	-	-	-
Mean	-	-	-	-	0.217	-0.037	0.108	-0.030	0.170	-0.102
Homogeneity	-	-	-	-	-	-	-0.323	0.129	-0.129	0.175
Variance	-	-	-		-	-	-	-	-0.347	0.147
% Variance	82.1	13.1	79.9	10.5	80.4	12.3	80.8	11.4	80.7	11.5

Table 5.6. Classification accuracy results for LDA trials in which SAR backscatter and texture statistic data are added to visible optical data.

| LDA Variables | # of Variables | Model/Test Agreement | | | | Test Class Agreement (%) | | | | Test Samples |
		Model Overall (%)	Model KHAT	Test Overall (%)	Test KHAT	Barren Land	Forested Land	Peat Island	Open Water	
QB 1-4	4	97.93	0.971	97.68	0.967	100.00	96.08	97.28	99.09	1764
QB 1-4 + σ°	5	97.58	0.966	97.79	0.969	100.00	95.91	97.91	99.09	1764
QB 1-4 + Mean	5	97.58	0.966	97.62	0.967	99.34	95.74	97.91	98.91	1764
QB 1-4 + Mean-Hom	6	97.70	0.968	97.79	0.969	100.00	96.25	97.70	98.91	1764
QB 1-4 + Mean-Hom-Var	7	97.01	0.958	97.00	0.958	98.01	94.89	97.91	98.18	1764

The addition of SAR data to a full VNIR optical data set does not show significantly improved classification accuracy over the VNIR discriminant model on its own. The VNIR/SAR model (Figure 5.5) creates excellent separation between all four broad land cover classes. Barren land is separated from the other land based classes in the second discriminant axis, which is dominated by visible QuickBird bands. SAR σ° and the QuickBird NIR band are correlated in the first discriminant axis. They both create greater separation of land classes from water classes. For the SAR data, this related to the scattering characteristics of open water and land. There is a greater forward scattering component for calm open water, so less σ° is returned to the sensor. For the optical NIR data this is related to absorption by water at this spectral range, so less EMR is reflected back to the optical sensor. Forested land is the most frequently misclassified land cover class, which is most often confused with peat island.
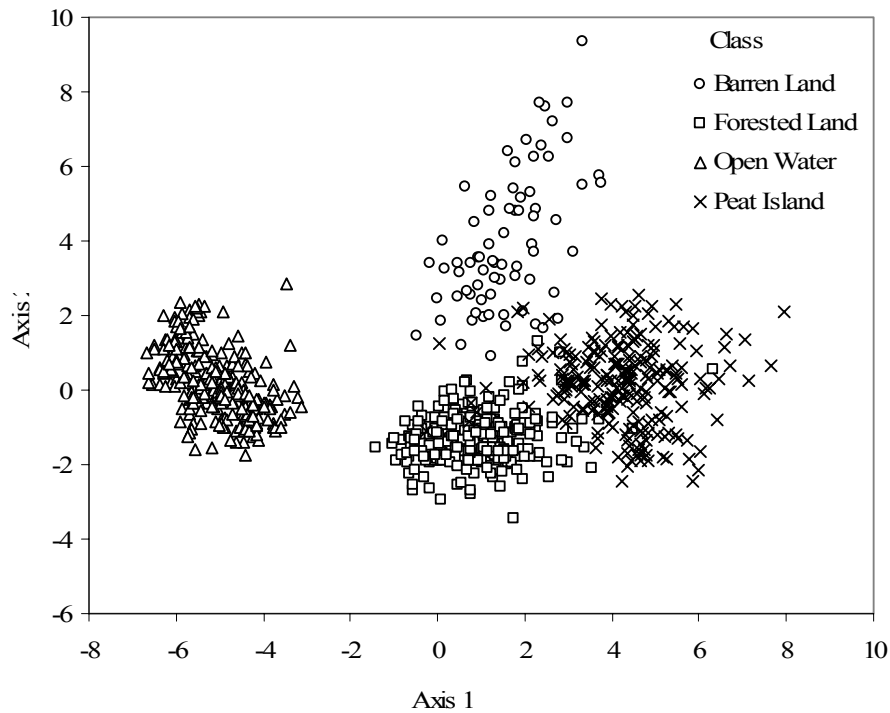
Figure 5.5. Scatter plot of discriminant axis scores scatter plot for the LDA trial in which SAR backscatter data is added to VNIR optical data.

Research question 1a demonstrates that when given a scenario where SAR texture statistic data is the primary data source the addition of optical data greatly improves overall classification accuracy of the studied land cover classes. Overall classification accuracy improved by 20% with the addition of a near-infrared data band, and by 30% with the addition of three visible data bands.

Research question 1b demonstrates that when given a scenario in which visible optical data is the primary data source, the addition of SAR $\sigma°$ improves overall classification accuracy. In this study overall classification accuracy improved by 10% to 95.67%. The addition of SAR texture statistics to the visible bands had no increased effect on overall classification accuracy over SAR $\sigma°$ by itself. The greatest improvement in classification accuracy came with the open water class. The addition of SAR $\sigma°$ to the

optical visible band discriminant model increased the classification accuracy of open water from 72.63% to 99.09%.

Research question 1c demonstrates that when given a scenario in which VNIR optical data is the primary data source, the addition of SAR σ° or texture statistic data does not significantly improve overall classification accuracy of broad land cover classes including peat islands.

5.3.4 Comparison of Remote Sensing Approaches

This study has demonstrated that optical VNIR data alone is better able to discriminate and classify (97.68 %) land and water cover classes of floating peatlands, forested land, barren land, and open water in a sub-arctic reservoir, than the use of visible data (84.69 %), or SAR texture statistic data (62.70%) alone.

An optical/SAR integration approach to discrimination revealed that in cases where only visible data are available the addition of SAR tone can improve classification results (94.67 %) over the use of visible data alone (84.69%). Likewise, the addition of visible data to SAR texture data dramatically improves classification accuracy from 62.70% to 93.20 %. SAR tone and optical NIR data are both able to discriminate between land and water; an integration of these two variables did not effectively enhance overall classification accuracies. The integrated approach to class discrimination is effective in certain cases, however it is not always practical to image with two separate systems. Issues such as cost, differences in water levels, differences in shoreline positions from multi-date data sets due to peat island movement, and resolution, complicate the combined use of these two sensors for the mapping and monitoring of peatland reservoir

change. An imaging application should rather look at the pros and cons of the two sensors to compliment each other rather than to outright improve classification accuracies.

In chapter 4, the use of SAR texture statistics for the discrimination of land from water was shown to greatly improve the classification over discrimination among the four land cover classes. Other studies have had similar outcomes. Arzandeh and Wang (2002) used Landsat TM and GLCM texture statistics derived from RADARSAT-1 fine beam imagery to classify wetland cover types. They found that optical Landsat TM data had better overall classification accuracy of eight wetland land cover types then any combination of texture statistic classifiers. They also found that overall classification accuracy improved greatly when discriminating between more general wetland and non-wetland cover types using SAR texture statistics. Another indication that optical and microwave sensors can be used to compliment each other in an application for discriminating the boundaries between land and water in a dynamic peatland reservoir. Where more detailed land cover class information is required, optical is useful, and when land and water boundaries are rapidly changing the use of SAR for guaranteed image acquisitions is invaluable.

In chapter 3, I demonstrated that turbid water resulting from high concentrations of TSS is often confused with other land cover classes due to high reflectance in the visible portion of the spectrum. The second scenario in this study found that given only visible bands of an optical data set, the addition of SAR $\sigma°$ can improve overall classification and improve the discrimination of open water. Although single-date, single-polarized SAR data has difficulty discriminating between different classes of vegetation, it has demonstrated great potential for use as a land and water masking tool. Optical data

acquisition for this study did not come easily. In 2005 a total of six attempts to collect QuickBird data was unsuccessful due to prevailing cloud cover during all attempts. In contrast, all four fine beam RADARSAT-1 SGX SAR images were acquired successfully on their programmed dates over 2005 and 2006. This is an important consideration when selecting spaceborne satellite data. In some cases SAR is therefore the only consistently attainable data for a given area. Because the process of peatland upheaval is very active in the first year following flooding, repeated image acquisitions would be required. In the absence of high resolution optical data and where image acquisitions need to be secured SAR makes an excellent tool for monitoring reservoir land and water changes over time.

Research question 2 demonstrates that optical VNIR data allows for a more robust land cover classification model than SAR data. Although SAR tone and texture data are able to discriminate readily between land and water alone, optical VNIR data allows for not only accurate discrimination between land and water, but also discrimination of more detailed land cover classes (i.e. peat island vs. forested mineral island).

5.3.5 Image Classification and Accuracy Assessment

An optical image classification model using the four VNIR bands of the QuickBird image was selected as the best available option for discrimination, classification, and mapping of land and water cover classes. Unsupervised class labeling relied on user based level 4 validation classes defined in Chapter 3. The dendrogram, based on class cluster distance, resulting from the ISODATA classification allows classes to be collapsed hierarchically down to higher order classes (Figure 5.6). Shadow related to forest canopies was not originally accounted for but occurs as a natural class as a result

of the ISODATA clustering algorithm and makes up a class in the final model, misclassification due to this class is considered to be negligible. A total of 95 natural spectral classes identified in the unsupervised classification were collapsed into floating peatland cover, forested land cover, barren land cover, and water. Results of the image classification are presented in Figure 5.7 (Ross Wright Bay), Figure 5.8 (O'Neil Bay), and Figure 5.9 (North Boisvert Island).

Classification accuracies of the image classification model are presented in Table 5.7. Overall classification accuracy was excellent at 95.5 % (K = 0.938). Misclassification was very low for all four classes, with the classification of open water being nearly perfect. Visual inspection of the classification reveals some additional confusion between forested land, barren land, and floating peatland classes, which is reflected in the error matrix (Table 5.7). Overall the results are excellent, and achieve the intended objective of developing an image classification model that can be used to map and monitor physical reservoir changes as a result of peatland disintegration, and mineral erosion processes. The advantage of this classification approach is that it is not only limited to the development of a general land and water mask but also to discrimination between the more detailed floating peatland, forested land, and barren land classes.
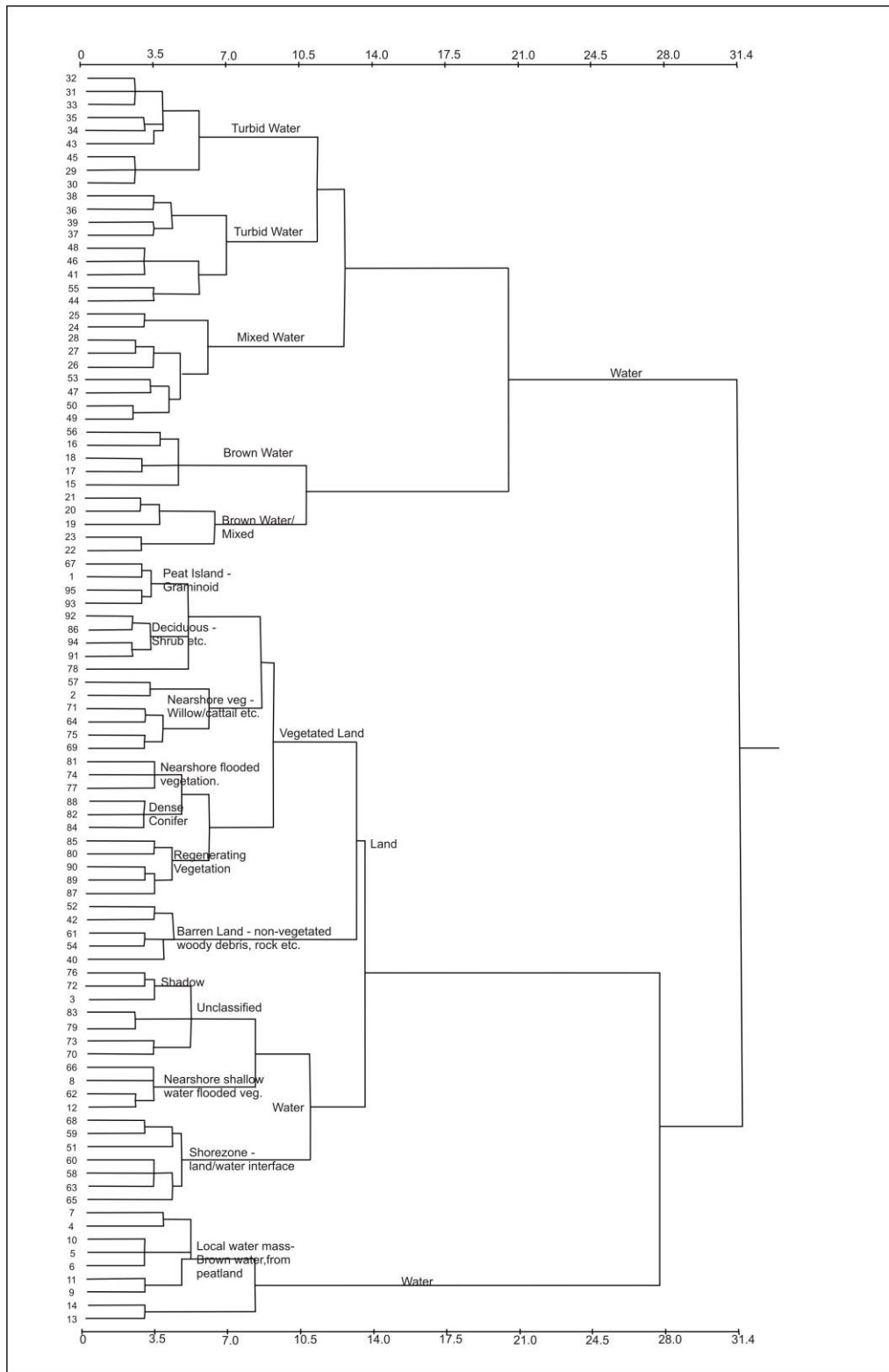
Figure 5.6. Dendrogram of the unsupervised ISODATA hierarchical classes. Grouping of related classes is achieved through Euclidean distance similarities measured in spectral space. Note that information labels are derived from the Chapter 3 hierarchical classification.
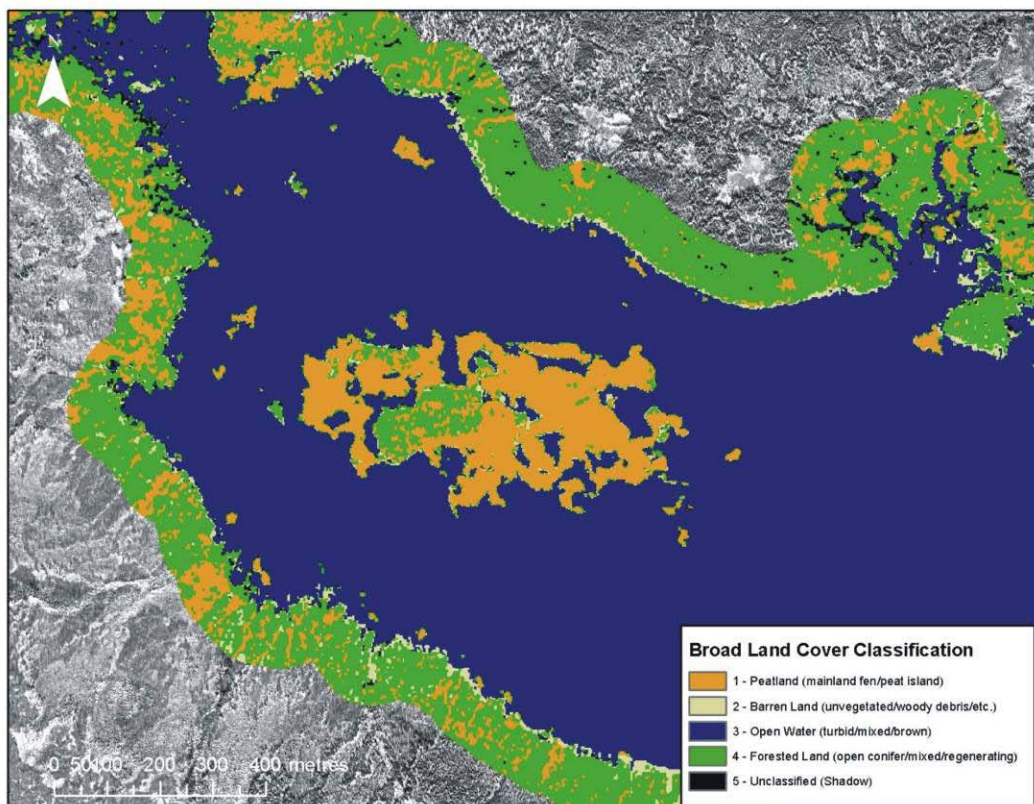
Figure 5.7. Final unsupervised QuickBird VNIR land cover classification map of the Ross Wright Bay study area. Copyright: DigitalGlobe 2006.
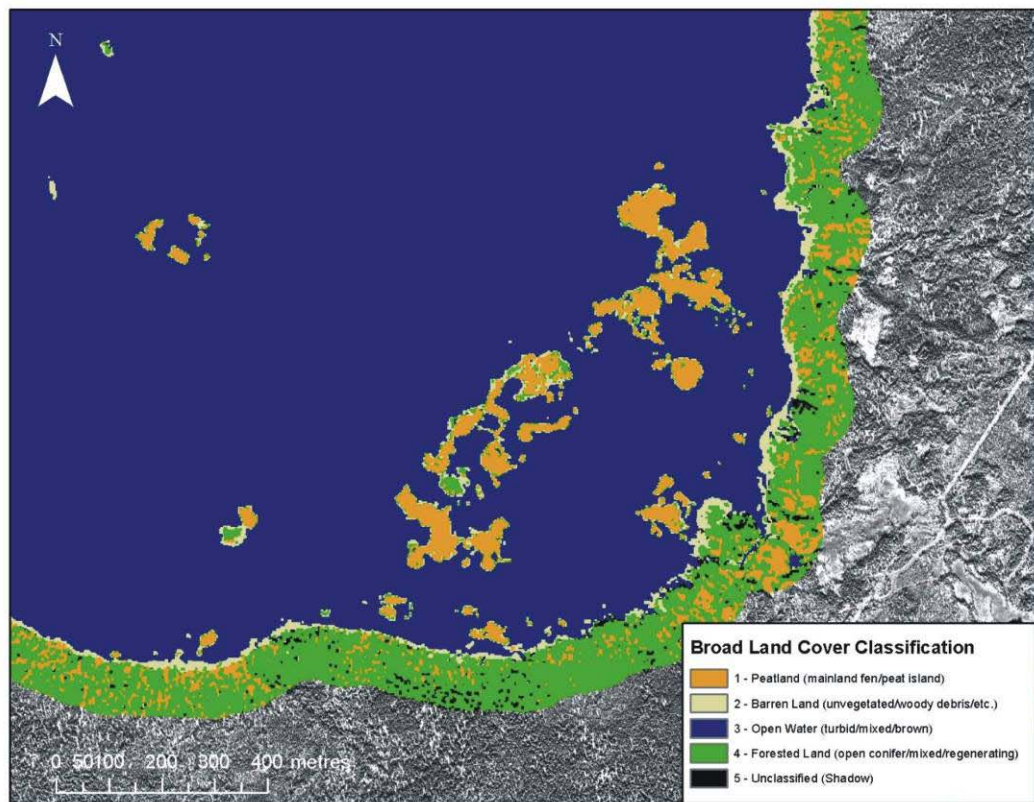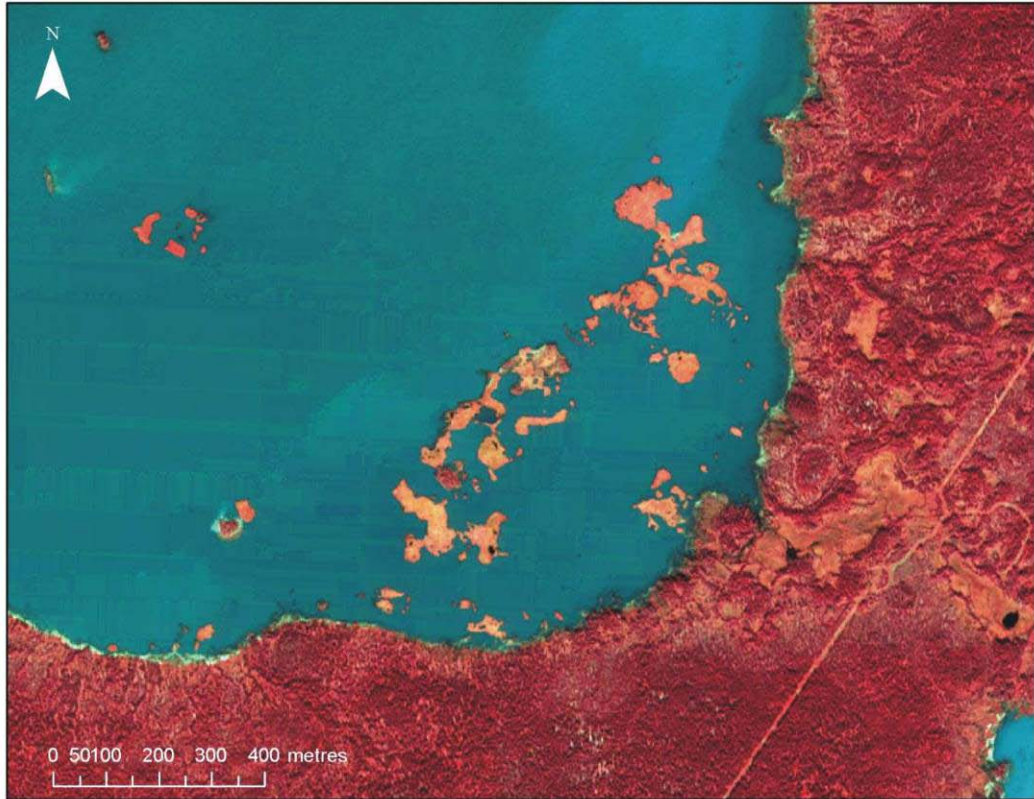
Figure 5.8. Final unsupervised QuickBird VNIR land cover classification map of the O'Neil Bay study area. Copyright: DigitalGlobe 2006.
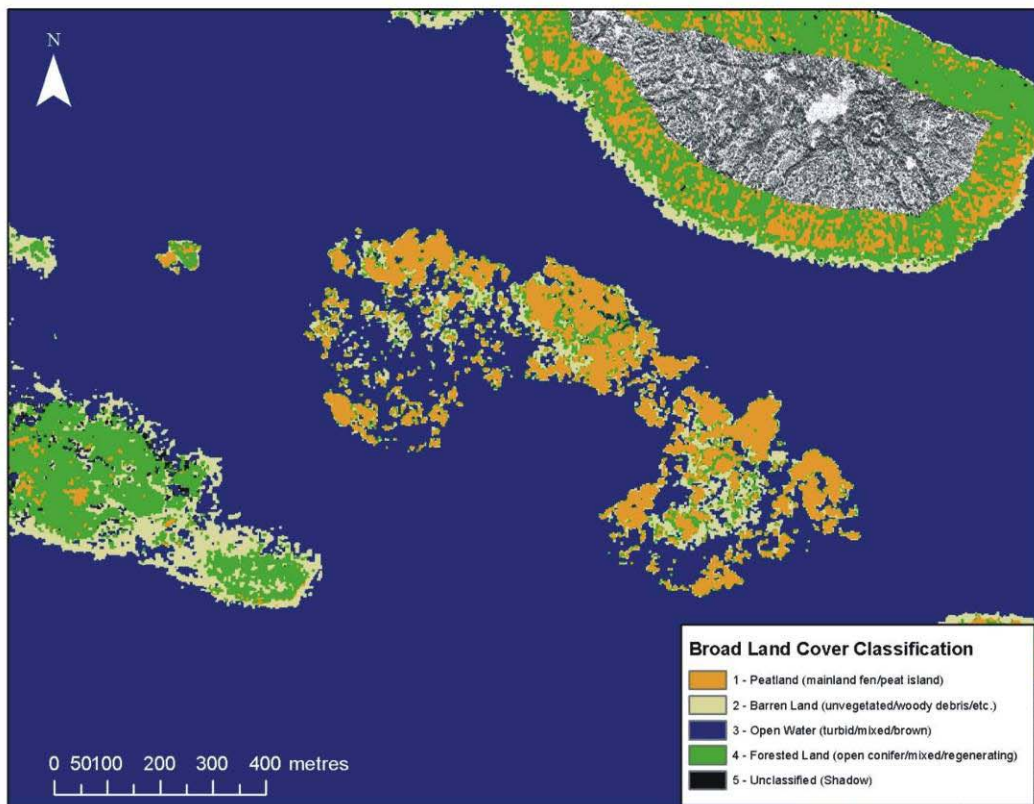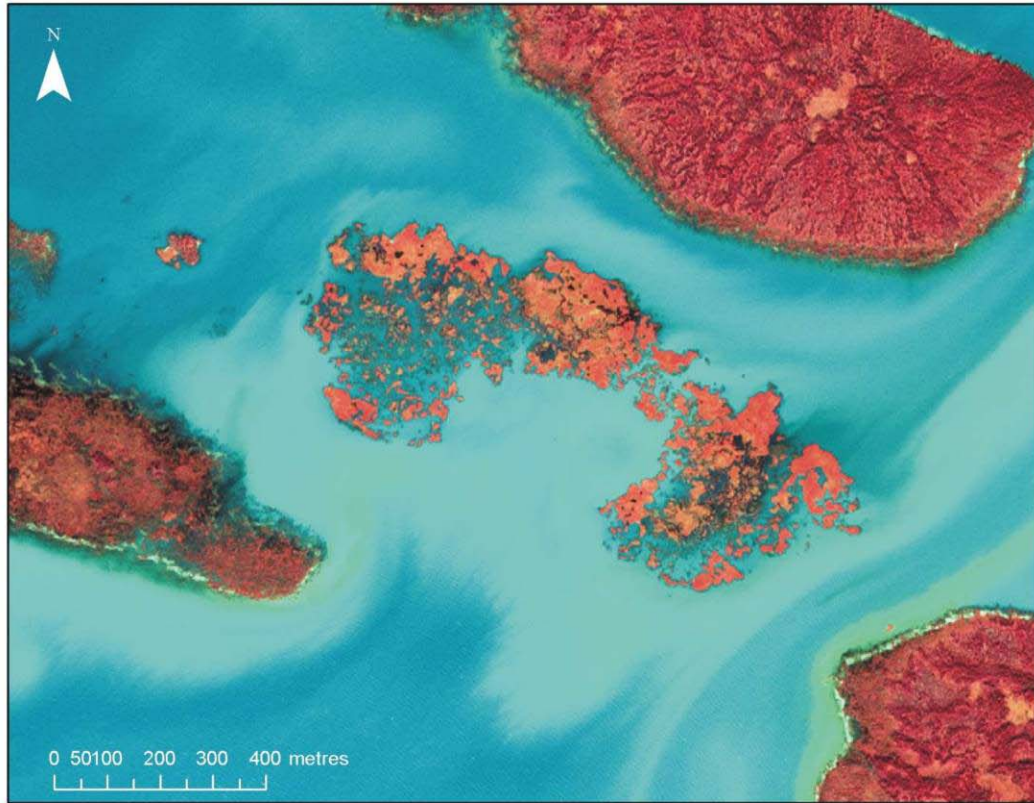
Figure 5.9. Final unsupervised QuickBird VNIR land cover classification map of the North Boisvert Island study area. Copyright: DigitalGlobe 2006.

Table 5.7. Error matrix for the QuickBird VNIR unsupervised land cover classification model.

	Barren Land	Forested Land	Open Water	Peat Island	Row Total
Barren Land	325	10	0	20	355
Forested Land	2	512	7	62	583
Open Water	0	0	850	0	850
Peat Island	1	15	0	820	836
Column Total	328	537	857	902	2624

Producers's Accuracy
Barren Land = 325 / 328 = 99.1%
Forested Land = 512 / 537 = 95.3%
Open Water = 850 / 857 = 99.2%
Peat Island = 820 / 902 = 90.9 %

User's Accuracy
Barren Land = 325 / 355 = 91.5%
Forested Land = 512 / 583 = 87.8%
Open Water = 850 / 850 = 100.0%
Peat Island = 820 / 836 = 98.1%

Overall Accuracy
= 2507 / 2624 = 95.5%

KHAT
= 0.938

181

5.5 CONCLUSION

The use of satellite image data to track and monitor changes to the boundaries of land and water within a peatland reservoir specifically related to peatland uplift, transport, and disintegration, mineral erosion, and water level fluctuation is a novel application. This study's first objective was to determine whether an optical, SAR, or an integration of these two remote sensing technologies provides a better method of discrimination between land and water cover classes in a sub-arctic peatland reservoir.

Research question 1a found that a SAR texture statistic discriminant model was greatly improved with the addition of QuickBird visible bands (i.e. 1, 2, and 3). This scenario demonstrated that in the absence of a full VNIR data set, discrimination and accurate classification of land and water classes is possible. In research question 1b a scenario was created where only visible optical data was available, the addition of SAR $\sigma°$ to a discriminant model improves the classification of open water, creating much improved overall classification accuracies. The third research question (1c), in which a full VNIR optical data set was the primary data source, found that the addition of SAR $\sigma°$ data does not significantly improve overall classification accuracy of peatland, forested land, barren land and water classes.

In answering research question 2 it was determined that QuickBird optical VNIR data provided the best overall discrimination and classification approach. The QuickBird optical solution not only provides excellent discrimination between land and water boundaries, but also allows for discrimination of more detailed land and water classes. The use of SAR as an approach to the discrimination of the boundary between land and water is valid, however discrimination between more detailed land-based classes is

difficult. An integrated remote sensing solution showed that SAR can be used to supplement an optical data set that is lacking a NIR band to achieve a comparable classification result. The use of the two technologies in a dynamic peatland reservoir application is better suited in a complementary manner. That is, SAR image acquisitions can fulfill time sensitive portions of an application, whereas optical images can be used to increase the class detail in an application. The process of peatland upheaval, transport, and disintegration is very active within the first couple of years, and would benefit from a higher frequency of image acquisitions during this time.

The second objective of this chapter was to develop an image classification model that could be used to map and monitor the changes to the boundary between land and water arising from the dynamic processes of peatland upheaval, transport, and disintegration. An unsupervised image classification of the QuickBird VNIR data set resulted in excellent classification accuracy of floating peatlands, forested land, barren land, and open water. The hierarchical nature of the resulting unsupervised spectral classes has additional utility for a number of related reservoir applications, provided the appropriate level of validation data is available for class labeling. More importantly the classes can be collapsed into a land and water mask for quantification of reservoir area change over time.

CHAPTER 6 : CHANGE DETECTION ANALYSIS OF A DYNAMIC PEATLAND RESERVOIR

6.1 INTRODUCTION

In this chapter I apply the optical image classification model developed in Chapter 5 to a land and water change detection analysis over a 7 year period (1999 – 2006) in a large back bay of Stephen's Lake. using a historical (1999) land/water mask of the same area. The results will demonstrate the utility in using remotely sensed image data sets in mapping peatland reservoir dynamics, and is intended to illustrate the effects of peatland upheaval, transport, and disintegration, mineral shoreline erosion, and water level management, on the land/water interface of the reservoir 35 years after flooding.

6.2 METHODS

6.2.1 Study Area and Data

This chapter focuses on O'Neil Bay, located on the west end of Stephens Lake (Figure 6.1). It currently occupies approximately 800 ha and runs approximately 5 km east to west and 2 km north to south. The bay receives water from two main tributaries, Looking Back Creek from the west, and a breach channel that connects the Nelson River through a water body known as Pond 13 from the south. The area, prior to inundation, was covered almost entirely by bog and fen peatland types (KHLP 2010). Since initial flooding the bay has undergone extensive peatland upheaval, transport, and disintegration in addition to mineral erosion.

The September 2, 2006 QuickBird high resolution (2.44 m) optical image previously classified in to four land cover classes (Chapter 5) is used to represent the state of O'Neil Bay in 2006. Digital ortho imagery (DOI) of Stephens Lake acquired August 16, 1999 was provided by Manitoba Hydro. The water level in the 2006 imagery was 140.81 m ASL at the time of acquisition and 140.47 m ASL for the 1999 air photo acquisition (Manitoba Hydro Unpublished Data). The 1999 imagery was collected at 1:60,000 and has the image pixel size of 1 m. Both images are projected to a UTM zone 15 NAD83 projection. Geometric correction of the QuickBird image is described in Chapter 3. The positional accuracy between the images appeared to be excellent.
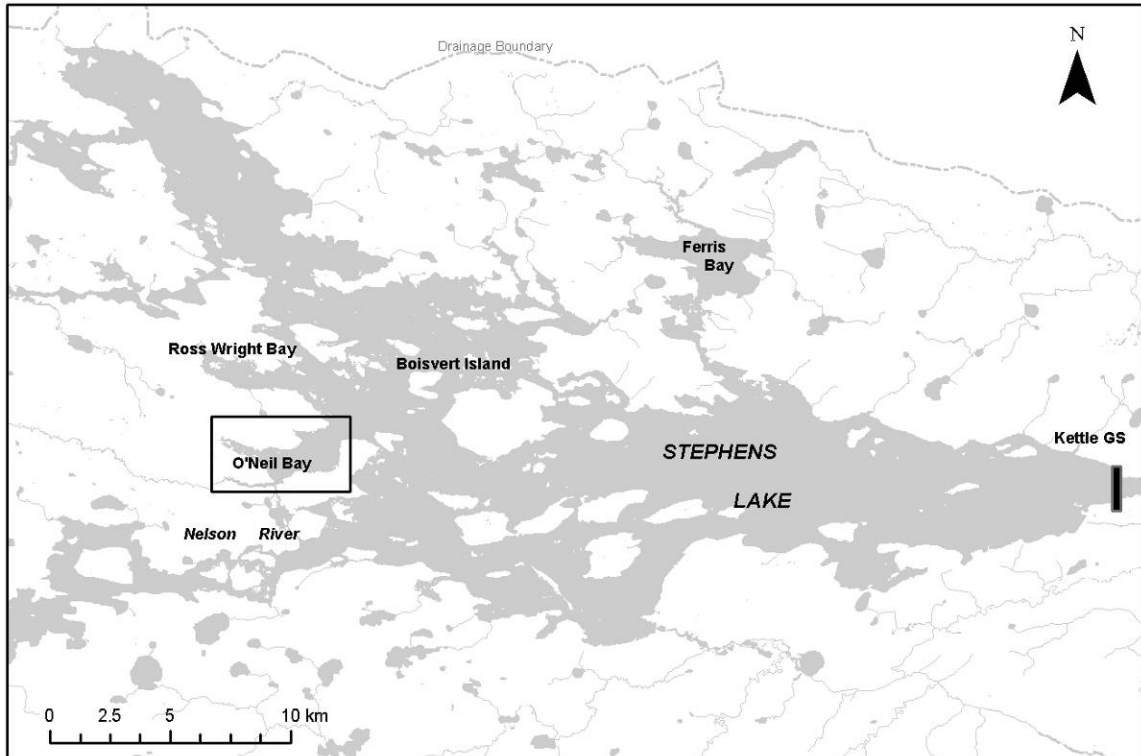
Figure 6.1. Location of the O'Neil Bay study area on Stephens Lake. (Spatial Data Source: Geogratis 1:50K NTDB, (C) Department of Natural Resources Canada).

6.2.2 Change Detection Analysis

The process of change detection involves the use of multi-temporal data sets to discriminate areas of land cover change between two dates of imaging (Lillesand and Kieffer 2000). In this analysis I employ a post-classification comparison (Lillesand and Kieffer 2000). Figure 6.2 illustrates the processing steps employed in this analysis. ArcGIS® 9.2 (ESRI) software was used to digitize a 1999 vector shoreline using a heads up digitizing approach. The vector shoreline was then converted to a 2.44 m land and water binary raster dataset (water = 0 and land =1) using ArcGIS Spatial Analyst. The QuickBird image previously classified to four broad land cover classes using an unsupervised classification algorithm (Chapter 5) was reclassified to a land and water binary data set. Finally, map algebra was applied to the two images. The 1999 land and

186

water mask was subtracted from the 2006 land and water mask, resulting in a change map

in which values of 0 represented pixels with no change between the two years, -1

represented areas that were land in 1999 and became water in 2006, and +1 represented

areas that were water in 1999 and became land in 2006. Areas of change between the two

maps were then calculated and summarized.
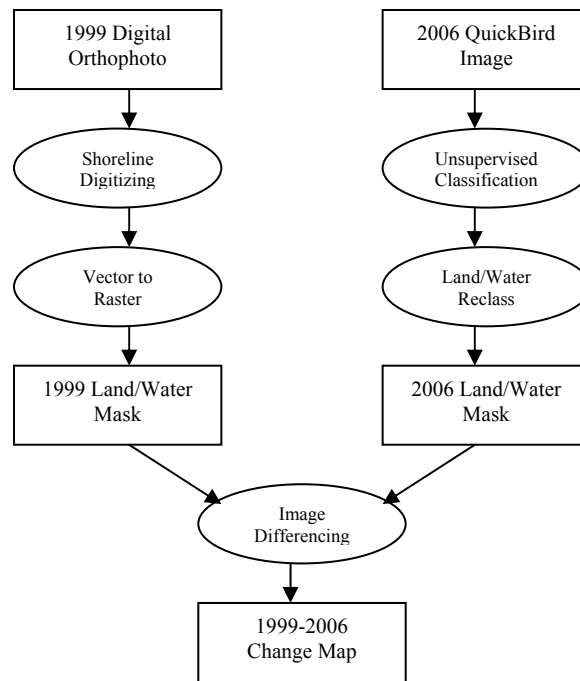
Figure 6.2. Flow diagram of the methods used to complete the change detection analysis in this study.

6.3 RESULTS AND DISCUSSION

Maps of the land and water masking procedures for 1999 (Figure 6.3) and 2006 (Figure 6.4) have, at first look, very similar results. However, further investigation reveals apparent differences between the two years. The most noticeable difference is the reduction in the size of the floating peat islands in the southeast corner of the image and the increased backwater effect at the mouth of Looking Back Creek in the southwest corner of the 2006 image. Further change is revealed after applying the map algebra between the two years of land and water masks.
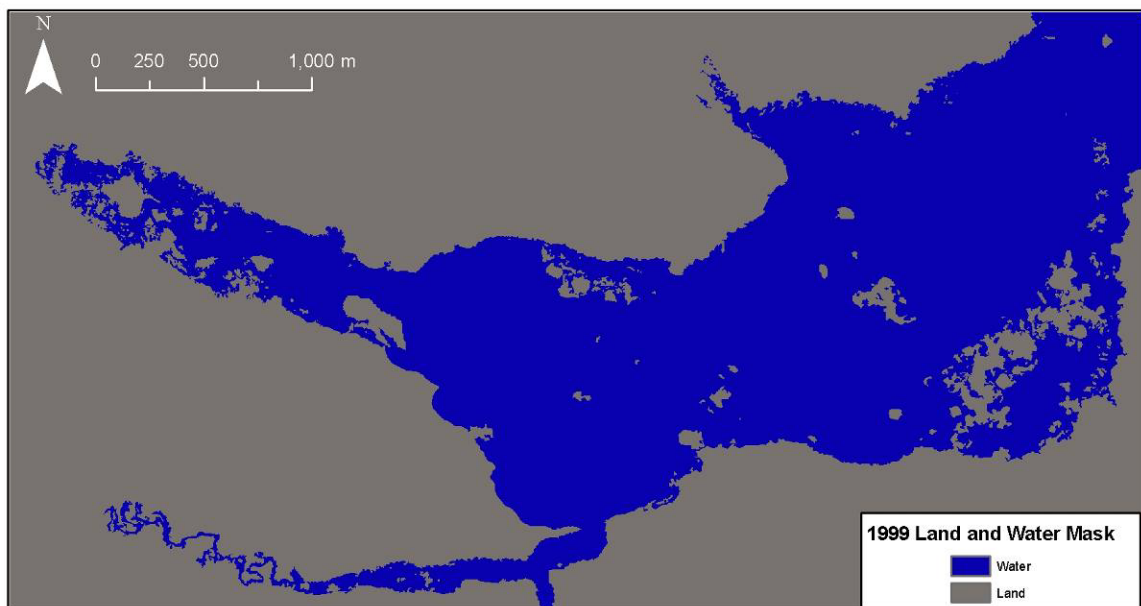

Figure 6.3. The 1999 land and water mask map derived from historical digital orthophoto digitization.
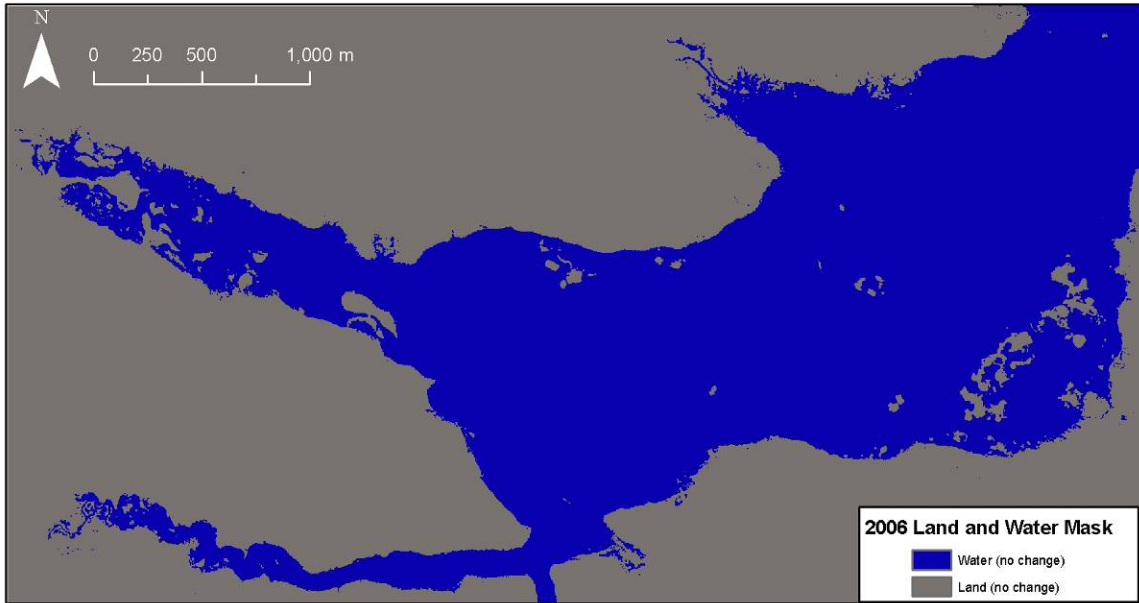
Figure 6.4. The 2006 land and water mask map derived from the image classification method developed in Chapter 5.

The final change detection map clearly shows the areas of change when overlaid on top of the 2006 land and water mask (Figure 6.5). Areas colored red indicate areas that were land in 1999 and changed to water in 2006. Areas that are green in the change detection map are areas that were water in 1999, which became land in 2006. Between 1999 and 2006 there was an increase in water area of 61.58 ha (7%) (Table 6.1, Figure 6.6). The loss in land during this same period is inversely proportional to the increase in water. Three main factors including, water level variation, peatland disintegration, and mineral erosion are likely responsible for the changes seen between the two years of land cover data. Other factors such as geometric and scale errors between the two years of land cover data may introduce error, but are assumed to be negligible for the purposes of

this analysis.
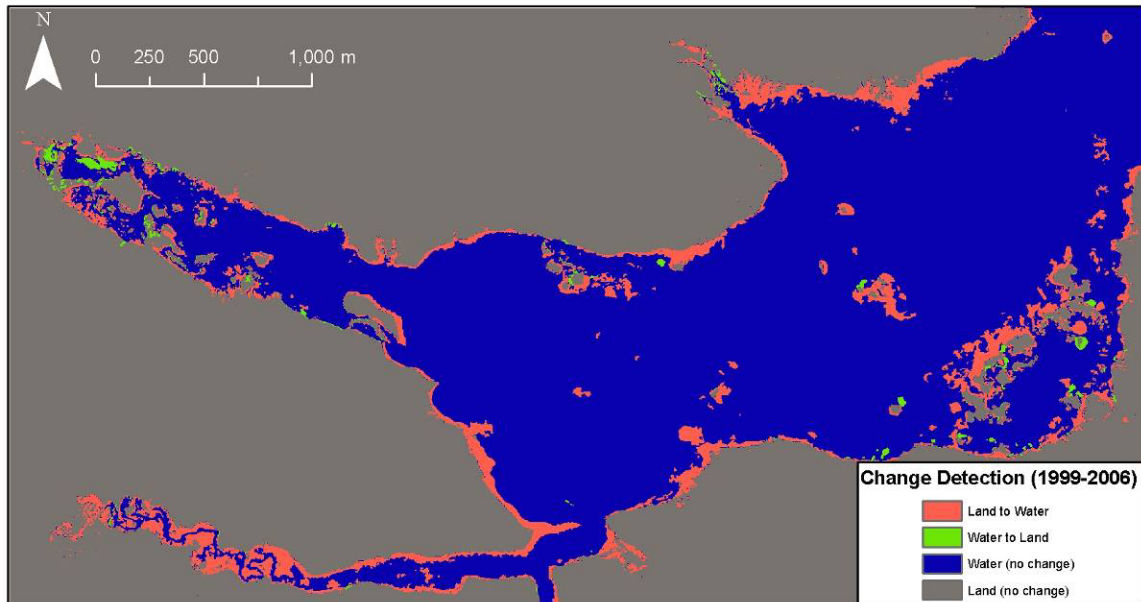
Figure 6.5. Change detection map created by subtracting the 1999 land and water mask from the 2006 land and water mask showing areas that were water and are now land and areas that were land and are now water.

Table 6.1. Summary of land and water areas in 1999, and 2006, and the amount of change in the seven year period between the two images.

| Class	1999		2006		Change	
	Area (ha)	% of Total	Area (ha)	% of Total	Area (ha)	%
Water	512.39	64.04%	573.96	71.74%	61.58	7.70%
Land	287.67	35.96%	226.10	28.26%	-61.58	-7.70%
Total	800.06	100.00%	800.06	100.00%	-	-
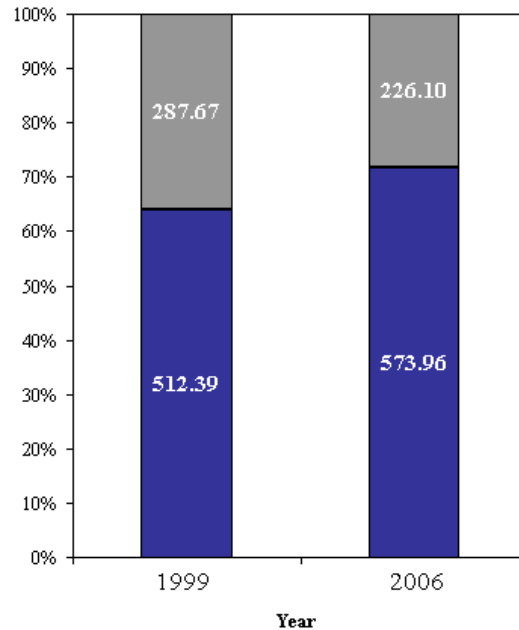
Figure 6.6. Stacked bar graph depicting land and water composition and total areas for the O'Neil Bay study area in 1999 and 2006.

Water levels were approximately 30 cm (measured at Kettle GS) higher in the 2006 land/water classification, contributing to the shore zone change indicated by the red areas around the periphery of the bay. The mouth of Looking Back Creek in the southwest corner of the image is completely inundated by water in 2006. The original creek channel seen in 1999 (Figure 6.3) is lost in the 2006 classification. Kettle GS is operated as a peaking-type plant. It's forebay is cycled on a daily, weekly, and seasonal basis, the annual range is 141.1 m to 139.5 m ASL (Manitoba Hydro 1996a). As a result water level variations between multi-date imagery are an important consideration. Changes to the land/water interface resulting from short term water level variation can be difficult to separate from the land water changes resulting from peatland disintegration or mineral erosion processes. A current detailed bathymetric or digital terrain model (DTM) could be used to estimate the surface area of O'Neil Bay given a water level elevation at Kettle GS. This in turn could be used to determine changes resulting entirely from

191

operational water level variation. The remainder of the changes (outside of the DTM) could be attributed to ongoing reservoir expansion resulting from mineral shore erosion and peatland disintegration.

Peatland reservoir dynamics involve peatland upheaval, transport, and disintegration and/or growth. The large peat island formation in the southeast corner of Figure 6.5 is magnified in Figure 6.7. Along with water level variation between the 1999 and 2006 land and water masks, a number of dynamic peatland processes can be identified. Green areas in the open area of the bay indicate floating peat island movement. Peat islands have detached from the main peat island formation or have migrated in from other areas of the bay. An example is the small floating peat island abutted against a forested mineral island in the southwest corner of the map (Figure 6.7). Closer to shore in the southeast corner of the map, small green areas may indicate shore zone peat resurfacing as a result of newly flooded peatland areas in the expanding reservoir. Red areas along the north edge of the large peat island formation are a result of water level variation, sinking of peat island fringes and detachment and movement of peat islands away from the larger central formation, which was confirmed by a bottom validation survey in 2006 (Larter and Cooley 2009) (Figure 6.8). Validation sites that showed sub-surface bottom types to be intact peat (organic fibric), indicated that floating peatlands had either sank or neglected to float with additional water level increase between the two years of image data. Likewise the red areas along the edge of the mainland shoreline are a

combination of water level variation and peatland disintegration.
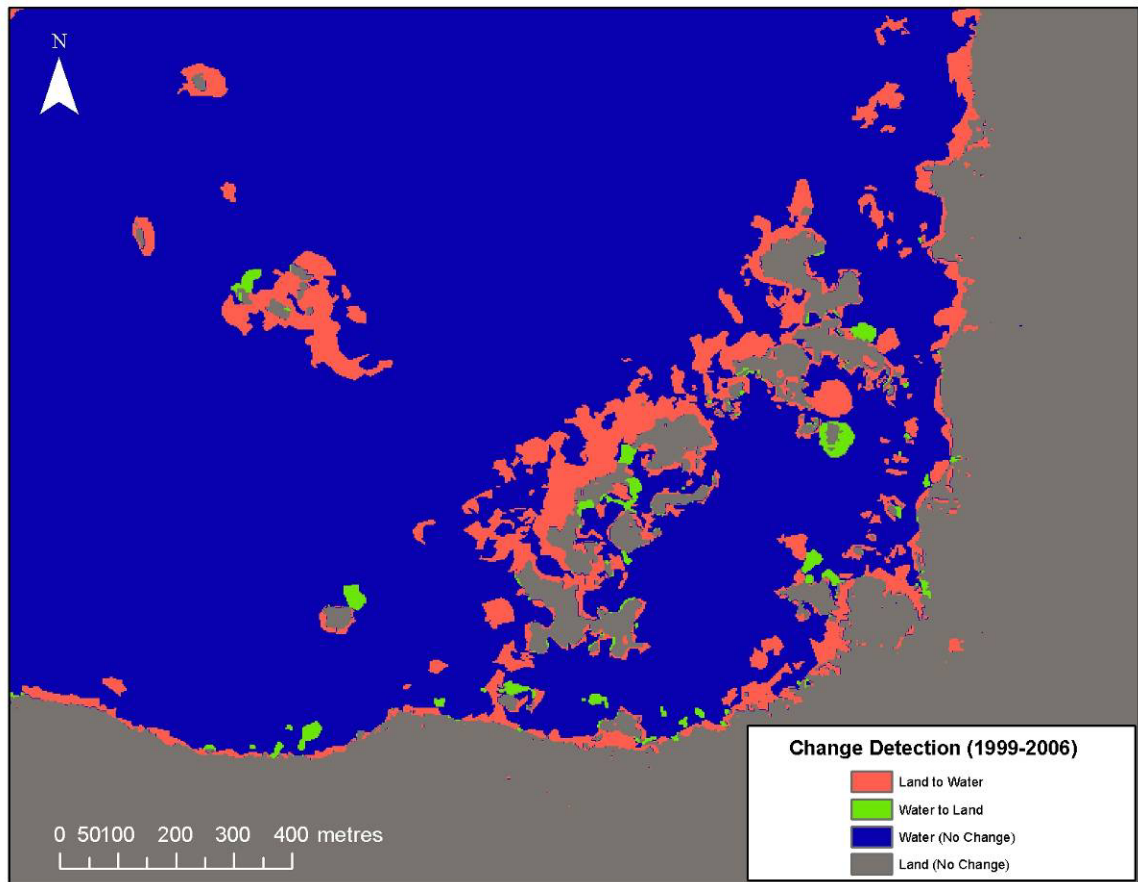
Figure 6.7. Change detection map of the large floating peatland area in the southeast corner of O'Neil Bay.
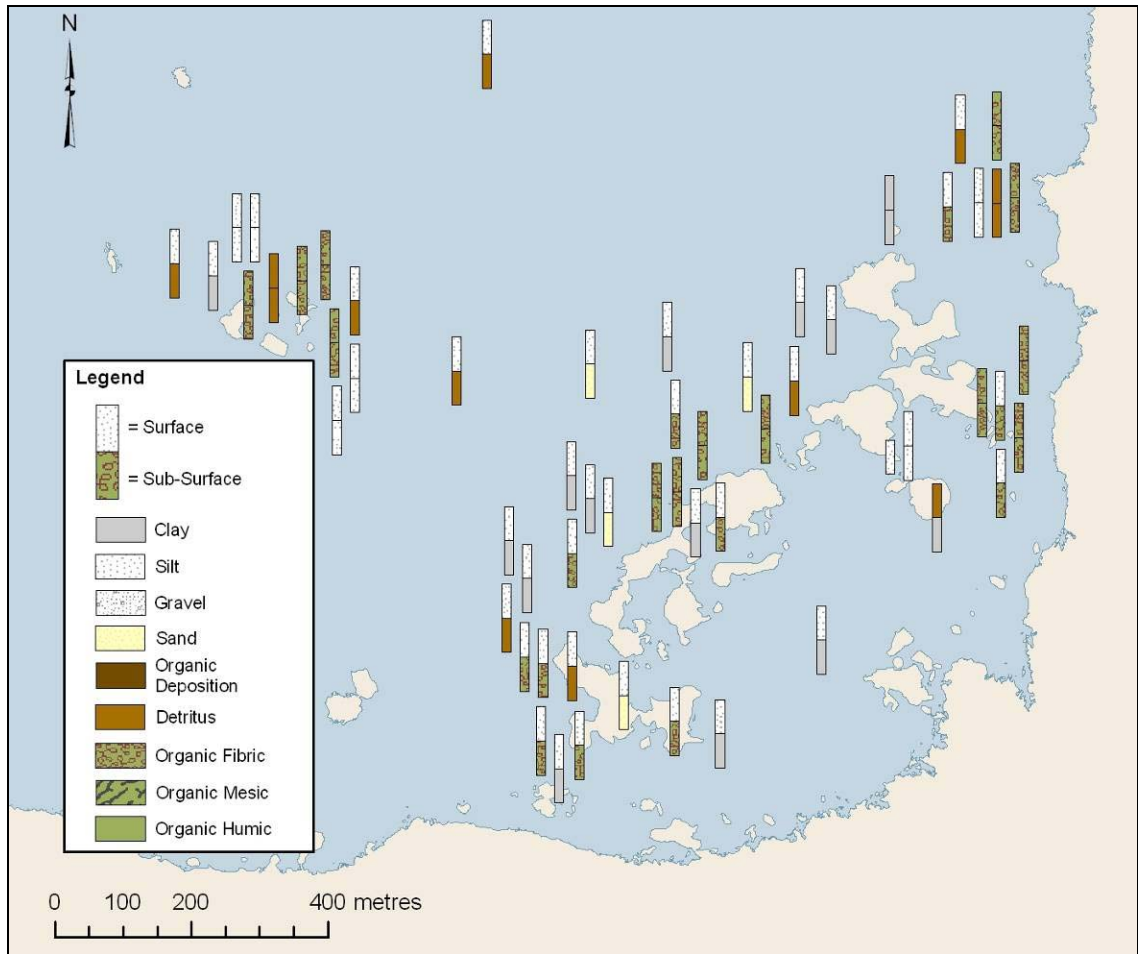
Figure 6.8. Locations of surface and sub-surface bottom type validation sites showing bottom type composition near the O'Neil Bay floating peatland formation.

Mineral erosion in addition to peatland disintegration has also occurred between the two dates. The south central area of the change detection map (Figure 6.3) shows a water course entering the bay. This channel connects Pond 13 to O'Neil Bay which was breached in recent years, connecting the Nelson River downstream of Gull Rapids to O'Neil Bay, changing the flow dynamics within the system. This increased flow through to O'Neil Bay caused the peninsula of a post-glacial esker to be completely eroded away in the area of the flow between 1999 and 2006.

6.4 CONCLUSION

In this chapter I demonstrated the use of a classified optical image directly applied in a multi-date land and water change detection analysis to quantify changes to terrestrial and aquatic habitats in a dynamic peatland reservoir. The results demonstrated that changes to the land/water interface, resulting from peatland upheaval, transport, and disintegration, and mineral erosion, are still occurring 35 years after initial flooding of the reservoir. Change detection quantification is hindered somewhat by operational water level variation. An up to date detailed bathymetric model could be used to determine shoreline extents resulting from forebay cycling in order to attribute remaining changes to ongoing peatland disintegration and mineral erosion processes.

CHAPTER 7 : SUMMARY, CONCLUSIONS, AND RECOMMENDATIONS

7.1 SUMMARY

Chapter 1 introduced the concept of peatland dynamics in sub-arctic hydroelectric reservoirs and proposed a potential means for utilizing optical and microwave remote sensing technologies for mapping and monitoring the changes occurring as a result of this dynamic process. Chapter 2 provided a context for understanding peatland development, the process of peatland disintegration, and floating peatland/peat island formation as well as a review of remote sensing principles and applications related to wetland and peatland monitoring and mapping. Chapter 3 explored the optical VNIR properties of dominant land cover classes and determined the ability of the QuickBird high-resolution optical sensor to discriminate between floating peatlands, forested land, open water, and barren land cover classes. Chapter 4 looked at the microwave backscattering properties of the dominant land and water cover classes and determined the discriminant ability of tone and image texture statistics derived from single date RADARSAT-1 fine beam SGX SAR imagery to classify floating peatlands, forested land, barren land, and open water cover classes. Chapter 5 explored the potential for integrating optical and microwave remote sensing data for improved classification of broad reservoir peatland classes and proposed a methodology for mapping land and water cover classes. In Chapter 6, an optical satellite image classified as land and water was used in a change detection analysis to describe changes in a sub-arctic peatland reservoir over a period of 7 years, 35 years after initial flooding.

7.2 CONCLUSIONS

The overarching objective of this thesis was to develop an approach to remote discrimination of land (i.e. floating peatlands, forested land, and barren land) from water in a sub-arctic peatland reservoir using optical and synthetic aperture radar data. The methodology developed herein provides a context for routine discrimination of the boundaries between land and open water in a sub-arctic peatland reservoir, which are continually changing as a result of peatland disintegration, mineral shoreline erosion, and water level fluctuation. In a dynamic peatland reservoir this methodology is paramount to mapping, monitoring, and quantifying the ongoing changes to aquatic and terrestrial environments, which in turn assists the ongoing stewardship of the natural environment.

In achieving thesis Objective 1 the optical spectral response and microwave backscattering signatures of land (i.e. forested land, peatland, barren land) and water cover classes were determined. Both the optical (Chapter 3) and SAR (Chapter 4) systems were able to readily discriminate between more general land and water classes. Although the two systems operate in different fashions discrimination between land and water boundaries resulted in similar excellent (> 90 %) classification accuracies. However when looking at more detailed land-based classes (i.e. peatland, forested land, barren land) SAR (RADARSAT-1) only had moderate classification accuracy results (~ 60%), whereas the optical sensor (QuickBird) had excellent classification results. From an operational point of view QuickBird image acquisitions can be hindered by cloud cover and prevailing weather conditions, and difficulties may arise when discriminating highly reflective turbid water from some land based classes. RADARSAT-1 can penetrate cloud cover and weather and image at any time of the day or night. SAR

backscatter from land cover targets can be affected by prevailing environmental conditions (waves, rainfall), and sensor incident angle. This should be considered when imaging a reservoir many times during varying weather conditions; however it should not severely hinder the overall objective of mapping land and water boundaries. In conclusion, Objective 1 found that the use of high-resolution optical QuickBird data is more adept at discriminating and classifying detailed land and water-based classes from each other, however both are proficient in discriminating the boundary between land and water only.

Thesis Objective 2 determined whether an optical, radar, or integrated sensor approach provided a better method of discrimination and classification of land and water classes. Results showed that NIR optical and SAR data are somewhat correlated. An integrated approach to discrimination of land and water cover types would be practical if the objective was to map more detailed land cover classes. Visible optical data could be supplemented with a SAR image band to map more detailed land cover classes and vice versa. In the end it was concluded that optical VNIR data provided the best overall classification approach as it allowed for excellent discrimination among land-based targets, which is important in discriminating floating peatlands from surrounding mineral based shorelines and islands. SAR can be viewed as a more dependable spaceborne sensor, in that it will image ground targets regardless of prevailing cloud cover or weather conditions. An understanding of the operational aspects of the two sensors allows for an appreciation of how they could be used to complement each other in a peatland reservoir remote sensing application. SAR imaging satisfies the need for repeated successful image acquisitions early (year 1-3) after initial flooding when most of

the peatland upheaval, transport, and disintegration processes are occurring. High-resolution optical imaging provides the ability to discriminate and map detailed land cover classes.

Thesis Objective 3 developed an image classification model to map floating peatlands, forested land, open water, and barren land cover classes. The QuickBird optical VNIR image was selected based on the results of the discriminant analyses in the first part of Chapter 5 (Objective 2). The classification accuracy of the unsupervised classification model was found to be excellent at 95.5%. The hierarchical nature of the classification allowed it to be collapsed down to a land and water mask classification. The advantage of this model is that it can be used not only as a land/water masking tool, but also as a tool for deriving a floating peatland inventory map, among additional applications.

Thesis Objective 4 completed a land and water change detection in order to determine changes in Stephen's Lake over a seven year period (1999 – 2006), 35 years after initial flooding. The resulting change detection map successfully revealed areas that were land in 1999 and had become water in 2006, and areas that were water in 1999, and were now replaced by land in 2006. These areas of change can be attributed to peatland upheaval, transport, and disintegration, mineral erosion, and water level variation due to forebay cycling. Dynamic peatland processes are still occurring 35 years after initial flooding.

7.3 RECOMMENDATIONS

Technological advances in high-resolution optical and SAR imaging systems have made data more accessible, provide greater coverage, and have improved accuracy. High-resolution optical sensors, which are planned for launch or have recently been launched, will have increased image area coverage, increased spatial resolution and an increased selection of optical channels covering smaller bandwidths (ex. DigitalGlobe's WorldView-2). These optical system enhancements will only increase the scale at which land cover can be mapped using remotely sensed methods. RADARSAT-2, which became operational in 2008, provides multi-polarized data, and increased spatial resolution. A maximum of four information bands can be attained from a single scene with this setup. The use of multi-polarized SAR data in the operational discrimination and classification of land cover types has been shown to be much greater than single-polarized data (Baghdadi et al. 2001) and should be explored in future studies.

 Further information gained from *in situ* optical VNIR and microwave data collection can only improve the understanding of the optical and microwave EMR response properties of floating peatland habitats. Future projects may benefit from *in situ* scatterometer measurements of microwave backscatter from peatland targets.

The inclusion of up to date detailed digital terrain models (DTM) can be used to help quantify maximum shoreline extents related to water level variations stemming from forebay cycling. This would allow for a better estimation of reservoir change directly related to mineral erosion and peatland disintegration processes. Some studies, for example, the proposed Keeyask GS project have accounted for this early on during environmental impact studies.

An intuitive imaging acquisition effort is required to map and monitor the changes to the land/water interface resulting from the processes of peatland upheaval, transport, and disintegration and mineral erosion, which the proposed Keeyask GS project is expected to experience (KHLP 2010). This effort would see the most benefit from a complimentary imaging program. SAR image acquisitions would fulfill the time-sensitive nature of the application and optical image acquisitions would allow for detailed land cover class mapping and validation. Imaging would ideally begin prior to initial reservoir filling in order to calibrate or bench mark future images captured after flooding. One SAR and one optical image prior to flooding would be prudent. SAR imaging should be frequent in the beginning with a recommended minimum of three images during each of the open water seasons in the first two years. A high-resolution optical image should be acquired, if possible, once during the middle of each of the open water seasons. After three years the frequency of acquisitions can be minimized to 1 SAR and 1 optical during the open water season. After 10 years most peatland change will have occurred, however as this thesis has demonstrated, change is still occurring 35 years after initial flooding in Stephens Lake.

REFERENCES

Agriculture and Agri-food Canada. 2003. Biophysical Land Classification of the Kettle Rapids (54D) and Split Lake (54A – SE1/4) Map Areas. Information Bulletin 2003-3. Prepared by Land Resource Group – Manitoba Semiarid Prairie Agricultural Research Centre, Research Branch, Agriculture and Agri-Food Canada for Manitoba Hydro. 45 p.

Andrefouiet, S., Kramer, P., Torres-Pulliza, D., Joyce, K.E., Hochberg, E.J., Garza-Perez, R., Mumby, P.J., Riegl, B., Yamano, H., White, W.H., Zubia, M., Brock, J.C., Phinn, S.R., Naseer, A., Hatcher, B.G., and F.E. Muller-Karger. 2003. Multi-site evaluation of IKONOS data for classification of tropical coral reef environments. Remote Sensing of Environment, 88: 128-143.

Arzandeh, S. and J. Wang. 2002. Texture evaluation of RADARSAT imagery for wetland mapping. Can. J. Remote Sensing. 28: 653 – 666.

Asada, T., Warner, B.G., and S.L. Schiff. 2005. Effects of shallow flooding on vegetation and carbon pools in boreal peatlands. Applied Vegetation Science, 8: 199-208.

Augusteijn, M.F. and C.E.Warrender. 1998. Wetland classification using optical and radar data and neural network classification. International Journal of Remote Sensing, 19: 1545-1560.

Baghdadi, N., Bernier, M., Gauthier, R., and I. Neeson. 2001. Evaluation of C-band SAR data for wetlands mapping. International Journal of Remote Sensing, 22: 71-88.

Baghdadi, N., Gaultier, S., and C. King. 2002. Retrieving surface roughness and soil moisture from synthetic aperture radar (SAR) data using neural networks. Can. J. Remote Sensing, Vol. 28: 701–711.

Balagurov, M.1967. Twenty-five years of service of the sequence of hydroelectric power stations on the upper Volga. Power Technology and Engineering (formerly Hydrotechnical Construction), 1: 516-524.

Barber, D.G. and E.F. LeDrew. 1991. SAR sea ice discrimination using texture statistics: A multivariate approach. Photogrammetric Engineering and Remote Sensing, 57: 385-395.

Barber, D.G. 1993. A comparison of second-order classifiers for SAR sea ice discrimination. Photogrammetric Engineering and Remote Sensing 59:1397-1408.

Barber, D.G., Hochheim, K.P., Dixon, R., Mosscrop, D.R., and M.J. McMullan. 1996. The role of earth observation technologies in flood mapping: A Manitoba case study. Canadian Journal of Remote Sensing, 22: 137 – 143.

Bartsch, A., Kidd, R.A., Pathe, C., Scipal, K., and W. Wagner. 2007. Satellite radar imagery for monitoring inland wetlands in boreal and sub-arctic environments. Aquatic Conservation: Marine and Freshwater Ecosystems, 17: 305-317.

Baxter, R.M. 1977. Environmental Effects of Dams and Impoundments. Annual Review of Ecology and Systematics, 8: 255-283.

Bélanger, S., J. Ouzilleau and J. Brunelle. 1991. Aménagement hydroélectrique d'Eastmain 1. Etude d'impact sur l'environment- Avant-project. Rapport sectoriel no. 9: Soulèvement des tourbières. Rapport présenté par Le Groupe Roche Boréal à la viceprésidence Environnement, Hydro-Québec. 20p.

Benallegue M., Taconet, O., Vidal-Madjar, D., and M. Normand. 1995. The use of radar backscattering signals for measuring soil moisture and surface roughness. Remote Sensing of Environment 53: 61-68.

Bodaly, R.A., St.Louis, V.L., Paterson, M.J. Fudge, R.J.P., Hall, B.D., Rosenberg, D.M., and J.W.M. 1997. Bioaccumulation of mercury in the aquatic food chain in newly flooded areas. *In* Mercury and its effects on environment and biology. *Edited by* H.Sigel and A. Sigel. Marcel Dekker, New York pp. 259 – 287.

Bryan, M.L.. 1981. Use of radar imagery for surface water investigations. In: Satellite hydrology; Proceedings of the Fifth Annual William T. Pecora Memorial Symposium on Remote Sensing, Sioux Falls, SD, June 10-15, 1979. (A81-43176 20-43) Minneapolis, MN, American Water Resources Association, 1981, p. 238-251.

Brezonik, P.L., K. Menken, and M.E. Bauer 2005. Landsat-based remote sensing of lake water quality characteristics, including chlorophyll and colored dissolved organic matter (CDOM). Lake and Reservoir Management 21: 373-382.

Brisco, B., and R.J. Brown. 1998. Agriculture applications with radar. In Principles and applications of imaging radar. Manual of remote sensing. John Wiley & Sons, Inc., New York, NY. 724p.

Brook R. K.. 2001. Structure and dynamics of the vegetation in Wapusk National Park and the Cape Churchill Wildlife Management Area of Manitoba, community and landscape scales. MNRM thesis. University of Manitoba, Canada. 274p.

Brook R.K. and N.C. Kenkel. 2002. A multivariate approach to vegetation mapping of Manitoba's Hudson Bay Lowlands. Int. J. Remote Sensing. 23: 4761-4776.

Canadian Centre for Remote Sensing (CCRS). 2009. Tutorial: Fundamentals of Remote Sensing. Natural Resources Canada. http://www.ccrs.nrcan.gc.ca/ resource/tutor/fundam/index_e.php

Charman, D. 2002. Peatlands and environmental change. Chichester, England:.John Wiley and Sons Ltd. 301p.

Clark, M.W., and K.R. Reddy. 1998. Analysis of floating and emergent vegetation formation in Orange Lake. Final Report. St. Johns River Water Management District, Palatka, FL.

Cohen, J. 1960. A coefficient of agreement for nominal scales. Educational and Psychological Measurement, 1: 37 – 40.

Congalton, R.G. 1991. A review of assessing the accuracy of classifications of remotely sensed data. Remote Sensing of Environment 37: 35-46.

Cooley, P.M. and D.G. Barber. 2003. Remote Sensing of the Coastal Zone of Tropical Lakes.*Internat. Assoc. Great Lakes Res.*, 29(2), 62-75.

Cooley, P., Dolce-Blanchard, L., and J.Larter. 2009. The effect of local and regional watersheds on the spectral composition and attenuation of light and water quality parameters in the surface waters of Stephens Lake, Manitoba. A report prepared for Manitoba Hydro by North/South Consultants Inc. 37p.

Corkery, M.T. 1996. Geology and landforms of Manitoba. *In*The geography of Manitoba: its land and its people. University of Manitoba Press, Canada.327p.

Dechka, J.A., Franklin, S.E., Watmough, M.D., Bennett, R.P., and D.W. Ingstrup 2002. Classification of wetland habitat and vegetation communities using multi-temporal Ikonos imagery in southern Saskatchewan. Can. J. Remote Sensing, 28: 679-685.

Desrochers, A. and G. van Duinen. 2006. Peatland fauna. In Boreal Peatland Ecosystems. Springer, Berlin. 435p.

Dixon, R. and J. Stewart. 1984. Peatland inventory of The Pas, Manitoba using Landsat. Manitoba Remote Sensing Centre. Report 32pp.

Dobson, M.C., and F.T. Ulaby. 1998. Mapping soil moisture distribution with imaging radar. In Principles and applications of imaging radar. Manual of remote sensing. John Wiley & Sons, Inc., New York, NY. 724p.

Downs, S.G., Macleod, C.L., and J.N. Lester. 1998. Mercury in precipitation and its relation to bioaccumulation in fish: A literature review. Water, Air, and Soil Pollution 108: 149–187.

Doxaran, D., Froidefond, J., Lavender, S., and P. Castaing. 2002. Spectral signature of highly turbid waters Application with SPOT data to quantify suspended particulate matter concentrations. Remote Sensing of Environment 81: 149-161.

Dryade. 1984. Soulèvement des tourbières sur les réservoirs du complexe La Grande.Rapport pour la direction Ingénierie et Environnement, Société d'énergie de la Baie James. Québec, Le Groupe Dryade ltée.

Duchemin, E., Lucotte, M., Canuel, R. and A. Chamberland. 1995. Production of the greenhouse gases CH_4 and CO_2 by hydroelectric reservoirs of the boreal region. Global Biogeochemical Cycles 9: 529-540.

Duda, O. and Hart, P.E., 1973. Pattern classification and scene analysis. New York: Wiley. 363p.

Elachi, C., and J. van Zyl. 2006. Introduction to the physics and techniques of remote sensing, second edition. John Wiley and Sons, New Jersey.

Environment Canada. 2007. Canadian monthly climate data and 1971-2000 normals. [Ottawa, Ont.]: Environment Canada, c2007.

Fechner-Levy, E.J. and Hemond, H.F.1996. Trapped methane volume and potential effects on methane ebullition in a northern peatland. Limnology and Oceanography, 41: 1375-1383.

Fitzgerald, W.F., Engstrom D.R., Mason R. P., and E.A. Nater. 1998. The case for atmospheric mercury contamination in remote areas. Environmental Science and Technology. 32: 1-7.

Frost, V.S., Stiles, J.A., Shanmugan, K.S., Holtzman, J.C., and S.A. Smith. 1981. An adaptive filter for smoothing noisy radar images. Proceedings of the IEEE, 69: 133-135.

Gamon, J.A, Huemmrich, K.F., Peddle, D.R., Chen, J., Fuentes, D.,.Hall, F G., Kimball, ,J.S., Goetz, S., Gu J., McDonald, K.C. Miller, J.R., Moghaddam, M. , Rahman, A.F., Roujean, J.-L., Smith, E.A., Walthall, C.L., Zarco-Tejada, P., Hui, B., Fernandes, R., and J. Cihlar. 2004. Remote sensing in BOREAS: Lessons learned. Remote Sensing of Environment, 89: $139 - 162$.

Giglio, L., Descloitresa, J., Justicec, C.O., and Y.J. Kaufman. 2003. An enhanced contextual fire detection algorithm for MODIS. Remote Sensing of Environment, 87: $273 - 282$.

Grenier, M., Demers, A., Labrecque, S., Benoit, M., Fournier, R.A., and B. Drolet. 2007. An object based method to map wetland using RADARSAT-1 and Landsat ETM images:test case on two sites in Quebec, Canada. Can. J. Remote Sensing, 33: 28 $- 45$.

Grondin, P. and J. Ouzilleau. 1980. Les toubieres du complexe NBR, terretoire de la Baie-James, Quebec. Tome 1. Classification et description. Rapport pour la direction Environnment, Societe d'energie de la Baie James. Le Groupe Dryade Itee, Quebec.

Han, L. 1997. Spectral reflectance with varying suspended sediment concentration in clear and algae-laden waters. Photogrammetric Engineering and Remote Sensing 63: $701 - 705$.

Haralick, R.M., Shanmugan, K., and I. Dinstein. 1973. Textural features for image classification. IEEE Transactions on Systems, Man, and Cybernetics, 3: 610-621.

Harris, A., Bryant, R.G., and A.J Baird. 2006. Mapping the effects of water stress on Sphagnum: Preliminary observations using airborne remote sensing. Remote Sensing of Environment,100: 363-378.

Hogg, E.H. and R.W. Wein. 1988. The contribution of typha components to floating mat buoyancy. Ecology, 69: 1025-1031.

Ivanov, I., Busel', N., and V. Kalenov. 1971. Power-economy effectiveness and experience with the 15-year operation of the first stage of the Irkutsk hydroelectric plant. Power Technology and Engineering (formerly Hydrotechnical Construction) 5: 605-610.

Karaska, M.A., Huguenin, R.L., Beacham, J.L., Wang, M., Jensen, J.R., and R.S. Kaufmann. 2004. AVIRIS measurements of chlorophyll, suspended minerals, dissolved organic carbon, and turbidity in the Neuse River, North Carolina. Photogrammetric Engineering and Remote Sensing, 70: 125-133.

Keeyask Hydropower Limited Partnership (KHLP) 2010. Keeyask generation project environmental impact statement: physical environment supporting volume (Draft – February 2010). Manitoba Hydro, Winnipeg, MB., Canada.

Kuan, D.T., Sawchuck, A.A., Strand, T.C., and P. Chavel. 1987. Adaptive restoration of images with speckle. IEEE Trans. Acoustics, Speech and Sig. Proc., 35: 373-383.

Kuhry, P. and Turunen, J. 2006. The postglacial development of boreal and subarctic peatlands. *In*Boreal peatland ecosystems. Springer, Berlin.435p.

Laba, M., Down, R., Smith, S., Welsh, S., Neider, C, White, S., Richmond, M., Philpot, W., and P. Baveye. 2007. Mapping invasive wetland plants in the Hudson River National Estuarine Research Reserve using quickbird satellite imagery. Remote Sensing of Environment, 112: 286 – 300.

Larter, J.L., and P.M. Cooley. 2009. Substratum and depth distribution in flooded habitat of Stephens Lake, Manitoba, thirty-five years after impoundment. A draft report prepared for Manitoba Hydro. by North/South Consultants Inc. 41p.

Leckie, D.G., and K.J. Ranson. 1998. Forestry applications using imaging radar. In Principles and applications of imaging radar. Manual of remote sensing. John Wiley & Sons, Inc., New York, NY. 724p.

Lee, J.S., 1981. Speckle Analysis and Smoothing of Synthetic Aperture Radar Images. Computer Graphics and Image Processing, 17: 24-32.

Lee, J.S., 1986. Speckle suppression and analysis for synthetic aperture radar images. Optical Engineering, 25: 636–643.

Legendre, P. and L. Legendre. 1998. Numerical Ecology. Second English edition. Elsevier Scientific Publishing Company, Amsterdam, 853p.

Lewis, A.J. 1998. Geomorphic and hydrologic applications of active microwave remote sensing. *In* Principles and applications of imaging radar. Manual of remote sensing. John Wiley and Sons Inc. ,New York 866p.

Lewis A.J. and F.M. Henderson.1998. Radar fundamentals: the geoscience perspective. *In* Principles and applications of imaging radar. Manual of remote sensing. John Wiley and Sons Inc., New York 866p.

Lewis, F.J., and E.S. Dowding. 1926. The vegetation and retrogressive changes of peat areas ("muskegs") in central Alberta. The Journal of Ecology, 14: 317-341.

Li, J. and W. Chen. 2005. A rule-based method for mapping Canada's wetlands using optical, radar and DEM data. International Journal of Remote Sensing, 26: 5051-5069.

Li, J., Chen, W., and R. Touzi. 2007. Optimum RADARSAT-1 configurations for wetland discrimination: a case study of the Mer Bleu peat bog. Canada. Can. J. Remote Sensing, 33: 46 – 55.

Lillesand, T.M. and.R.W. Kieffer. 2000. Remote sensing and image interpretation. John Wiley & Sons, Inc., New York, NY. 724p.

Loechel, S. E., Walthall, C. L., de Colstoun, E. B., Chen, J. M., and B.L. Markham. 1996. Spatial and temporal variability of surface cover at BOREAS using reflectance from a helicopter platform. Geoscience and Remote Sensing Symposium, 1996. IGARSS '96. 'Remote Sensing for a Sustainable Future.', 1: 586-589.

Manitoba Hydro. 1996a. History and First Order Effects: Manitoba Hydro Projects and Related Activities in the Split Lake Cree Study Area: Split Lake Cree Post Project Environmental Review Volume 2. Split Lake Cree – Manitoba Hydro Joint Study Group. 64 p.

Manitoba Hydro. 1996b. First Rapids Generating Station, First Rapids Erosion Study. Geotechnical Department, Engineering Division, Manitoba Hydro. March 1996. 14 p.

Manitoba Hydro and Nisichawayasihk Cree Nation (NCN). 2003. Wuskwatim generation project: environmental impact statement. Volumes 1 – 10. Manitoba Hydro, Winnipeg, MB.

Mather, P.M. 2004. Computer processing of remotely-sensed images: an introduction. Jon Wiley & Sons Ltd., Chichester, England. 324p.

Menken, K., Brezonik, P.L., and M. Bauer. 2006. Influence of chlorophyll and humic color on reflectance spectra of lakes: implications for measurement of lake-water properties by remote sensing. Journal of Lake and Reservoir Management.

Mills, G.F., Veldhuis, H., and D.B. Forester. 1976. A guide to biophysical land classification Kettle Rapids 54D, Manitoba. Northern Resource Information Program.

Mitchell, C.C. and W.A. Niering. 1993. Vegetation change in a topogenic bog following beaver flooding. Bulletin of the Torrey Botanical Club.120: 136-147.

Moore, T., and N. Basiliko. 2006. Decomposition in boreal peatlands. *In* Boreal peatland ecosystems. Springer, Berlin.435p.

Mouchot, M., and R. Garello. 1998. SAR for oceanography. In Principles and applications of imaging radar. Manual of remote sensing. John Wiley & Sons, Inc., New York, NY. 724p.

Mumby, P.J. and A.J. Edwards. 2002. Mapping marine environments with IKONOS imagery: enhanced spatial resolution can deliver greater thematic accuracy. Remote Sensing of Environment 82: 248-257.

Munyati, C.. 2004. Use of principal component analysis (PCA) of remote sensing images in wetland change detection on the Kafue Flats, Zambia. Geocarto International, 19: 11-22.

National Wetlands Working Group. 1997. The Canadian wetland classification system. Wetlands Research Centre, University of Waterloo, Ontario.

Nichol, C.J., Huemmrich, K.F., Black, T.A., Jarvis, P.G., Walthall, C.L., Grace, J., and F.G. Hall. 2000. Remote sensing of photosynthetic-light-use efficiency of boreal forest. Agricultural and Forest Meteorology 101: 131-142.

Ouzillaeau, J.. 1977. Floating peat islands in the Cabonga Reservoir. Report on Programme 77, Service Environment Division Etudes.

Ozesmi, S.L. and M.E. Bauer. 2002. Satellite remote sensing of wetlands. Wetlands Ecology and Management. 10: 381-402.

Peake, W.H., and T.L. Oliver. 1971. The response of terrestrial surfaces at microwave frequencies. Ohio State University Technical Report 2440-7.

Pietroniro, A. and R. Leconte. 2000. A review of Canadian remote sensing applications in hydrology, 1995–1999. Hydro. Process. 14: 1641–1666.

Poulin, M., Careau, D., Rochefort, L. and A. Desrochers. 2002. From satellite imagery to peatland vegetation diversity: how reliable are habitat maps?. Conservation Ecology. 6:16.

Quinty, F., and L. Rochefort. 2003. Peatland restoration guide, second edition.

RADARSAT International (RSI), 2000. Radarsat Data Product Specifications.Report No. RSI-GS-026, Radarsat International, Richmond, BC.

Rahel, F.J.. 1984. Factors structuring fish assemblages along a bog successional gradient. Ecology, 65: 1276 – 1289.

Raney, R.K. 1998. Radar fundamentals: technical perspective. *In* Principles and applications of imaging radar. Manual of remote sensing. John Wiley & Sons, Inc., New York, NY. 724p.

Robert, D. 2000. Suivi des toubieres flottantes dans le Reservoir de LG-1. A report for Barrage et Ouvrages de Genie Civil Direction Regionale La Grande Riviere et Direction Production.

Ronka, E. and R. Uusinoka. 1976. The problem of peat upheaval in finnish artificial reservoirs. Bulletin of Engineering Geology and the Environment. 13: 71-74.

Rosenberg, D.M., Berkes, F., Bodaly, R.A., Hecky, R.E., Kelly, C.A., and J.W.M. Rudd. 1997. Large-scale impacts of hydroelectric development. Environ. Rev. 5: 27-54.

Rosenberg, D.M., Chambers, P.A., Culp, J.M., Franzin, W.G., Nelson, P.A., Salaki, A.G., Stainton, R.A., Bodaly, R.A., and R.W. Newbury. 2005. Nelson and Churchill River Basins. In Rivers of North America, Edited by C.Benke and C.E. Cushing. Elsevier: Canada. 1144p.

Rydin, H. and J. Jeglum. 2006. The biology of peatlands. Oxford University Press, New York. 343p.

Saint-Laurent, D., Touileb, B.N., Saucet, J., Whalen, A., Gagnon, B., and T. Nzakimuena. 2001. Effects of simulated water level management on shoreline erosion rates. Case study: Baskatong Reservoir, Quebec, Canada. Can. J. Civ. Eng. 28: 482–495

Saquet, M.A.M.. 2003. Greenhouse gas flux and budget from an experimentally flooded wetland using stable isotopes and geochemistry. University of Waterloo. 158p.

Sawaya, K.E., Olmanson, L.G., Heinert, N.J., Brezonik, P.L., and M.E.Bauer. 2003. Extending satellite remote sensing to local scales: land and water resource monitoring using high-resolution imagery: IKONOS Fine Spatial Resolution Land Observation. Remote Sensing of Environment. 88: 144-156.

Schaepman, M., Keller, P., Schläpfer, D., Cathomen, C., and K.I. Itten. 1997. Experimental determination of adjacency effects over an eutrophic lake using a helicopter mounted spectroradiometer for the correction of imaging spectrometer data. Third International Airborne Remote Sensing Conference and Exhibition, 7–10 July, Copenhagen, Denmark

Scott, G.A.J.1995. Canada's vegetation: a world perspective. McGill-Queen's University Press.

Scott, G.A.J. 1996. Manitoba's ecoclimatic regions. *In*The geography of Manitoba: its land and its people. The University of Manitoba Press, Canada.

Scott, K.J., C.A. Kelly, and J.W.M. Rudd . 1999. The importance of floating peat to methane fluxes from flooded peatlands. Biogeochemistry, 47: 187-202.

Sokol, J., NcNairn, H., and T.J. Pultz. 2004. Case studies demonstrating the hydrological applications of C-band multipolarized and polarimetric SAR. Can. J. Remote Sensing, 30: 470–483.

Somodi, I. and Z. Botta-Dukat.2004. Determinants of floating island vegetation and succession in a recently flooded shallow lake, Kis-Balaton (Hungary). Aquatic Botany 79: 357-366.

St.Louis, V.L., Partridge, A.D., Kelly, C.A., and J.W.M. Rudd. 2003. Mineralization rates of peat from eroding peat islands in reservoirs. Biogeochemistry 64**:** 97-100.

St.Louis, V.L., Rudd, J.W.M., Kelly, C.A., Bodaly, R.A., Paterson, M.J., Beaty, K.G., Hesslein, R.H., Heyes, A., and A.R Majewski. 2004. The rise and fall of mercury methylation in an experimental reservoir. Environ. Sci. Technol. 38: 1348-1358.

Stumpf, R.P., and K.Holdried. 2003. Determination of water depth with high-resolution satellite imagery over variable bottom types. Limnol. Oceanogr., 48: 547 – 556.

Tarnocai, C. 2006. The effect of climate change on carbon in Canadian peatlands. Global and Planetary Change. 53:222-232.

Tarnocai, C., Kettles, I.M., and Lacelle, B. 2000. Peatlands of Canada; Geological Survey of Canada, Open File 3834, scale 1:6 500 000.

Tarnocai, C., Kettles I.M., and Lacelle, B. 2002. Peatlands of Canada Database. Geological Survey of Canada, Open File 4002)

Thomas, V., Treitz, P., Jelinski, D., Miller, J., Lafleur, P., and J. H. McCaughey. 2003. Image classification of a northern peatland complex using spectral and plant community data. Remote Sensing of Environment, 84: 83 – 99.

Tou, J. and Gonzales, R. 1974. Pattern recognition principles. Reading, MA: Addison-Wesley.

Townsend, P. and S. Walsh. 1998. Modeling floodplain inundation using an integrated GIS with radar and optical remote sensing. Geomorphology, 21: 295-312.

Townsend, P. and S. Walsh. 2001. Remote sensing of forested wetlands: application of multitemporal and multispectral satellite imagery to determine plant community composition and structure in southeastern USA. Plant Ecology157: 129-149.

Toyra, J. Pietroniro, A., and L.W. Martz. 2001. Multisensor hydrologic assessment of a freshwater wetland. Remote Sensing of Environment 75:162-173.

Toyra, J. and A. Pietroniro. 2005. Towards operational monitoring of a northern wetland using geomatics-based techniques. Remote Sensing of Environment. 97: 177-197.

Ulaby, F.T., Moore, R.K. and A.K. Fung. 1981. Microwave remote sensing. Volume 1, Addison-Wesley, Reading, MA. 456p.

Ulaby, F.T., Kouyate, F., Brisco, B., and T.H.L. Williams. 1986. Textural information in SAR images: Geoscience and Remote Sensing, IEEE Transactions on. Geoscience and Remote Sensing. 24: 235-245.

Vachon, P.W., Campbell, J.W.M., Bjerkelund, C.A., Dobson, F.W., and M.T. Rey. 1997. Ship detection by the RADARSAT SAR: validation of detection model predictions. Can. J. Remote Sensing 23: 48-59.

Vasilevskii, A., Kazarov, S., and E. Shtern,. 1975. Improved utilization of water resources at hydroelectric plants. Power Technology and Engineering (formerly Hydrotechnical Construction) 9: 47-52.

Vertucci, F.A. and G.E. Likens. 1989. Spectral reflectance and water quality of Adirondack Mountain Region Lakes. Limnology and Oceanography 34: 1656-1672.

Vitt, D.H.. 2006. Functional characteristics and indicators of boreal peatlands. *In* Boreal peatland ecosystems. Springer, Berlin.435p

Vogelmann, J.E., and D.M. Moss. 1993. Spectral reflectance measurements in the genus sphagnum. Remote Sensing of Environment, 45: 273 – 279.

Von Post, L. 1924. Das genetische System der organogenen Bildungen Schwedens. Comite International de Pedologic IV Commission No.22.

Wei, A., and P. Chow-Fraser. 2007. Use of IKONOS imagery to map coastal wetlands of Georgian Bay. Fisheries, 32: 167-173.

Weider, R.K., Vitt, D.H., and B.W. Benscoter. 2006. Peatlands and the boreal forest. *In* Boreal peatland ecosystems. Springer, Berlin.435p

Weyhenmeyer,C.E. 1999. Methane emissions from beaver ponds: Rates, patterns, and transport mechanisms. Global Biogeochemical Cycles 13: 1079-1090.

Wolter, P.T., Johnston, C.A., and G.J. Niemi. 2005. Mapping submergent aquatic vegetation in the US Great Lakes using Quickbird satellite data. International Journal of Remote Sensing, 26: 5255 – 5274.

Woodhouse, I.H.. 2006. Introduction to microwave remote sensing. Taylor and Francis Group, Florida. 370p.

Xie, H., Ulaby, F.T., Pierce, L.E., and M.C. Dobson. 1999. Performance Metrics for SAR Speckle-Suppression Filters. In Proc. IGARSS '99. vol.3: 1540-1543.